Universidade de Aveiro Departamento de Química
2010

Diana Mónica de Mesquita Sousa Fernandes

Eléctrodos modificados com polioxotungstatos do tipo Keggin

Modified electrodes with Keggin-type polyoxotungstates

Universidade de Aveiro Departamento de Química
2010

Diana Mónica de Mesquita Sousa Fernandes

Eléctrodos modificados com polioxotungstatos do tipo Keggin

Modified electrodes with Keggin-type polyoxotungstates

Tese apresentada à Universidade de Aveiro para cumprimento dos requisitos necessários à obtenção do grau de Doutor em Química, realizada sob a orientação científica da Doutora Ana Maria V. S. Viana Cavaleiro, Professora Catedrática do Departamento de Química da Universidade de Aveiro e do Doutor Christopher Michael Ashton Brett, Professor Catedrático da Universidade de Coimbra

Apoio financeiro do POCTI no âmbito do III Quadro Comunitário de Apoio.

Apoio financeiro da FCT e do FSE no âmbito do III Quadro Comunitário de Apoio.

Dedico este trabalho à minha orientadora Doutora Helena Carapuça (1965-2008) pela sua inspiração, apoio incansável e constante amizade.

o júri

presidente

Prof. Doutor Casimiro Adrião Pio
professor catedrático da Universidade de Aveiro

Prof. Doutora Ana Maria Vieira da Silva Cavaleiro
professora catedrática da Universidade de Aveiro

Prof. Doutor Christopher Michael Ashton Brett
professor catedrático da Faculdade de Ciências e Tecnologia da Universidade de Coimbra

Prof. Doutor Baltazar Manuel Romão de Castro
professor catedrático da Faculdade de Ciências da Universidade do Porto

Prof. Doutora Maria Isabel da Silva Pereira
professora associada com agregação da Faculdade de Ciências da Universidade de Lisboa

Prof. Doutora Helena Isabel Seguro Nogueira
professora auxiliar da Universidade de Aveiro

agradecimentos

No final desta etapa não posso deixar de agradecer o meu sincero agradecimento às pessoas que, directa ou indirectamente, contribuíram para a concretização desta investigação.

Aos meus orientadores científicos, Doutora Helena Carapuça, Doutora Ana Cavaleiro e Doutor Christopher Brett, muito obrigada por tudo o que me ensinaram, pela dedicação, disponibilidade, incentivo e por toda a amizade e simpatia ao longo destes anos.

À Universidade de Aveiro, em particular ao CICECO e ao Departamento de Química, por me terem disponibilizado todas as condições necessárias à realização deste trabalho. À Fundação para a Ciência e a Tecnologia pela bolsa de Doutoramento.

À Drª Celeste Azevedo pela realização das análises térmicas e pela simpatia sempre demonstrada.

Obrigada aos amigos e colegas do DQ pelo companheirismo, amizade e carinho em especial ao João Rodrigues, à Joana Marques e à Violeta Girão.

Obrigada aos colegas e amigos de Coimbra por me terem recebido com tanta simpatia e em especial à Madi por todo o apoio com os estudos de impedância.

À Mestre Susana Simões pelo apoio no laboratório, pelas nossas conversas científicas e por toda a amizade demonstrada.

Aos meus amigos Nélio, Pedro, Tana, Paula e Jorge muito obrigada por estarem sempre presentes apesar da distância.

Às minhas meninas, Luciana Rocha, Patrícia Silva, Diana Lima e Catarina Coelho muito obrigada pela amizade incondicional, carinho e pelo amparo nos momentos mais difíceis. Aveiro não seria a mesma se não vos tivesse conhecido.

Ao Renato pelo carinho, compreensão e muita paciência.

Aos meus avós João e Isolina, à minha querida irmã Xaninha e em especial aos meus pais José e Fernanda pelo amor constante, pela confiança e por estarem sempre presentes e me apoiarem em todos os momentos da minha vida.

palavras-chave

Polioxotungstatos do tipo Keggin, eléctrodos modificados, voltametria cíclica, espectroscopia de impedância electroquímica.

resumo

O objectivo deste trabalho é a produção de novos eléctrodos modificados com polioxotungstatos (POMs) do tipo Keggin, incluindo POMs lacunares e substituídos por metais de transição. A preparação e caracterização dos polioxotungstatos encontram-se descritas no Capítulo 2. No Capítulo 3 descreve-se a produção de eléctrodos de carbono vítreo funcionalizados com sais híbridos de tetra-*n*-butilamónio de vários silicotungstatos pelo método de evaporação da gota. As propriedades electroquímicas dos polioxotungstatos imobilizados foram comparadas com as das espécies solúveis correspondentes. A morfologia dos depósitos foi avaliada por microscopia óptica e por microscopia electrónica de varrimento. No capítulo 4 descreve-se a preparação de novos eléctrodos compósitos de carbono e poli(hexilmetacrilato) com fosfotungstatos. Os estudos electroquímicos revelaram que as principais características dos POMs são mantidas e que os processos de redução são controlados por difusão, dependendo da difusão dos protões da solução. O Capítulo 5 descreve a construção de filmes em multicamadas ultrafinos contendo POMs e polietilenimina, preparados pelo método de auto-montagem camada-sobre-camada em eléctrodos de carbono vítreo. Os filmes em multicamada foram caracterizados por voltametria cíclica e por microscopia electrónica de varrimento e foi usada a espectroscopia de absorção de UV-Vis em placas de quartzo para monitorar o crescimento de filme. Os resultados voltamétricos revelaram que os processos de redução dos POM são confinados à superfície. Alguns destes eléctrodos modificados revelaram propriedades electrocatalíticas relativamente à redução dos aniões nitrito, bromato e/ou iodato. A espectroscopia de impedância electroquímica também foi usada na caracterização destes filmes e os resultados revelaram que a resistência à transferência de carga aumenta com o aumento do número de bicamadas para ambas as espécies redox, indicando que a espessura do filme tem um efeito importante sobre a cinética de reacções de transferência de carga. No capítulo 6 descreve-se a síntese de filmes híbridos orgânicos/inorgânicos compostos por poli(3,4-etilenodioxitiofeno) (PEDOT) e por silicotungstatos do tipo Keggin através da polimerização electroquímica, em condições aquosas, na superfície de electrodos de carbono vítreo. A voltametria cíclica revelou que as características principais dos POMs são mantidas nos filmes. Verificou-se que estes filmes são muito estáveis, possivelmente devido a fortes interacções electrostáticas entre os POMs aniónicos e o polímero positivamente carregado. A espectroscopia de impedância electroquímica foi também utilizada e os resultados mostraram que a resistência de transferência de carga aumenta com o aumento do pH e para valores de potenciais mais elevados. O capítulo 7 apresenta as conclusões finais e possíveis trabalhos futuros.

keywords

α-Keggin type polyoxotungstates, modified electrodes, cyclic voltammetry, electrochemical impedance spectroscopy.

abstract

The aim of the present work is the fabrication of novel modified electrodes with Keggin-type polyoxotungstates (POMs), including lacunary and transition metal-substituted POMs. The preparation and characterization of the polyoxotungstates is described in Chapter 2. In Chapter 3 is described the production of glassy carbon electrodes functionalised with tetra-*n*-butylammonium hybrid salts of several silicotungstate anions by the droplet evaporation method. The electrochemical features of immobilized polyoxotungstates were compared with those of corresponding soluble species. The morphology of the deposits was evaluated by optical and scanning electron microscopy. In Chapter 4 is described the preparation of novel poly(hexylmethacrylate) carbon composite electrodes with phosphotungstates. The electrochemical studies showed that the main features of the POMs are maintained and that the reduction processes are diffusion-controlled, depending on the uptake of protons from the solution. Chapter 5 describes the construction of ultrathin multilayer films containing POMs and poly(ethylenimine) prepared by the electrostatic layer-by-layer self-assembly method on glassy carbon electrodes. The multilayer films were characterized by cyclic voltammetry and scanning electron microscopy, and UV-Vis absorption spectroscopy on a quartz slide was used to monitor film growth. Voltammetric results revealed that the POMs tungsten reduction processes are surface-confined. Some of these modified electrodes showed electrocatalytic properties towards the reduction of nitrite, bromate and/or iodate. Electrochemical impedance spectroscopy (EIS) was also used and showed that the charge transfer resistance increases with increasing number of bilayers for both redox probes indicating that the thickness of the multilayer film has an important effect on the kinetics of the charge transfer reactions. In Chapter 6 is described the synthesis of hybrid organic/inorganic films composed of poly(3,4-ethylenedioxythiophene) (PEDOT) and silicotungstates by electrochemical polymerization under aqueous conditions on the surface of glassy carbon electrodes. Cyclic voltammetry showed that the main features of POMs are maintained in the films. The films presented high stability, possibly due to strong electrostatic interactions between anionic POM and positively charged polymer. Electrochemical impedance spectroscopy was also used and the results showed that the charge transfer resistance increased with increasing pH and for higher values of potentials used. Conclusions and future perspectives are indicated in Chapter 7.

General Index

Publications List

1. Diana M. Fernandes, Susana M. N. Simões, Helena M. Carapuça, Ana M. V. Cavaleiro, "Functionalisation of glassy carbon electrodes with adsorbed tetra-butylammonium microcrystalline salts of lacunary and metal substituted α-Keggin-polyoxosilicotungstates", Electrochimica Acta 53 (2008) 6580.

2. Diana M. Fernandes, Susana M. N. Simões, Helena M. Carapuça, Christopher M. A. Brett, Ana M. V. Cavaleiro, "Novel poly(hexylmethacrylate) composite carbon electrodes modified with Keggin-type tungstophosphate tetra-butylammonium salts", Journal of Electroanalytical Chemistry 639 (2010) 83.

3. Diana M. Fernandes, Helena M. Carapuça, Christopher M. A. Brett, Ana M. V. Cavaleiro, "Electrochemical behaviour of self–assembly multilayer films based on iron–substituted α–Keggin polyoxotungstates, Thin Solid Films 518 (2010) 5881.

4. Diana M. Fernandes, Christopher M. A. Brett, Ana M. V. Cavaleiro, " Layer-by-Layer self-assembly and electrocatalytic properties of poly(ethylenimine)-silicotungstate multilayer composite films", Journal of Solid State Electrochemistry, DOI 10.1007/s10008-010-1154-1 (in press).

5. Diana M. Fernandes, Mariana E. Ghica, Christopher M. A. Brett, Ana M. V. Cavaleiro, "Electrochemical impedance study of layer-by-layer iron-silicotunsgtate/ poly(ethylenimine) modified electrodes", submitted in Electrochimica Acta.

6. Diana M. Fernandes, Christopher M. A. Brett, Ana M. V. Cavaleiro, "Preparation and electrochemical properties of modified electrodes with Keggin-type silicotungstates and PEDOT", submitted in Journal of Electroanalytical Chemistry.

Abbreviations List

COP	Conducting organic polymers
CPEs	Carbon paste electrodes
CV	Cyclic voltammetry
DMF	Dimethylformamide
DMSO	Dimethylsulfoxide
EIS	Electrochemical impedance spectroscopy
GCE	Glassy carbon electrode
ITO	Indium tin oxide
IUPAC	International Union of Pure and Applied Chemistry
LbL	Layer-by-layer
MCM	Mobil composition of matter
NMR	Nuclear magnetic resonance
PAni	Polyaniline
PDDA	Poly(diallyldimethylammonium chloride)
PEDOT	Poly(ethylenedioxythiophene)
PEI	Poly(ethylenimine)
POMs	Polyoxometalates
PPy	Polypyrrole
PT	Polythiophene
SEM	Scanning electron microscopy
TBA	Tetra-n-butylammonium $[N(C_4H_9)_4]^+$
TG	Thermogravimetry
UV-Vis	Ultraviolet-visible
XW_{11}	Lacunary anion $[XW_{11}O_{39}]^{(n+4)-}$, X = P, Si, etc
$XW_{11}M$	Mono-substituted anion $[XW_{11}M(H_2O)O_{39}]^{m-}$, X = P, Si, and M = Fe, Co, Mn, etc
XW_{12}	Keggin anion $[XW_{12}O_{40}]^{n-}$, X = P, Si, etc

Symbols List

A	Geometric area of the electrode
A_λ	Absorbance at specific wavelength
C	Capacitance
C_d	Double layer capacity
CPE	Constant phase element
$E_{1/2}$	Mid wave potential
E_{pa}	Anodic peak potential
E_{pc}	Cathodic peak potential
F	Faraday's constant
I_{pa}	Anodic peak current
I_{pc}	Cathodic peak current
n	Number of electrons transferred
R_{ct}	Charge transfer resistance
R_Ω	Cell resistance
T	Temperature
Z_W	Warburg element
Γ	Surface coverage
ΔE_p	Peak-to-peak separation
ε_λ	Isotropic molar absorption coefficients
v	Scan rate

Figure Index

Chapter 1

Chapter 2

Chapter 3

Chapter 4

Chapter 5

Chapter 6

Table Index

Chapter 2

Chapter 3

Chapter 4

Chapter 5

Chapter 6

CHAPTER 1

INTRODUCTION

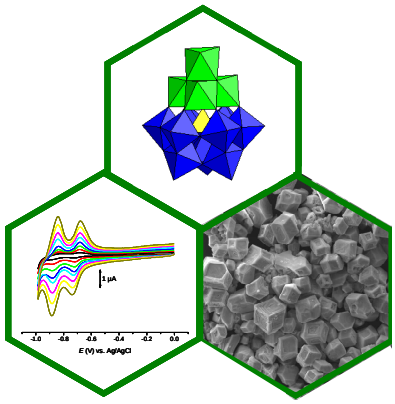

This chapter has the aim of introducing the polyoxometalates (POMs), mainly Keggin-type polyoxometalates, and their importance and application in the electrochemistry field. Therefore, first will be given a general introduction to POMs, presenting what they are and some of their main features, with particular reference to the Keggin anions and their derivatives. These compounds have been of growing interest over recent decades, in areas such as catalysis, medicine and materials science due to their important properties, reactivity, and molecular and electronic versatility. Secondly, an overview will be given of the electrochemical behaviour of these compounds and on what has been studied in the field of modified electrodes using polyoxometalates. Finally, the fundamentals of the main electrochemical techniques used will be presented.

1.1. Polyoxometalates

Polyoxometalates are a set of inorganic clusters in the vast field of coordination chemistry compounds. They are characterized by metallic centres, M = V, Mo, W (or less frequently Nb and Ta), called the addenda atoms, surrounded by bridging or terminal oxygen atoms. Apart from M and O, other elements can be part of the POM cluster. We can distinguish two types of POM families: the isopolyanions ($[M_xO_y]^{m-}$) and the heteropolyanions ($[X_zM_xO_y]^{n-}$), where the elements X are the so-called primary heteroatoms. This heteroatom is essential for the complete polyanion structure, from where it cannot be removed or chemically substituted without destroying the anion. In some cases, there are secondary heteroatoms that may in principle, and generally in

practice, be excised from the heteropolyanion structure to leave an independently stable polyanion [1,2].

The IUPAC nomenclature for POMs proposes names that are normally quite long and not easily applied, for this reason the more common designations among those who work in this area will be used in this thesis. In a review article, Jeannin explains how to connect a name to the structure according to the IUPAC rules [3].

In this work, only the Keggin-type and related heteropolyanions are studied (often referred as polyanions) and, those where the M element is tungsten (W), so the polyoxometalates studied are all polyoxotungstates.

1.1.1. Structure of Keggin anions

The increasing diversity of structures classified in the literature as polyoxometalates turns the definition of this group of compounds gradually more diffuse. This diversity is a consequence of many and unusual properties of POMs. The vast diversity of polyanions known present structures, which are usually composed of MO_6 octahedra linked together through oxygen bridges. The strong polarization of the external layer of oxygens (terminal oxygens) in relation to the interior of the octahedra (due to π bonding), explains why, when the stage of the heteropolyanion species is reached, by combining MO_6, the polymerization process does not continue, leading to infinite chains, but ends with the achievement of discrete units [4].

Among the most studied polyoxometalates are the Keggin anions and their derivatives. The Keggin anion of general formula α-$[XM_{12}O_{40}]^{n-}$, M = Mo^{VI}, W^{VI}; X = P^{V}, As^{V}, Ge^{IV}, Si^{IV}, B^{III}, Fe^{III}, Co^{II}, amongst others, has a overall T_d symmetry, when M = W and *T* symmetry when M = Mo (Fig. 1.1) [1].

The Keggin anion may have more than one type of addenda atom, as in $[PV_2W_{10}O_{40}]^{5-}$ or $[SiMo_3W_9O_{40}]^{4-}$. These are called mixed heteropolyanions.

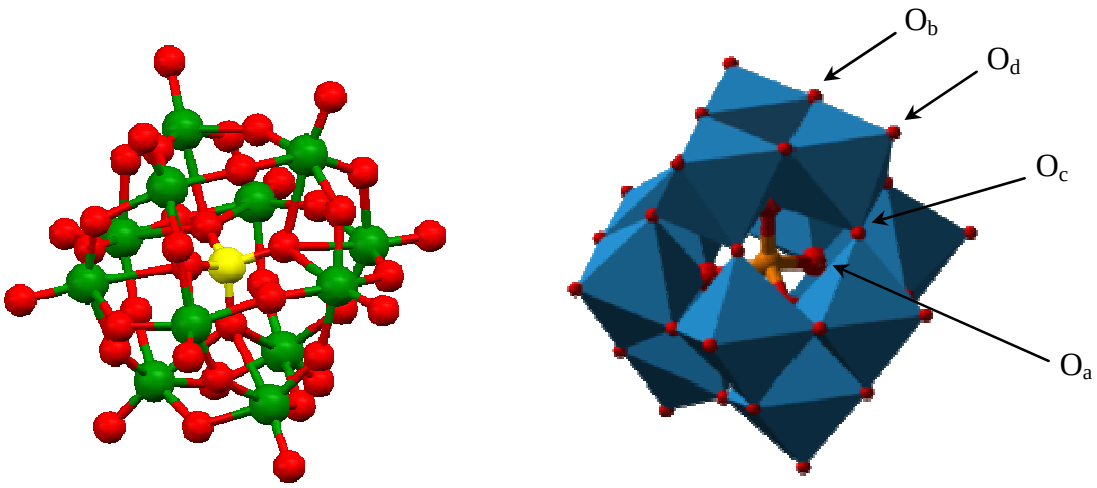

Figure 1.1. Representation of the α-Keggin polyanion structure. (a) Ball and stick structure (the central yellow ball represents the heteroatom X, the green balls are the addenda atoms and the red ones the oxygen atoms, (b) Polyhedral representation with indication of the different types of oxygen in the structure.

In the Keggin anion, the central XO_4 tetrahedron is surrounded by twelve MO_6 octahedra arranged in four groups of three edge-shared octahedra, M_3O_{13} [1]. Every M atom has one terminal oxygen atom. Each MO_6 group shares three oxygen atoms inside the M_3O_{13} group, and two other with the octahedra of neighbouring M_3O_{13} groups. Inside the same M_3O_{13} group, each metal M shares two oxygen atoms with the two neighbouring M and the third with the primary heteroatom X. The metal atom M is displaced outwards from the central position of the octahedra MO_6, in the direction of the unshared oxygen. As a result, four types of oxygen atoms in the structure can be identified (Fig. 1.1):

- ❖ O_a: oxygen shared between each three octahedra of M_3O_{13} group and with the XO_4 group
- ❖ O_b: oxygen shared between octahedra of the same M_3O_{13} group
- ❖ O_c: oxygen shared between octahedra of different M_3O_{13} groups
- ❖ O_d: unshared oxygen from the MO_6 group (terminal oxygen).

Although the polyhedral representation may suggest otherwise, the Keggin structure, like that of most polyanions, is a closed-pack arrangement of oxygen atoms [1,2,5]. Pope showed that based on metal atom displacement, polyanions can be divided

into two categories: type I, displacement towards one, always terminal, oxygen atom, and type II, towards two cis, usually but not always, terminal oxygen atoms [1]. The Keggin-type anions belong to the first category.

The formula of these Keggin polyanions, for M = W, is presented through this thesis by the abbreviation XW_{12} (where X = P^{V} and Si^{IV}).

The Keggin anions can present different geometric isomers, β, γ, δ and ε, which were proposed by Baker and Figgis (Fig. 1.2) and are pointed out as possible structures related with the Keggin anion (α isomer).

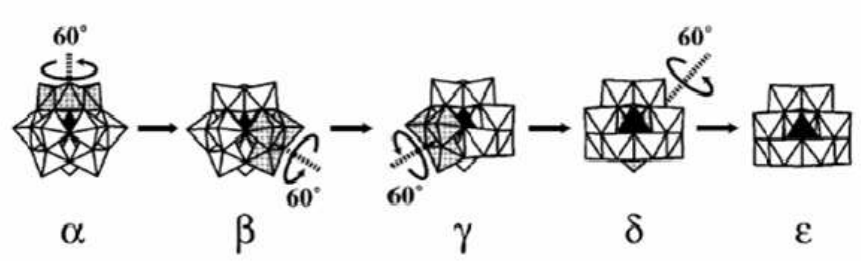

Figure 1.2. The five Baker-Figgis isomers of the Keggin structure (α isomer). In the β, γ, δ and ε structures, one, two, three and four M_3O_{13} groups have been rotated by 60°[1].

These isomers are related to the Keggin anion by the rotation of 60° of a M_3O_{13} group relatively to the α isomer. Thus, when one, two, three and four groups are moved, the geometric isomers, β, γ, δ and ε, are respectively obtained. In fact, although the δ and ε isomers have never been observed, the β isomer has been recorded for the polyanions XM_{12} (X = P, Si, Al and M = W, Mo) and the γ isomer for the $[SiW_{12}O_{40}]^{4-}$ anion [1,6-8].

For heteropolytungstates, in the β isomer, new corner-shared W-O-W linkages between the rotated group and the rest of the anion involve shorter W···W separations and more acute W-O-W angles than the α structure. Both of these features may account for the lower stability of β, compared with α, owing to increased coulombic repulsion (due to higher proximity of metal centres) and less favourable pπ-dπ interactions (responsible for the π W-O bond) [1,8,9]. In addition, an increase in the number of octahedra that are corner-shared can be observed in the sequence α → β → γ → δ → ε, which implies lower stability of the resulting isomers, due to higher coulombic repulsions [1].

All the polyanions prepared and studied in this work are α isomers and, for this reason, the prefix α is omitted throughout this thesis.

1.1.2. Derivatives of the Keggin anion and related heteropolyoxometalates

From the Keggin anion, lacunary species can be obtained by removal of one, or more, MO_x groups. In the mono-lacunary anions this corresponds to the elimination of a MO^{4+} group formed by any of the twelve addenda atoms (M) of the Keggin MX_{12} anion with its terminal oxygen.

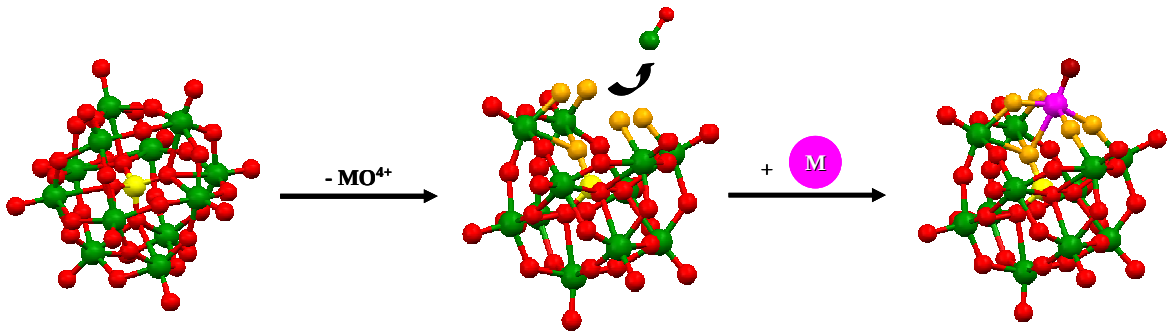

(a) (b) (c)

Figure 1.3. Polyhedral representation of the (a) α-Keggin anion, (b) lacunary anion and (c) mono substituted anion.

In this work, only the mono-lacunary species are used and are represented by the general formula $[XM_{11}O_{39}]^{(n+4)-}$. The formula of these polyanions for M = W is presented several times through this thesis by the abbreviation XW_{11} (where X = P^{V} and Si^{IV}). This lacunary species has a lacuna with five oxygen atoms that can potentially coordinate (Fig. 1.3b).

Other isomeric forms of the lacunary anion can be obtained by the removal of an MO^{4+} group of the β isomers of the Keggin anion. Only one α isomeric lacunary form results from the α structure. However, the β isomer can give rise to three isomeric structures: β_1, β_2 and β_3 that differ from each other in the position of the removed octahedra. The β_1 and β_2 correspond to the removal of an MO^{4+} in the adjacent group to the rotated W_3O_{13} and β_3 refers to the removal of an MO^{4+} group in the rotated W_3O_{13} group [1].

The lacunary anions react with transition metal ions to form complexes with global stoichiometry 1:1 (metal:ligand). In these 1:1 complexes, the five oxygen atoms of the lacunary anion may bind to the metal, with the polyanion ligand functioning, in general, in a pentadentate manner. The sixth coordination site on the metal in these complexes may be occupied by a variety of ligands, L, where the more common are H_2O, OH^-, O^{2-} or an

amine [1]. The general formula for the mono-substituted polyanion can therefore be written as $[XM_{11}M'(L)O_{39}]^{m-}$ (Fig. 1.3c). The metal cation M' must have appropriate dimensions to occupy the lacuna and to maintain the Keggin structure [1]. Larger ions, such as lanthanides Ln^{3+}, bind preferentially to two lacunary moieties (tetradentate), forming complexes with 1:2 (metal:ligand) stoichiometry.

There is a wide variety of mono-substituted heteropolyanions and in some cases the element that occupies the X and M' positions in the structure is the same (generally Fe^{III}, Co^{II}, Zn^{II}, Al^{III}, Ti^{IV} and Ga^{III}) [1,2,10]. Other polyanions can also be found in the literature with a large variety of metal ions in the lacuna, like V^{III}, $Cr^{III,V}$, $Mn^{II,III,IV}$, Fe^{II}, Co^{III}, $Ru^{II,III,IV}$, Ni^{II}, Cu^{II}, Rh^{III}, Pd^{II}, In^{III}, Tl^{III}, Ge^{IV}, $Sn^{II,IV}$, $Pb^{II,IV}$, $Sb^{III,V}$, Ir^{IV}, Os^{VI}, Tc^{V}, $Re^{V,VI,VII}$ [1,10,11].

From the Keggin anion, more than one MO^{4+} group can be removed. For example, the tri-lacunary $[XM_9O_{34}]^{(n+6)-}$ results from the removal of three MO^{4+} groups from three different octahedra and from some associated oxygen atoms (fragment $M_3O_6^{6+}$) of the Keggin anion. Several isomers are possible [1]. These tri-lacunary anions, like the mono-lacunary anion, are potentially coordinative, leading to several complexes with transition metal cations, particularly, tri-substituted anions and sandwich type anions such as, for example $[M'_4(H_2O)_2(PW_9O_{34})_2]^{10-}$ (Fig. 1.4a).

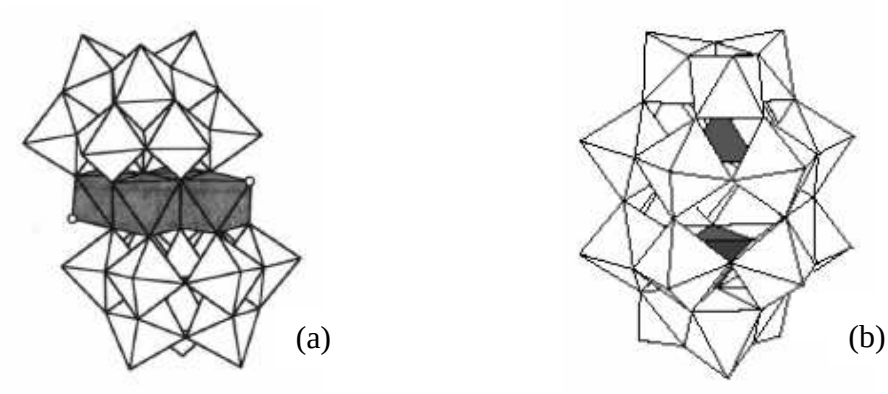

Figure 1.4. Polyhedral representation of the (a) sandwich anion, (b) Dawson anion.

Another type of polyanion related to the Keggin anions are the Dawson anions such as, for example $[P_2W_{18}O_{62}]^{6-}$ (Fig. 1.4b), that can be envisaged as resulting from two $[PM_9O_{34}]^{9-}$ units fused into a cluster [1]. These types of polyanion are related to mono- and tri- substituted Dawson anions or to sandwich type polyoxometalates, the parent anion being of a family of heteropolyanions identical to that of the Keggin anions. These types of polyanion were not prepared in this work but they are sometimes referred in order to compare their properties with the Keggin anions used.

1.1.3. Properties and applications

Interest in polyoxometalates is increasing worldwide due to their enormous variety of structures and to their unique set of properties. Their ionic size may be extremely high and they can reach molar masses of approximately 40000 g mol^{-1} [12].

These polyanions have different charges depending on the structure and of the type of elements present. In the crystals, the electrostatic attractions between the heteropolyanions and the counter-cations have low intensity, due to the increased distance of mass centres. The fact that the exteriors of the heteropolyanions consist largely, or entirely, of oxygen atoms that are very strongly polarized toward the addenda, and, therefore, not polarisable in other directions, creates a condition where one might expect van der Waals attractions between the complexes to be essentially nonexistent if they involve species having only exterior oxygen atoms that are adjacent to addenda atoms only [4]. These two reasons are responsible for low lattice energy of salts containing heteropolyanions. Given that the complex's solvation energy for a typical heteropolyanion is also low, solubility of the salts is essentially given by the type of counter-cation. Therefore, salts of K^+, Na^+, NH_4^+ are water soluble and tetra-butylammonium salts (TBA) are soluble in organic solvents [4].

For the Keggin-type anions and their derivatives, in particular for the polyoxotungstates, their interesting properties also include high thermal stability, rich redox chemistry, photochemical and catalytic features towards a number of industrially and biologically significant reactions [1,10,13-15]. These compounds are also resistant to oxidative degradation due to the fact that their fundamental elements (addenda atoms) are, generally, in their higher oxidation state [1,2,4,16]. These properties make them very attractive in many fields such as catalysis (including photocatalysis), where they can be used as acid or oxidative catalysts, in solution or in the solid state, with the possibility of being applied in heterogeneous or homogeneous catalysis [17]. Other important application fields are medicine (antitumoral, antiviral and even anti-HIV activity), electrochemistry, analytical chemistry, materials science and energy storage [1,10,13-15,18-26]. These fields are the focus of much current and undergoing research. Among their properties, the ability to undergo reversible multi-electron redox processes makes them very attractive for chemically modified electrodes and electrocatalysis [1,13,14].

The application of polyoxometalates in the fields mentioned above has been seen improved with increased interest due to the fact that their synthesis can be carried out in large quantities and using common reagents with fairly low-price.

1.2. Electrochemical behaviour of polyoxometalates

The study of the electrochemical behaviour of POMs was pioneered by the Souchay group in the early forties [1], having been retaken in the late sixties by other research groups [27-31]. Since then, the electrochemical study of these compounds has widened, especially in homogeneous electrolytic systems. Recently, POMs have been applied in the preparation of modified electrodes, in which the polyanions are deposited onto the electrode surface, changing their properties in this way [1,13,29].

A vast number of POMs can undergo a series of reversible reductions of one or two electrons. The occurrence of reversible reductions can be found for type I polyoxotungstates where the WO_6 octahedra have only one terminal oxygen atom and is associated with the fact that the electrons added to M enter an orbital that is predominantly non-bonding, with minimal subsequent bond length alteration. On the other hand, in the type II polyoxotungstates, the WO_6 octahedra have two terminal oxygen atoms and the added electrons enter an anti-bonding orbital, resulting in large structural changes [1,13].

The parent, lacunary and mono-substituted Keggin type anions are well studied in aqueous media, by electrochemical methods such as cyclic voltammetry [4,11,13,32]. Studies with parent and lacunary anions in organic media are also reported in the literature [33-36]. Nevertheless, studies in organic solution with mono-substituted Keggin type anions are scarce [37,38]. In aqueous solution, many studies show that pH has a large influence on the reduction of these polyanions. Generally, there is a linear dependence between the redox potentials attributed to the reduction of tungsten atoms or of the transition substituting metal and the pH value, resulting from protonation of the reduced species [12,31,32,39,40]. The slopes depend on the number of protons and electrons exchanged in the redox process. When the pH value of the solution is favourable to protonation, in general more electrons can be transferred to the POM structure [28].

Polyoxometalates can also contain, in their structure, different transition metal ions that have different reduction potentials, giving rise to different oxidation-reduction processes.

1.2.1. Keggin and lacunary anions

The number of electrons that can be transferred reversibly to the tungsten atoms in the structure of Keggin type POM is limited. In general, the polyanion structure is not significantly altered when the number of electrons is lower or equal to four [13]. In these conditions the "heteropoly blues" (constituted by W^{VI} and W^{V} [41]) are formed. When, six, or more than six electrons are added to the polyanion structure, brown polyanions are formed which present structural and electrochemical properties different from the non-reduced polyanions and from the heteropoly blues. In the brown polyanions (constituted by W^{VI} and W^{IV}), the electrons added to the structure through successive reductions are not delocalized in the structure, but originate $W^{IV}_3O_{13}$ groups [1,41].

The redox chemistry of some heteropolyanions, especially of the Keggin complexes, $[XW_{12}O_{40}]^{n-}$, have been studied in detail, knowing that these are reduced and re-oxidized with preservation of their structures [42]. Souchay was the first to study the reduction of Keggin anions $[PW_{12}O_{40}]^{3-}$, $[SiW_{12}O_{40}]^{4-}$, and $[H_2W_{12}O_{40}]^{6-}$, in aqueous media [43]. These redox processes are attributed to the reduction and oxidation of tungsten atoms [1].

The partial reduction of polyanions leads to the appearance of an intense blue colour, the heteropoly blues. These were first described by Berzelius and have been the base for many analytical procedures [44]. The blue coloration is due to the partial reduction of the addenda atoms (W, Mo) of the Keggin type polyanions and the intensity of the colour increases with increasing number of transferred electrons [28,29]. More specifically, the blue colour is attributed to intervalence electronic transition due to the existence of addenda atoms in the oxidation state +6 and +5. When an electron enters the polyanion structure, it is rapidly delocalized through the addenda atoms. When a second electron is added to the structure, it is also delocalized quickly between the different addenda atoms. However, the two electrons never meet each other in the same addenda atom. The electronic delocalization may, or may not, occur in the whole polyanion structure. However, ^{183}W NMR studies show that the delocalization of electrons, within the polyanion structure, occurs more easily between addenda atoms of the same W_3O_{13} group than between different groups, since the distance between tungsten atoms inside the same W_3O_{13} group is smaller than between different groups [41,45].

The formation of blue heteropolyanions involves a fast and reversible reduction process, the corresponding cyclic voltammograms being constituted by several reversible waves. The reduction process progress leads to the disappearance of the blue colour, but

the term blue heteropolyanion may indicate, for some authors, a reduced heteropolyanion, regardless of its colour [1].

Pope and Varga [13] studied the reduction of $[PW_{12}O_{40}]^{3-}$, $[SiW_{12}O_{40}]^{4-}$, $[FeW_{12}O_{40}]^{5-}$, $[CoW_{12}O_{40}]^{6-}$ and $[H_2W_{12}O_{40}]^{6-}$ by polarographic and potentiometric methods, showing that these anions can undergo two reductions of one electron, without decomposition. In acidic solutions, these anions can accept more than two electrons, these reductions being accompanied by protonation, keeping the overall ionic charge at -6. In neutral solutions (pH > 5) reduction proceeds until the charge of the reduced species is -8 [13]. In the presence of a higher concentration of protons in solution (lower pH), the two reductions of one electron are converted in one two electron reduction and it is accompanied by the addition of two protons to the polyanion structure. In aqueous solution where no protonation accompanies the reduction for $[XW_{12}O_{40}]^{n-}$ (X = P^{V}, Si^{IV}, Ge^{IV}, Fe^{III}, B^{III}, Co^{II}, H_2, Cu^{I}) the potentials of the two-electron reduction waves observed are linearly dependent on the ionic charge by -0.18V per unit charge [13,46]. A similar trend was also reported in organic solvents [47].

Similar studies were conducted in non aqueous solvents such as DMSO and DMF, for example, and it was observed that in these media, the formal potentials of the oxidation-reduction processes associated with the tungsten structure shift to more negative values. So, this way is more difficult to reduce these Keggin anions, as well as other polyanions, in non-aqueous solvents [13,48-50].

The relative stability of the reduced forms of the α and β isomers of the Keggin anions XW_{12}, has been studied in aqueous media and in acetonitrile solutions [13,32,49]. The α-$[SiW_{12}O_{40}]^{4-}$, when reduced, is more stable than the β-$[SiW_{12}O_{40}]^{4-}$ isomer, in aqueous media than in a non-aqueous solvent [13]. Himeno *et al.* studied the electrochemical behaviour of the α and β isomers of $[PW_{12}O_{40}]^{3-}$ in water/acetonitrile mixtures [49]. The electrochemical behaviour of these two isomers, only in acetonitrile, is very similar where a four-step one-electron reduction waves can be observed for both isomers. With the addition of CF_3SO_3H, the one-electron reduction waves were converted into two two-electron waves, followed by an ill-defined wave and the addition of water to the CH_3CN/CF_3SO_3H system caused the first two-electron wave to split into two one-electron waves [49].

The lacunary polyanions α-XW_{11} (X = Si, P and Ge) were studied in aqueous media. Toth and Anson reported that two reductions of two-electron were observed at more negative potentials than the corresponding Keggin anions, the reduction being accompanied by protonation processes [39]. The authors also refer that there is a partial

transformation of the α-$[SiW_{11}O_{39}]^{8-}$ into the β isomer. This isomer is reduced at more positive potentials than the α isomer and the appearance of a new anodic peak was identified as being due to the β isomer. The same behaviour was observed by other authors [32].

The lacunary polyoxotungstates XW_{11} (X = P, Si) have also been studied in acetonitrile solution and gave well-defined cyclic voltammograms with two and three one electron redox waves at negative potentials, respectively [37].

1.2.2. Mono-substituted Keggin anions

A large number of transition metal-substituted heteropolyanions have been reported. The introduction of different atoms in the structure is responsible for different electrochemical behaviour in comparison with the original Keggin and lacunary polyanions.

The metals incorporated in the heteropolyanions reside in an octahedral environment, with one coordination site occupied by a solvent molecule ($[XW_{11}M(L)O_{39}]^{m-}$). Because the heteropolyanions are, in most cases, studied in aqueous solution, the solvent molecule is a labile water molecule. In general, the aquametal (III) may be reducible to the aquametal (II) and oxidizable to the corresponding oxometal (IV), hydroxometal (IV), and oxometal (V) derivatives depending on the character of the incorporated metals [13].

The transition metal in the mono-substituted polyanions gives rise to a region of higher negative charge at the POM surface. This region in the polyanion structure of higher concentration of negative charge produces a repulsive effect towards electrons and this is the possible explanation for the greater difficulty of reduction of the tungsten atoms in the mono-substituted polyanions compared with the Keggin and lacunary polyanions [51].

The polyanions $[XW_{11}M(L)O_{39}]^{m-}$ are used in electrocatalysis and the transition metal (depending on the metal) is frequently referred to as the active centre of the catalytic reduction. The formal redox potential of the transition metal is influenced by several factors such as the nature of the ligands, L, the nature of the heteroatom, X and the charge of the polyanion [27].

The lacuna can also be filled by V^{V} or Mo^{VI} and then a mixed anion is formed. When one electron is added to the POM with different addenda atoms, this electron is initially transferred to the most reducible addenda atom. For example, $[XW_{11}VO_{40}]^{(n-1)-}$ and

$[XW_{11}MoO_{40}]^{n-}$ are reduced at a higher potential than $[XW_{12}O_{40}]^{n-}$, because V^{V} and Mo^{VI} are more difficult to oxidise than W^{VI} [13,27].

Anson's group [39,52,53] and Dong's group [54] have investigated the electrochemical behaviour of iron(III) substituted α-Keggin type polyanions, $[XW_{11}O_{39}Fe^{III}(H_2O)]^{n-}$, X = P, As with n = 4 and X = Si, Ge with n = 5 in aqueous solution. When an iron(III) centre is substituted into the vacant site of the lacunary ion, a new, reversible, one-electron wave appears at a more positive potential and the positions of the pair of two-electron waves of the lacunary ion are slightly shifted. The new, one-electron wave has been assigned to the reduction of the bound iron(III) to iron(II) and the two-electron waves at more negative potentials have been assigned to the reduction of tungsten centres in the polyoxometalate framework [39,52,53]. The reduction of this metallic centre is independent of pH, with no protonation of the reduced anion, $[XW_{11}Fe^{II}O_{39}]^{n-}$ [55]. The heteroatom nature has more influence on the reduction potential of Fe^{III} than in the W^{VI} reduction [39]. The iron-substituted heteropolyanions have large negative charge densities which would favour ion pairing with counter-cations or protons. Therefore, the formal potentials of reversible Fe(III/II) couples and the two ligand-centered two-electron reductions depend on both the pH and the countercation concentration because of competition between protonation and ion pairing [13]. Both reactions occur in order to diminish the negative charge of the reduced polyanions. In highly acidic medium, protonation occurs in overlap to the ion pairing, but the opposite happens in solutions with high pH values [39].

Polyanions mono-substituted by Co^{II} (X = P, Si, B and Zn) and by Co^{III} (X = Si and B) were also studied in aqueous media [32,56]. For the $[XW_{11}CoO_{39}]^{n-}$, with X = Si and P, two reversible, or quasi-reversible, two-electron waves corresponding to reduction of tungsten atoms being observed. When X = B, irreversible transformations take place, producing cyclic voltammograms without anodic counterparts. However, one two-electron reversible couple is observed if the potential scan is reversed at values less than -700 mV (at pH =2.2). No redox process occurring at the metal (Co) was observed [32].

Several polyanions mono-substituted by other metals were also studied in aqueous media: Mn^{III} (X = P, Si, B and Zn) [56-58], Ni^{II} (X = P, Si, B and Zn) [32,56], Cr^{III} (X = P, Si, B and Zn) [32,56,59], Cu^{II} (X = Zn) [56], Zn^{II} (X = Zn) [56], Pb^{II} (X = Si, P) [60].

Electrochemical studies in acetonitrile of $[XW_{11}M(H_2O)O_{39}]^{m-}$, X = P, Si, M^{II} = Co, Ni, M^{III} = Fe, Mn, can also be found in the literature [37].

1.3. Electrode modification using polyoxometalates

Polyoxometalates have gained particular attention due to their applications in many fields, resulting from their chemical, structural and electronic properties. Among these properties, the ability to undergo reversible multi-electron redox processes makes them very attractive for chemically modified electrodes and electrocatalysis [13,14]. The need to immobilize catalysts on surfaces, while maintaining, controlling and/or enhancing their beneficial properties, constitutes a challenge which has been receiving increasing attention over recent decades. The term chemically modified electrode was initially used in electrochemistry by Murray and its co-workers, to refer to electrodes with chemically active species immobilized on the surface of these devices [61,62]. Electrodes are usually chemically modified by one of four approaches [63]:

- **Chemisorption:** adsorption in which the forces involved are the valence forces of the same kind as those operating in the formation of the chemical compounds. The chemical film is strongly and, ideally, irreversibly adsorbed (chemisorbed) onto the electrode surface. This approach usually yields a monolayer (or less) coverage.
- **Covalent bonding:** linking agents, such as organosilanes, are used to covalently attach from one to several monomolecular layers of the chemical modifier to the electrode surface.
- **Polymer film coating:** electron conductive and nonconductive polymer films are held on the electrode surface by some combination of chemisorption and low solubility in the containing solution or by physical anchoring in a porous electrode. The polymer can be organic, organometallic or inorganic. It can already contain the desired chemical modifier or it is added to the polymer in a second, functionalizing step.
- **Composite:** the chemical modifier is simply mixed with an electrode matrix material, as in the case of an electron-transfer mediator combined with carbon particles (plus binder) of a carbon paste electrode.

Polymer film coated electrodes may be further subdivided by the process used to apply the film into dip-coating, solvent evaporation, spin coating, electrochemical deposition, electrochemical polymerization, radiofrequency polymerization and cross-linking [63].

A number of strategies have been developed to prepare chemically modified electrodes with a variety of POMs. Several groups have immobilized POMs using procedures such as electrochemical deposition [64,65], entrapment into polymeric matrices [64-68] and adsorption of a POM anion mono-layer from an aqueous solution

generally followed by the adsorption of a second layer of a counter-cation (e.g. $[NH_3(CH_2)_xNH_3]^{2+}$ or $[Os(bpy)_3]^{2+}$) [13,69,70]. This modification procedure, which is similar to a method reported by Kulesza and Faulkner [71,72], can be generalised for a larger variety of cations. Adsorption of a monolayer of POM creates a negative diffuse layer potential on the surface of the modified electrode due to the high negative charge of these anions. This negative excess charge can be used to adsorb cations more or less irreversibly by electrostatic interactions. Besides metal complexes like $[Os(bpy)_3]^{2+}$ and $[Ru(bpy)_3]^{2+}$normal metal cations can also be used. However, these electrodes often have a limited stability because electrode surfaces cannot be renewed in the case of leakage, contamination or passivation.

Other approaches have been the immobilization of organic–inorganic hybrids, e.g., POM salts of large organic cations incorporated into gel films on pyrolytic graphite [73] or surface deposition of POM salts onto carbon electrodes [74,75]. This latter procedure consists in the deposition of a small quantity of solution containing the POM over the electrode surface and subsequent solvent evaporation. The solvent evaporation may be at room temperature or under an air flux. The main advantage of this method relies on the fact that it is possible to know the quantity of POM on the electrode surface, from the solution concentration and the volume of the applied drop. However, the homogeneity of the deposit may differ.

Among the various types of chemically modified electrodes, these that have received particular attention in this thesis are carbon paste electrodes, and electrodes modified by electrochemical polymerization or by the layer-by-layer method. The use of Keggin-type polyoxometalates in these modifications will be discussed in the following sections.

1.3.1. Electrochemical polymerization

A polymeric film deposited on an electrode is a useful electron transfer mediator, and methods to assemble a monomer onto an electrode surface have been studied extensively. In electrochemical polymerization, a monomer in solution is oxidized, or reduced, to an active form that polymerizes and leads to the formation of a polymer film directly on the electrode surface. This can be achieved using cyclic voltammetry where an increase in the peak currents of the redox couple indicates film formation. The reaction products on the electrode are polymeric and insoluble in the solvent used. Unless the

polymer film is redox-active or conducting, electrode passivation occurs and further film growth is prevented [63].

An important and interesting possibility is a modified electrode containing hybrid organic–inorganic films that can have different properties, depending on the compounds used. In this section we will concentrate on organic–inorganic hybrid films based on conducting polymers (COP) and polyoxometalates.

A general approach for the introduction of a molecular species into a COP network takes advantage of the doping process itself. The doping of these polymers involves the introduction of holes (p-doped) or electrons (n-doped) into their conjugated chains. These processes take place with simultaneous incorporation of charge-balancing species into the structure, anions for the p-doped and cations for the n-doped [23]. It is commonly accepted that most polyoxometalates can be easily incorporated as dopants inside polymer matrixes [67,76]. Thus, by electropolymerization of the monomer unit, in the presence of the polyanion, a hybrid organic-inorganic material can be synthesized at the electrode surface. The vast majority of reports dealing with COP materials involve the study of p-doped polymers, most frequently polypyrrole (PPy), polyaniline (PAni), or polythiophene (PT) and their derivatives (Fig. 1.5) [23].

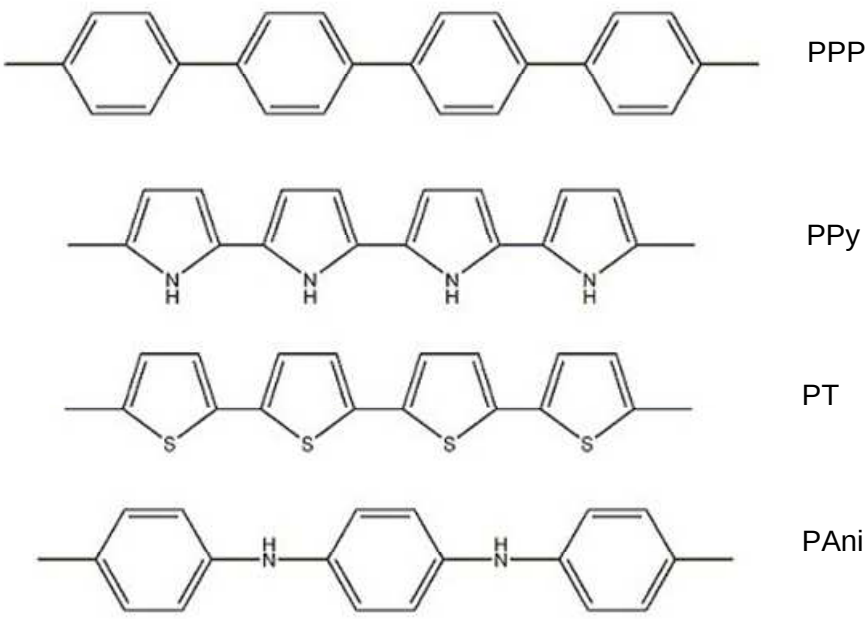

Figure 1.5. Structures of conducting polymers, from top to bottom: poly(para)phenylene, polypyrrole, polythiophene and polyaniline [77].

Amongst all of the known conducting polymers, polypyrrole is probably as the most investigated, with thousands of papers devoted to it. The mechanism of electrochemical pyrrole oligomerization is similar for the other conducting polymers [78] and will be described in more detail for the polythiophenes.

Polypyrrole itself is an electrochromic material and is also able to store electric charge. These properties have been extensively studied due to the many possibilities of applications. Specific hybrid materials formed by polypyrrole doped with polyoxometalates are expected to combine the redox properties of both of the two independent constituents. So far, several groups have prepared modified electrodes using POMs and polypyrrole [76,79-90]. In fact, these hybrids have already been employed in many electrocatalytic reactions [79-81], and their possibilities in the field of charge storage devices have also been pointed out [82,83,90].

Gomez-Romero *et al.* have prepared films combining Keggin-type $[PMo_{12}O_{40}]^{3-}$ with polypyrrole [83]. Otero's group studied the electrosynthesis of hybrid films of polypyrrole/$PW_{12}O_{40}^{3-}$ and the influence of the conditions of synthesis on the efficiency of the charge consumed during polymerization and on the specific charge stored in each electrogenerated film [84,85]. Bidan *et al.* [76] studied the electrosynthesis of the material on glassy carbon electrodes by anodic oxidation of the monomer under consecutive potential cycling, stating that the electrochemical behaviour of the heteropolyanions ($[SiW_{12}O_{40}]^{4-}$ and $[PW_{12}O_{40}]^{3-}$) inside the hybrid is different from that shown in bulk solutions. Dong's group studied the electrosynthesis of phosphomolybdate anion doped polypyrrole [80]. The growth of the hybrid material was followed through the evolution of the current peaks, or corresponding charge, in consecutive voltammograms [81,82].

In polyaniline (PAni) the conductivity results from a process of partial oxidation or reduction. Polyaniline compounds can be designed to achieve the required conductivity for a given application, the resultant blends being as conductive as silicon and germanium or as insulating as glass [91]. Gomez-Romero *et al.* studied the electropolymerization of polyaniline and the Keggin-type $[PMo_{12}O_{40}]^{3-}$ [92]. Others have also used the anions $[PMo_{12}O_{40}]^{3-}$ and $[PW_{12}O_{40}]^{3-}$ to prepare modified electrodes with polyaniline [93-97]. Lekha *et al.* were interested in studying the conduction mechanism using impedance spectroscopy because PAni yields a complicated structure, being a highly disordered material when doped with POMs. Comparison of the behaviour of the polyoxometalates in aqueous solution with their behaviour after entrapment in polymer matrices by electrodeposition has also been reported [98]. Fabre and Bidan studied the electrosynthesis of different electronic conducting polymer films of polyaniline,

polythiophene and poly(3-methylthiophene) doped with an iron-substituted heteropolytungstate [99]. This was one of the first attempts to use the metal substituted anions.

Polythiophenes (PTs) (Fig. 1.6) are one of the most important classes of conjugated polymers, with a wide range of applications such as conducting films, electrochromic, and field-effect transistors, which have been the subject of a number of publications [100,101]. They result from the polymerization of thiophenes that become conducting materials when electrons are added or removed from the conjugated π-orbitals via doping, done by intentionally adding elemental impurities [102].

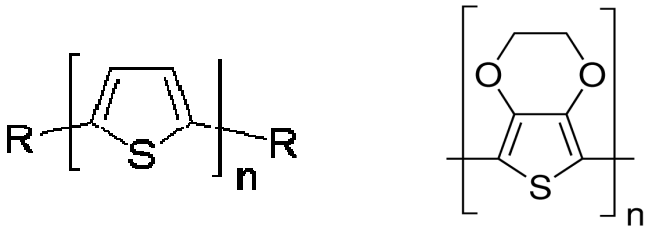

Figure 1.6. Examples of polythiophenes: (a) poly(thiophene-2,5-diyl), PTh and (b) poly(ethylenedioxythiophene), PEDOT.

Despite the large amount of work devoted to electrogenerated PTs, the mechanism of the electropolymerization of thiophene has been little considered. This probably arises from the fact that it is generally admitted that the electropolymerization of aromatic compounds occurs via a unique mechanism which has been more extensively analyzed using pyrrole as a model compound [103,104]. An important aspect of the electropolymerization reaction is that it proceeds with a specific electrochemical stoichiometry. The oxidation of the monomer requires 2 electrons/molecule while the excess of charge corresponds to the reversible oxidation or doping of the polymer.

Figure 1.7 shows, as an example, the mechanism of electropolymerization of five-member ring heterocycles [105]. The first electrochemical step (E) consists in the oxidation of the monomer to its radical cation. Since the electron-transfer reaction is much faster than diffusion of the monomer from the bulk solution, it follows that a high concentration of radicals is continuously maintained near the electrode surface. The second step involves the coupling of two radicals to produce a dihydro dimer dication which leads to a dimer after loss of two protons and rearomatization. This rearomatization constitutes the driving force of the chemical step (C). Due to the applied potential, the dimer, which is more easily oxidized than the monomer, loses an electron to give its

radical form and undergoes further coupling with a monomer radical. Electropolymerization then proceeds through successive electrochemical and chemical steps according to a general E(CE), scheme, until the oligomer becomes insoluble in the electrolytic medium and precipitates onto the electrode surface. It is firmly established that the oxidation of the monomer leads to the radical cation and that the electropolymerization process is not diffusion-limited. The initial deposition step and the propagation process during electropolymerization are less clearly understood and are still a matter of controversy.

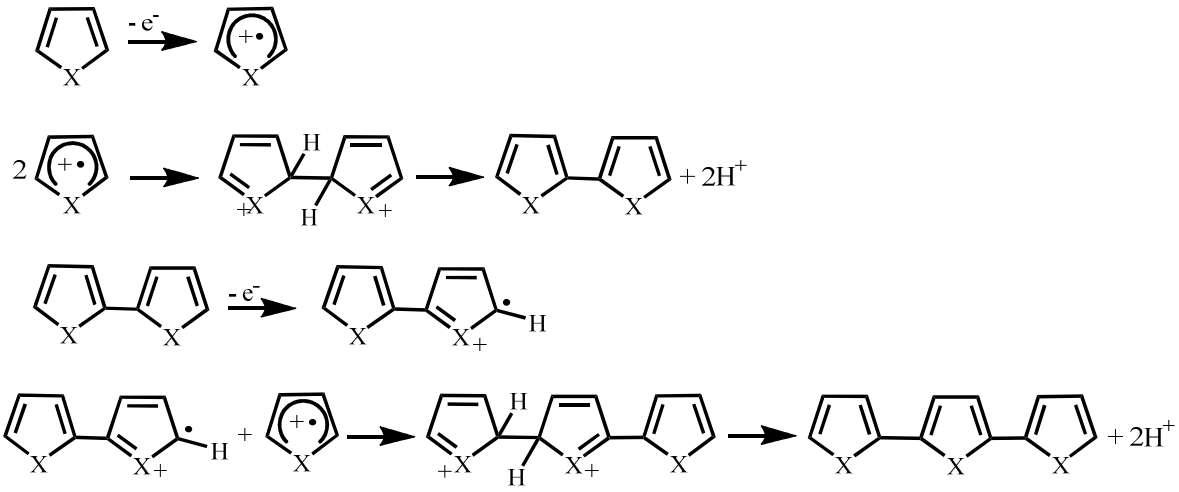

Figure 1.7. Mechanism of electropolymerization of heterocycles [adapted from 105].

Polythiophenes and their derivatives have been less used in the field of electropolymerization with polyoxometalates than polyaniline and polypyrrole. However, some examples can still be found in the literature. Most of papers published concerning the modification of electrodes by electrodeposition of polythiophenes with incorporation of polyoxometalates belong to Bidan and collaborators [106-111]. In their studies the Keggin-type $[PMo_{12}O_{40}]^{3-}$, $[PW_{12}O_{40}]^{3-}$ and $[SiW_{12}O_{40}]^{4-}$ were used [106-109], as well as the Dawson structure $[P_2W_{18}O_{62}]^{6-}$ [110,111]. Out of many derivatives of polythiophenes, poly(ethylenedioxythiophene), PEDOT, has recently been of interest as a particularly stable, highly conductive and electroactive polymer. Recent reports are consistent with the view that PEDOT shows promise for the design of novel composite materials with improved stability [112,113] for electrode modification. Examples with this polymer will be discussed in Chapter 6.

1.3.2. Layer-by-layer Method

In recent years, the construction of self-assembled ultrathin films has attracted considerable attention due to their potential applications in molecular and nano-devices. Layer-by-layer (LbL) self-assembly has proved to be a promising method for the fabrication of ultrathin films. It is based on the alternate adsorption on the substrate surface of oppositely charged species from dilute solutions, and film formation is attributed primarily to electrostatic interactions and van der Waals forces [114-117]. Consecutive cycles with alternating adsorption of oppositely charged species result in stepwise growth of films as illustrated in Fig. 1.8.

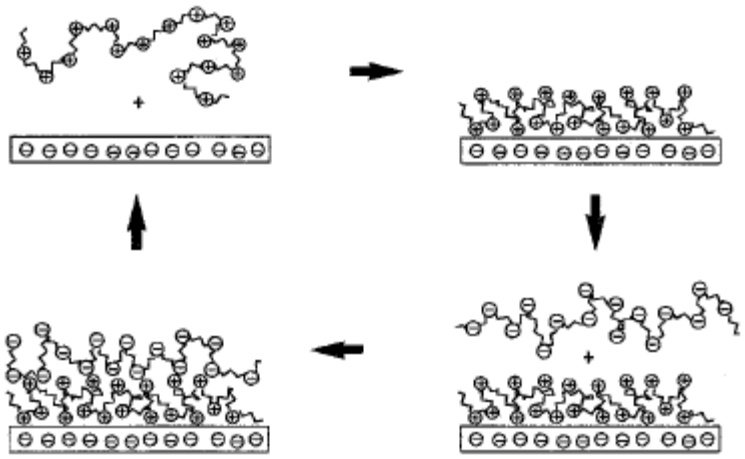

Figure 1.8. Scheme of the electrostatic layer-by-layer self-assembly of oppositely charged polyelectrolytes [116].

Combinations of cationic and anionic polyelectrolytes, or of these with smaller ionic species, have been reported. Given the large number of materials which can be easily incorporated into multilayer films, layer-by-layer deposition is a rather general approach for the fabrication of complex surface coatings [116].

Since the layer-by-layer method is based on the attractive interaction of complementary charges, the compound used needs to have a minimal number of charged groups, below which the method does not work. The presence of large hydrophobic fragments in the polyelectrolytes reduces the charge density, and may sterically hamper the necessary ion-ion interactions which may be disadvantageous [18,116]. This

interpretation was linked to the idea of a critical minimum value of charge density for LbL, which is necessary to enable successful film growth. Experiments with weak polyelectrolytes, in the form of statistical copolymers of charged and non-charged repeat units, supported this idea [118-120].

However, this concept of a minimum value of charge density is oversimplified, since some polymers with an unexpectedly low charge density have been successfully grown in multilayer films by layer-by-layer [121,122]. Fisher *et al.* suggested that successful deposition requires appropriate matching of the charge density of the polyelectrolyte pair used, rather than a minimum charge density [123], although this does not necessary exclude film formation [123].

There is a large number of polyelectrolytes that are used for film formation using the layer-by-layer process. The most used, commercially available, ones are presented in Fig. 1.9. From these, the best studied system is by far the poly(allylamine)(c)/poly(styrene sulfonate)(e) pair.

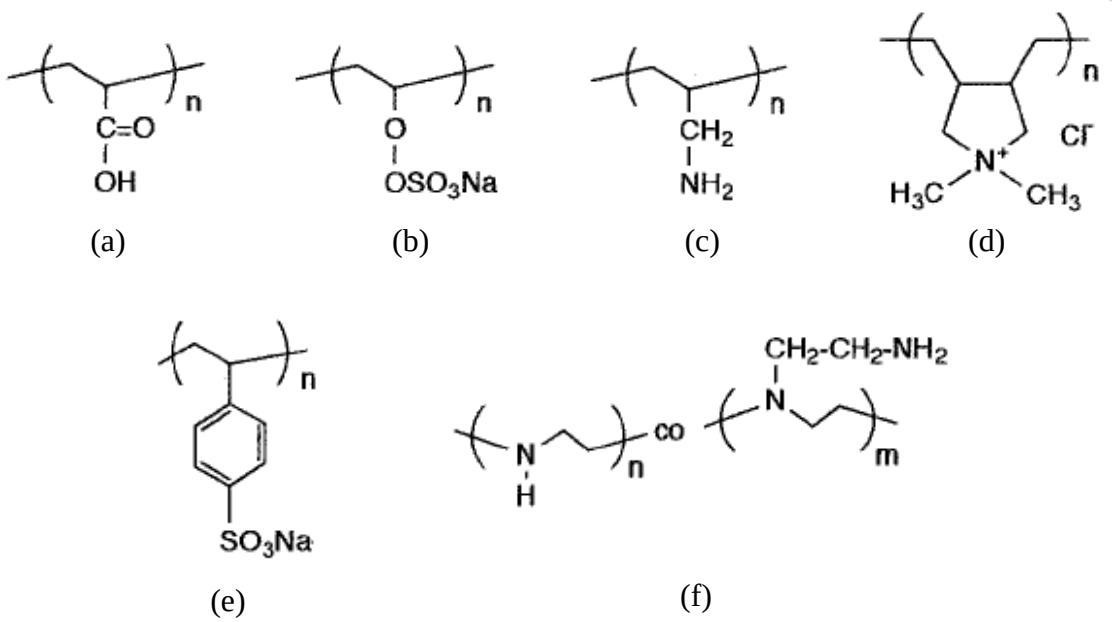

Figure 1.9. Examples of standard polyelectrolytes used in layer-by-layer method: (a) poly(acrylic acid), (b) poly(vinylsulfate), (c) poly(allylamine), (d) poly(diallyldimethylammonium chloride), (e) poly(styrene sulfonate) and (f) poly(ethyleneimine).

An important feature of the layer-by-layer method is that different substrates can be used. Usually, the choice of substrate depends on the analytical methods that will be used. Glass, quartz, silicon wafers, gold coated supports and glassy carbon are materials used most frequently. Due to their transparency, ITO, glass and quartz are often applied

for characterization by UV-Visible and Infrared spectroscopy. Gold-coated surfaces and glassy carbon enable electrochemical studies to be carried out [116].

This method is of great versatility due to the broad processing window and to the many control parameters that can be changed such as concentration, adsorption time, ionic strength, temperature, pH, among others. It also provides thickness control at the nanometer level, can be easily adapted for automated fabrication and permits co-assembly with different functional components [18,124].

Owing to its numerous advantages, the layer-by-layer approach has been successfully utilized to fabricate POM-containing multilayer films consisting of synthesized or natural polyelectrolytes. For example, thin films based on large polyoxometalates, such as $[Co_4(H_2O)_2P_4W_{30}O_{112}]^{16-}$, $[Eu(H_2O)P_5W_{30}O_{110}]^{12-}$ and $[Na(H_2O)P_5W_{30}O_{110}]^{14-}$ [124], have been successfully fabricated on ITO electrodes, using poly(ethylenimine) (positively charged) and poly(styrenesulfonate) (negatively charged), as the anchorage layers, and poly(allylamine hydrochloride) as the source of polycations.

Keggin–type polyoxometalates were also used for the preparation of ultrathin multilayer films with polyelectrolytes on the surface of different types of electrodes. Early studies have been reviewed [13]. Several studies use the parent Keggin silicotungstate $[SiW_{12}O_{40}]^{4-}$ as the anion and, for example, polyaniline [125], chitosan [126], or poly(diallyldimethylammonium chloride) [127] as the counter cation source. Other Keggin-type and related polyoxometalates such as $[Eu(SiW_{11}O_{39})_2]^{13-}$, $[SiMo_{11}VO_{40}]^{5-}$ and $[ZnW_{11}M(H_2O)O_{39}]^{n-}$ (M = Cr, Mn, Fe, Co, Ni, Cu or Zn) were successfully immobilized on a 4-aminobenzoic acid modified glassy carbon electrode, through layer-by-layer assembly with a quaternized poly(4-vinylpyridine) partially complexed with $[Os(bpy)_2Cl]^{1+/2+}$ (QPVP-Os) as counterion [128-131]. Poly(ethylenimine) has also been used as the polycation source [132,133] this will be discussed in Chapter 5.

The use of polymeric cations is not necessary for growing films with Keggin anions. For example, complex films based on the heteropolyacids $H_3PW_{12}O_{40}$, $H_3PMo_{12}O_{40}$ or $H_4SiMo_{12}O_{40}$, have been built onto glassy carbon electrodes with methyl viologen and with the cationic meso-tetra(4N-methylpyridyl porphyrin) [134]. This cation was also used to immobilize the Keggin-type polyoxometalates $[SiW_{12}O_{40}]^{4-}$, $[EuPW_{11}O_{39}]^{4-}$ [135] and $[SiW_{11}Fe^{III}(H_2O)O_{39}]^{5-}$ [136]. There are only a few examples of use of transition metal mono-substituted Keggin polyoxotungstate anions in films prepared by the layer-by-layer self-assembly method [131,136].

1.3.3. Carbon Paste Electrodes

Carbon paste electrodes (CPEs) are composite electrodes because they result from the combination of two or more materials. They consist of a mixture of, at least, an electrically conducting carbon powder and an organic liquid (binder). A portion of this paste is then packed into the cavity of the carbon paste electrode body and the surface smoothed on a weighing paper. They have been widely applied in electrochemistry owing to their many advantages: inexpensive, easy to prepare, easy to handle, have low background currents and their surface renewal is rapid [137].

Among the advantageous properties and characteristics listed above, CPEs allow the preparation of electrodes with a desired composition and, hence, with pre-determined properties. The choice of carbon paste components (carbon powder and pasting liquid), their ratio in the mixture and the way in which the CPEs are prepared (homogenization of the paste, packing of the paste in the electrode body, etc.) are important aspects that determine the properties, characteristics and behaviour of CPEs [138]. Generally, the organic liquid used as the binder component of pastes is a non-conductive mineral oil, such as nujol or liquid paraffin. Owing to their chemical inertness, as well as good adhesive ability, these viscous liquids have been widely used in the process of fabricating traditional CPEs. However, since these binders are not conductive which, to some extent, weakens the electrochemical response, other pasting binders have been used to improve the carbon paste electrode response. Much has been published about CPEs using ionic liquids mixed with organic binders, or as their substitutes [139-141]. Other carbon composite electrodes based on graphite and cellulose acetate [142], or graphite and poly(vinyl chloride) [143,144], have also been developed. Graphite-epoxy composite electrodes have been used as substrates for electrochemical biosensors [145].

Four preparative methods can be used to modify the surface or composition of the CPE, namely adsorption, covalent binding, dissolution and direct mixing, among which direct mixing is the most common [137]. In general, the modifiers used with direct mixing should be insoluble in the analyte solution or they should, at least, strongly adsorb to the paste components in order to avoid dissolution of the modifier from the electrode surface during measurements. Therefore, for studies in aqueous solutions, the traditional salts of POMs and alkali metals, like Na^+ or K^+, cannot be directly used as bulk modifiers of CPEs owing to their good solubility in water. However, inorganic–organic hybrids of POMs such as tetra-butylammonium (TBA) salts of the lacunary and transition-metal monosubstituted Keggin-type anions are insoluble in aqueous solutions [11].

Several research groups have devoted their studies to the preparation of carbon paste electrodes using polyoxometalates. Most work published in the literature concerns the parent Keggin anions [88,146-152]. Wang's group developed several different CPEs using the Keggin type $[PMo_{12}O_{40}]^{3-}$ and $[SiMo_{12}O_{40}]^{4-}$ [88,150-152]. Some were prepared just by direct mixing of POM with the graphite powder. However, they also developed PMo_{12}-doped conducting PPy composite material bulk-modified CPEs [88], and CPEs with hybrid nanoparticles [152]. Other authors describe the fabrication of non-conventional CPEs. Li *et al.* developed CPEs containing Keggin type $[PMo_{12}O_{40}]^{3-}$ anions encapsulated in modified mesoporous MCM-41 molecular sieves [148]. Liang *et al.* reported a PMo_{12} bacterial cellulose nanofiber-based CPE [153]. In the literature several papers concerning CPEs with POMs can also be found where organic binders have been substituted by other pasting binders such as ionic liquids, to improve the carbon paste electrode response [141,154].

The preparation of CPEs using mono-substituted polyoxometalates is less common and only a few are available in the literature. Hamidi *et al.* reported the preparation of CPEs with $PW_{11}Fe$ supported on amorphous silica, organofunctionalized with 3-aminopropyl(triethoxy)silane (APS) [155]. Other authors have used the mono-substituted $PMo_{11}M'$ with M' = Co and Zn [38] and $SiW_{11}Co$ [156].

1.4. Electrochemical techniques

1.4.1. Cyclic voltammetry

Cyclic voltammetry is an effective, versatile technique which allows the characterization of electroactive compounds, i.e., that can be oxidized and/or reduced, and studying the reversibility of the oxidation and/or reduction [157]. It also allows evaluating the presence of chemical steps associated with electron transfer, verifying the occurrence of adsorption of reagents or of products on the electrode surface.

This technique consists in applying a potential sweep to the working electrode, within limits E_{min} and E_{max}. The initial potential, E_i, and final potential, E_f, may or may not be the same as E_{min} or E_{max}, and the initial sweep can be in the positive direction (to cause an oxidation) or negative direction (to cause a reduction).

The response, current versus potential is called a cyclic voltammogram. Figure 1.10 shows a typical cyclic voltammogram of a reversible process and the characteristic parameters that can be easily obtained graphically.

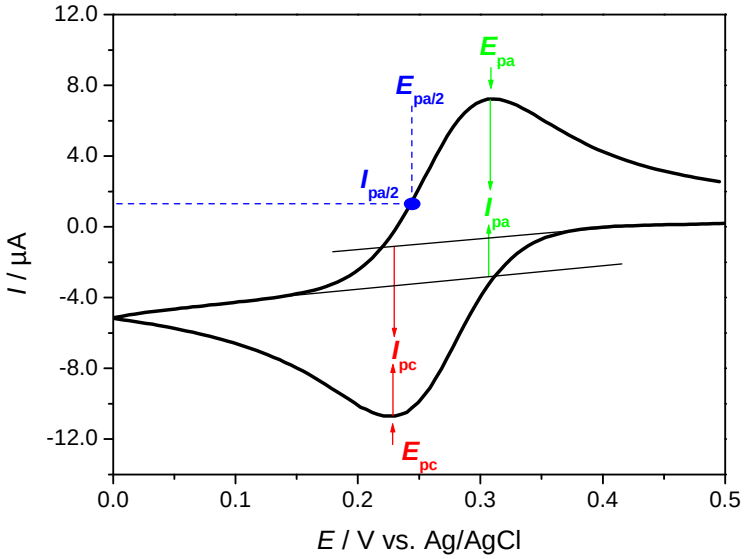

Figure 1.10. Cyclic voltammogram for a reversible system: 1 mM $K_3[Fe(CN)_6]$ + 1 M KCl, scan rate 20 mV s^{-1}.

In the cyclic voltammetry of reversible reactions, i. e. those with fast electrode kinetics relative to the time-scale of the sweep, the product of the initial oxidation or reduction is then reduced or oxidised, respectively, on reversing the scan direction. Theoretical analysis of the wave shape leads to following equation for the peak current, exemplified for an oxidation (Randles-Sevcik equation) [158,159]:

$$I_{pa} = 2.69 \times 10^5 \, n^{3/2} \, A \, D_R^{1/2} \, [R]_\infty \, \nu^{1/2}$$

where n is the number of electrons involved in the process, A is the electrode surface area (cm^2), D_R the diffusion coefficient (cm^2 s^{-1}), $[R]_\infty$ the bulk concentration of species (mol cm^{-3}), ν is the scan rate (V s^{-1}) and I_{pa} the anodic peak current (A).

It must be emphasised that a reversible cyclic voltammogram can only be observed if both O and R ($O + ne^- \rightarrow R$) are stable and the kinetics of the electron transfer process are fast, so that at all potentials and potential scan rates the electron transfer process on

the surface is in equilibrium so that surface concentrations follow the Nernst equation [160].

The information obtained from previous equation is, generally, presented in the form of a diagnostic test for cyclic voltammograms of reversible processes [158-160]:

- $I_p \propto \nu^{1/2}$
- E_p independent of ν
- $|E_p - E_{p/2}| = 56.6 / n$ (mV)
- $|\Delta E_p| = |E_{pa} - E_{pc}| = 57.0 / n$ (mV)
- $|I_{pa} / I_{pc}| = 1$

For a completely irreversible reaction only the oxidation and reduction corresponding to the initial sweep direction appears, since re-reduction or re-oxidation, respectively, cannot occur, i.e. there is no reverse peak [159]. However the majority of redox couples fall between the two extremes and exhibit quasi-reversible behaviour. This means that the reverse peak appears but is smaller than the forward peak [158]. For electrochemically quasi-reversible reactions, the surface concentrations are controlled both by kinetics and diffusion. The peaks separation (ΔE_p) increases when scan rate increases and smaller currents are observed, but peak current continues to be proportional to $v^{1/2}$.

If the reagent or the product of an electrode reaction is adsorbed strongly or weakly at the electrode, there is a change in the shape of the cyclic voltammogram [158,159]. The features exhibited by a cyclic voltammogram of adsorbed species on a surface differ from the typical voltammogram obtained for species in solution. This occurs since the mass transfer component of the current can be disregarded due to adsorption of the electroactive species at the electrode surface. If the electron transfer is reversible, symmetric cyclic voltammograms can be obtained due to the fixed amount of reactant adsorbed on the surface [157]. In the case of adsorbed species, ΔE_p tends to zero for reversible reactions and I_p is directly proportional to ν [157].

1.4.2. Electrochemical impedance spectroscopy

Electrochemical impedance spectroscopy (EIS) can be considered nowadays as a key technique for characterisation of electrochemical systems. It provides a global vision

of the electrical features of the electrode/solution interface. Analysis of the system response contains information about the interface, its structure and reactions taking place and this information is of great use in electrochemistry.

From the theoretical point of view, impedance is the most complete parameter that can be measured in an electrochemical system since if it is measured throughout an infinite range of frequencies, it contains all the information that can be obtained about the system through purely electric means [161]. The power of EIS resides in the fact that, being considered a stationary state technique, it allows the study of processes with time constants that vary throughout several orders of magnitude. Its stationary character permits that each measurement is the result of an average of values, obtaining this way high levels of precision, while the large range of frequencies of the instrument makes possible the study of a wide range of interfacial processes [161].

The principle of this technique consists in applying a small perturbation to the system. A sinusoidal variation of potential of small amplitude is superimposed on an applied fixed potential, while in the methods based on linear potential sweep, the system is disturbed far from equilibrium. The fact that the perturbation is small is advantageous in terms of the mathematical equation resolution because it is possible to use limiting forms of these equations, that are normally linear, besides the fact that it allows the investigation of electrochemical phenomena close to equilibrium and over a wide range of frequencies. Generally the response to the applied perturbation is sinusoidal and may differ in phase and amplitude from the applied signal. The measurement of phase difference and amplitude (i.e. impedance) allows the analysis of electrode processes in relation to the contributions of diffusion, kinetics, double layer, amongst others [159].

Electrochemical impedance spectroscopy results can be analysed by two distinct approaches. The first consists in developing mathematical methods based on the kinetics of heterogeneous reactions involved and the second uses the concept of equivalent electrical circuit [162], based on the fact that, in principle, every electrochemical cell can be represented by an electrical model.

For a simple electrode process, commonly used combinations for faradaic reactions include a component representing the transport by diffusion, a component representing the kinetics (purely resistive) and another component representing the interfacial region/double layer (capacitive). Considering the application of a sinusoidal signal:

$$E(t) = E_0 \sin(\omega t)$$

where ω represents the perturbation frequency (rad s^{-1}), the response is:

$$I(t) = \frac{E_0}{|Z|}\sin(\omega t + \varphi)$$

where φ is the phase angle between the perturbation and the response. The proportionality factor, Z, between the perturbation and the response is the electrical impedance. The impedance is characterized by the amplitude and phase angle and can be described as follows:

$$Z = Z' + iZ'' \qquad Z' = (E_0/I_0)\cos\varphi \qquad Z'' = (E_0/I_0)\sin\varphi$$

So:

$$\left\{(Z')^2 + (Z'')^2\right\}^{1/2} = |Z| = E_0/I_0$$

This way, any electrochemical cell can be represented in terms of an equivalent electrical circuit, [159] e.g. a Randles circuit (Fig. 1.11), which includes the following parameters: a cell resistance R_Ω (resistance of solution, electrode materials, electrical leads etc.), a double layer capacitance C_d and the impedance of the faradaic process Z_f.

The impedance Z_f can be subdivided in two equivalent ways:

1. A resistance, R_s, in series with a pseudo capacitance, C_s.
2. A charge transfer resistance, R_{ct}, and an impedance measuring the difficulty of mass transfer of electroactive species, called the Warburg impedance, Z_w.

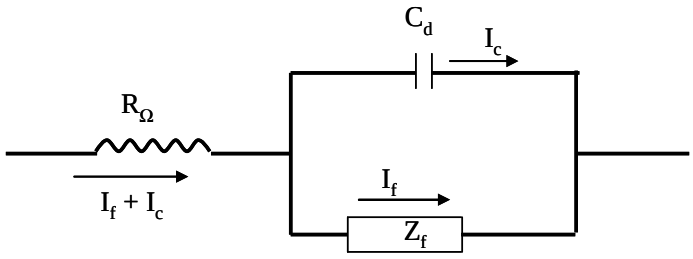

Figure 1.11. Equivalent electrical circuit of an electrochemical cell for a simple electrode process [159].

The most often used representation of the impedance spectrum is complex plane (Nyquist) plots, in which the imaginary part of impedance (Z'') is plotted vs. the real part

(Z'), for each frequency. Another representation is the Bode plots (log |*Z*| and *φ vs*. Log (*ω*)) [163].

Figure 1.12 shows a complete Randles type equivalent circuit of a simple charge transfer reaction.

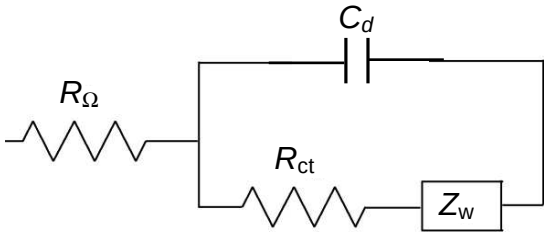

Figure 1.12. Complete Randles type equivalent electric circuit. The circuit comprises a cell resistance, R_Ω, in series with a parallel combination of a double layer capacity, C_d, and a charge transfer resistance, R_{ct}, together with a Warburg impedance, Z_W.

Separating the components in and out of phase, it can be shown that:

$$Z' = R_\Omega + \frac{R_{ct} + \sigma\omega^{-1/2}}{\left(\sigma\omega^{1/2}C_d + 1\right)^2 + \omega^2 C_d^2 \left(R_{ct} + \sigma\omega^{-1/2}\right)^2}$$

$$-Z'' = \frac{\omega C_d \left(R_{ct} + \sigma\omega^{-1/2}\right)^2 + \sigma^2 C_d + \sigma\omega^{-1/2}}{\left(\sigma\omega^{1/2}C_d + 1\right)^2 + \omega^2 C_d^2 \left(R_{ct} + \sigma\omega^{-1/2}\right)^2}$$

These components are represented in a plot in the complex plane (Fig. 1.13) called the Sluyters or Cole-Cole plot. Two limiting forms of these equations [159] are:

1. When $\omega \rightarrow 0$:

$$Z' = R_\Omega + R_{ct} + \sigma\omega^{-1/2}$$

$$Z'' = -\sigma\omega^{-1/2} - 2\sigma^2 C_d$$

This low frequency limit is a straight line with a slope of 1 that extrapolated to the real axis, gives an intercept of (R_Ω + R_{ct} - $2\sigma^2 C_d$). The line corresponds to a reaction controlled only by diffusion, and the impedance is the open circuit, infinite diffusion Warburg impedance, the phase angle being $\pi/4$.

2. When $\omega \rightarrow \infty$ (kinetic control):

In the high frequency limit the control is purely kinetic and $R_{ct} >> Z_w$. The electric analogy is a parallel combination *RC*. Eliminating the diffusion terms:

$$Z' = R_\Omega + \frac{R_{ct}}{1 + \omega^2 C_d^2 R_{ct}^2}$$

$$Z'' = -\frac{\omega C_d R_{ct}^2}{1 + \omega^2 C_d^2 R_{ct}^2}$$

The real component of impedance tends to at high frequencies R_Ω, and to $R_\Omega + R_{ct}$ at low frequencies. Eliminating the frequency parameter from the previous expressions the relationship between the imaginary and real components of impedance, can be obtained:

$$\left(Z' - R_\Omega - \frac{R_{ct}}{2}\right)^2 + (Z'')^2 = \left(\frac{R_{ct}}{2}\right)^2$$

This expression is the equation of a circle of radius $R_{ct}/2$ with intercepts on the Z' axis of R_Ω ($\omega \rightarrow \infty$) and of $R_\Omega + R_{ct}$ ($\omega \rightarrow 0$).

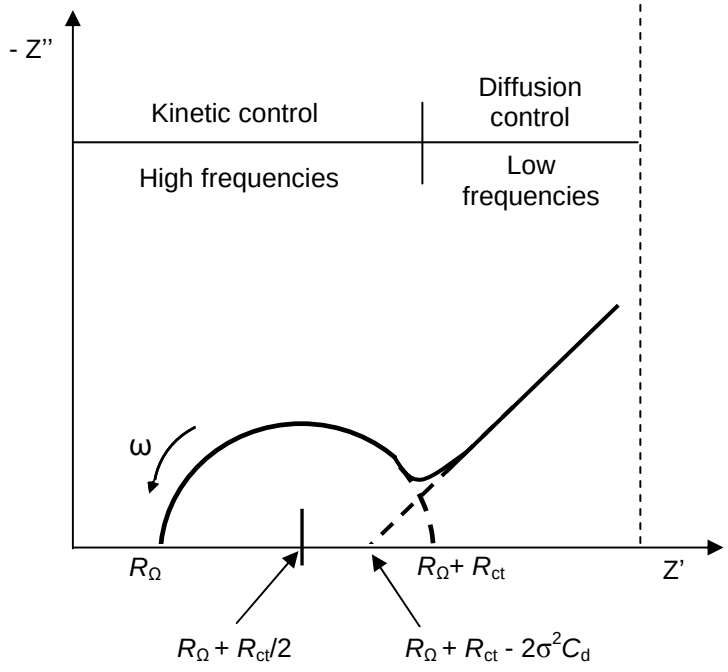

Figure 1.13. Complex plane impedance plot for a simple electrochemical system: O + ne^- → R.

Real systems, using solid electrodes, rarely conform to this ideal behaviour. The roughness and the porosity, usually encountered when using solid electrodes, give rise to changes in behaviour that can be modelled using the so-called constant phase element (CPE). In such systems, for electron transfer reactions the CPE often manifests itself as a non-ideal capacitor; in the case of a blocked interface this element is described by:

$$Q_{CPE} = -1/(i\omega C)^{n}$$

It has been demonstrated that at the limit of porous electrodes, the CPE exponent is n = 0.5 while for perfect uniform electrode surface it is n = 1 [159].

1.5. Scope of the work

The work presented in this thesis had as main goal the development of new modified electrodes incorporating polyoxotungstates through different methodologies.

Chapter 2 concerns the synthesis of different types of Keggin type polyoxotungstates which include the potassium (water soluble) and tetra-butylammonium salts of the lacunary anions, $[XW_{11}O_{39}]^{(n+4)-}$ (where X = P^{V} and Si^{IV}), and of the metal substituted $[XW_{11}M'(L)O_{39}]^{m-}$ (where M = Fe, Co and Mn). All prepared compounds were characterized by thermal and elemental analysis, thermogravimetry, and infrared absortion spectroscopy.

Chapter 3 describes the functionalisation of glassy carbon electrodes by deposition of tetra-butylammonium salts of the lacunary (X = Si) and of the mono-substituted anions (M = Fe and Co), using the droplet evaporation method. The electrochemical behaviour of the immobilized POMs was evaluated by cyclic voltammetry. The morphological features of the modified electrodes were also assessed by scanning electron microscopy. The study of the behaviour, in aqueous solution, of the prepared potassium salts of silicotungstates was performed for comparison and is also presented in this chapter.

Chapter 4 presents the preparation of carbon composite electrodes with tetra-butylammonium salts of the lacunary (X = P) and of the mono-substituted anion (M = Co), with and without poly(hexylmethacrylate). These modified electrodes were characterized

using $[Fe(CN)_6]^{3-/4-}$ model electroactive species, in aqueous solution, by cyclic voltammetry.

Chapter 5 describes the preparation of modified GCE, by the layer-by-layer methodology, using the potassium salts of the lacunary (X = Si) and of the mono-substituted anions (M = Fe, Co for X= Si and M = Fe for X = P), and poly(ethylenimine). The modified electrodes were characterized using cyclic voltammetry, electrochemical impedance spectroscopy and scanning electron microscopy. The growth of the multilayer films adsorbed on a quartz slide was monitored by UV–Vis absorption spectroscopy.

Chapter 6 presents the preparation of parent, lacunary and mono-substituted (M = Fe, Co) silicotungstates doped PEDOT modified electrodes. These modified electrodes were prepared by controlled electrodeposition of composite (hybrid) films of PEDOT, with the Keggin-type SiW_{12}, SiW_{11}, $SiW_{11}Fe$ and $SiW_{11}Co$. The electrochemical behaviour of the immobilized POMs was examined.

Chapter 7 of this thesis is dedicated to the final conclusions.

1.6. References

[1] M. T. Pope, Heteropoly and Isopoly Oxometalates, Springer Verlag, 1983.

[2] M. T. Pope, Comprehensive Coordination Chemistry, G. Wilkinson (ed.), Pergamon Press, 1987, chapter 3.

[3] Y. P. Jeannin, *Chem. Rev.* 98 (1998) 51.

[4] L. C. W. Baker, D. C. Glick, *Chem. Rev.* 98 (1998) 3.

[5] J. F. Keggin, *Nature* 131 (1933) 908.

[6] S. Himeno, M. Takamoto, T. Ueda, *J. Electroanal. Chem.* 465 (1999) 129.

[7] A. Tézé, J. Canny, L. Gurban, R. Thouvenot, G. Hervé, *Inorg. Chem.* 35 (1996) 1001.

[8] J. J. Cowan, A. J. Bailey, R. A. Heintz, B. T. Do, K. I. Hardcastle, C. L. Hill, I. A. Weinstock, *Inorg. Chem.* 40 (2001) 6666.

[9] A. Tézé, G. Hervé, *J. Inorg. Nucl. Chem.* 39 (1977) 2151.

[10] C. L. Hill, C. M. Prosser-McCartha, *Coord. Chem. Rev.* 143 (1995) 407.

[11] A. M. V. Cavaleiro, J. D. Pedrosa de Jesus, H. I. S. Nogueira, Metals Clusters in Chemistry, P. Braunstein, L. A. Oro, P. R. Raithly (eds), Wiley-VCH, 1999, chapter1.

[12] A. Müller, F. Peters, M. T. Pope, D. Gatteschi, *Chem. Rev*. 98 (1998) 239.

[13] M. Sadakane, M.E. Steckhan, *Chem. Rev.* 98 (1998) 219.

[14] B. Keita, L. Nadjo, *J. Mol. Catal. A: Chem.* 262 (2007) 190.

[15] R. Neumann in: J. E. Bäckvall (Ed.), *Modern Oxidative Methods*, Wiley-VCH, Weinheim, 2004, ch. 8.

[16] C. L. Hill, *Chem. Rev.* 98 (1998) 1.

[17] I. V. Kozhevnikov, *Chem. Rev.* 98 (1998) 171.

[18] D.G. Kurth, D. Volkmer, R.V.Klitzing in: G. Decher, J. B. Schlenoff (Eds.), Multilayer Thin Films: Sequential Assembly of Nanocomposite Materials, Wiley – VCH, Weinheim, 2003.

[19] M. T. Pope, A. Müller (eds.), Polyoxometalate Chemistry. From Topology via Self-assembly to Applications, Kluwer, Dordrecht, 2001.

[20] E. Coronado, C. Giménez-Saiz, C. J. Gómez-Garcia, *Coord. Chem. Rev.* 249 (2005) 1776.

[21] E. Coronado, C. J. Gómez-Garcia, *Chem. Rev.* 98 (1998) 273.

[22] J.M. Clemente-Juan, E. Coronado, *Coord. Chem. Rev.* 193–195 (1999) 361.

[23] P. Gomez-Romero, *Adv. Mater.* 13 (2001) 163.

[24] D.E. Katsoulis, *Chem. Rev.* 98 (1998) 359.

[25] J.T. Rhule, C.L. Hill, D.A. Judd, *Chem. Rev.* 98 (1998) 327.

[26] R. Neumann, *Prog. Inorg. Chem.* 47 (1998) 317.

[27] J. M. Fruchart, G. Hervé, J. P. Launay, R. Massart, *J. Inorg. Nucl. Chem.* 88 (1976) 1627.

[28] M. T. Pope, G. M. Varga, *Inorg. Chem.* 5 (1966) 1249.

[29] B. Keita, L. Nadjo, R. Parsons, *J. Electroanal. Chem.* 258 (1989) 207.

[30] G. Hervé, *Ann. Chim.* 6 (1971) 219.

[31] G. Hervé, *Ann Chim.* 6 (1971) 287.

[32] F. A. R. Couto, A. M. V. Cavaleiro, J. D. Pedrosa de Jesus, J. Simão, *Inorg. Chim.* Acta 281 (1998) 225.

[33] Y. Cui, L. Xu, W. J. Wang, G. G. Gao, E. B. Wang, *Chin. J. Chem.* 24 (2006) 316.

[34] M. Takamoto, T. Ueda, S. Himeno, *J. Electroanal. Chem.* 521 (2002) 132.

[35] K. Maeda, S. Himmeno, T. Osakai, T. Hori, *J. Electroanal. Chem.* 364 (1994) 149.

[36] N. M. Alpatova, V. E. Kazarinov, M. D. Levi, E. V. Ovsyannikova, *Russ. J. Electrochem.* 30 (1994) 775.

[37] M. S. Balula, J. A. Gamelas, H. M. Carapuça, A. M. V. Cavaleiro, W. Schlindwein, *Eur. J. Inorg. Chem.* (2004) 619.

[38] X. Liu, G. Gao, L. Xu, F. Li, L. Liu, N. Jiang, Y. Yang, *Solid State Sci.* 11 (2009) 1433.

[39] J. E. Toth, F. C. Anson, *J. Electroanal. Chem.* 256 (1988) 361.

[40] M. Sadakane, E. Steckhan, *Acta Chem. Scan.* 53 (1999) 837.

[41] M. T. Pope, A. Müller, *Angew. Chem. Int. Ed. Engl* 30 (1991) 34.

[42] F. Zonnevijlle, C. M. Tourné, G. F. Tourné, *Inorg. Chem.* 21 (1982) 2742.

[43] P. Souchay, *Ann. Chim.* 18 (1943) 169.

[44] F. Osmond, *Bull Soc. Chim.* 47 (1887) 745.

[45] M. T. Pope, A. Müller, Polyoxometalates: From Platonic Solids to Anti-Retroviral Activity (1994) 191.

[46] T. Okuhara, N. Misuno, M. Misono, *Adv. Catal.* 41 (1996) 113.

[47] K. Maeda, H. Katano, T. Osakai, S. Himeno, A. Saito, *J. Electroanal. Chem.* 389 (1995) 167.

[48] B. Keita, L. Nadjo, *J. Electroanal. Chem.* 227 (1987) 77.

[49] S. Himeno, M. Takamoto, T. Ueda, *J. Electroanal. Chem.* 465 (1999) 129.

[50] W. Sun, H. Liu, J. Kong, G. Xie, J. Deng, *J. Electroanal. Chem.* 437 (1997) 67.

[51] A. Müller, L. Dloczik, E. Diemann, M. T. Pope, *Inorg. Chim. Acta,* 257 (1997) 231.

[52] J. E. Toth, F. C. Anson, *J. Am. Chem. Soc.* 111 (1989) 2444.

[53] J. E. Toth, J. D. Melton, D. Cabelli, B. H. J. Bielski, F. C. Anson, *Inorg. Chem.* 29 (1990) 1952.

[54] S. Dong, M. Liu, *J. Electroanal. Chem.* 372 (1994) 95.

[55] F. Zonnevijlle, C. M. Tourné, G. F. Tourné, *Inorg. Chem.* 21 (1982) 2751.

[56] L. Cheng, H. Sun, B. Liu, J. Liu, S. Dong, *J. Chem. Soc. Dalton Trans.* (1999) 2619.

[57] X. Zang, M. T. Pope, M. R. Chance, G. B. Jameson, *Polyhedron* 14 (1995) 1381.

[58] M. Sadakane, E. Steckhan, *J. Mol. Cat. A* 114 (1996) 221.

[59] C.Rong, F. C. Anson, *Inorg. Chem.* 33 (1994) 1064.

[60] A. Schouten, B. Cros, *Can. J. Chem.* 60 (1982) 1368.

[61] R. W. Murray, A. G. Ewing, R. A. Durst, *Anal. Chem.* 59 (1987) 379.

[62] P. R. Moses, P. Wier, R. W. Murray, *Anal. Chem.* 47 (1975) 1882.

[63] R. A. Durst, A. J. Bäumner, R. W. Murray, R. P. Buck, C. P. Andrieux, *Pure & Appl. Chem.* 69 (1997) 1317.

[64] B. Keita, L. Nadjo, *J. Electroanal. Chem.* 243 (1988) 87.

[65] K. Reybier, J.-P. Malugani, S. Fantini, M. Herlem, B. Fahys, *J. Electrochem. Soc.* 149 (2002) E96.
[66] B. Keita, D. Bouaziz, L. Nadjo, *J. Electroanal. Chem.* 284 (1990) 431.
[67] B. Keita, K. Essaadi, L. Nadjo, *J. Electroanal. Chem.* 259 (1989) 127.
[68] B. Keita, L. Nadjo, *J. Electroanal. Chem.* 240 (1988) 325.
[69] D. Martel, A. Kuhn, *Electrochim. Acta* 45 (2000) 1829.
[70] A. Kuhn, N. Mano, C. Vidal, *J. Electroanal. Chem.* 462 (1999) 187.
[71] P.J. Kulesza, G. Roslonek, L.R. Faulkner, *J. Electroanal. Chem.* 280 (1990) 233.
[72] D. Ingersoll, P.J. Kulesza, P.J. Faulkner, *J. Electrochem. Soc.* 141 (1994) 140.
[73] X. Wang, Z. Kang, E. Wang, C. Hu, *J. Electroanal. Chem.* 523 (2002) 142.
[74] M.I. Prodromidis, P.G. Veltsistas, C.E. Efstathiou, M.I. Karayannis, *Electroanalysis* 13 (2001) 960.
[75] H.M. Carapuça, M.S. Balula, A.P. Fonseca, A.M.V. Cavaleiro, *J. Solid State Electrochem.*10 (2006) 10.
[76] G. Bidan, E. M. Genies, M. Lapkowski, *J. Electroanal. Chem.* 251 (1988) 297.
[77] http://98.131.55.98/is_a_ele_ecp.asp (25/07/2010).
[78] E.M. Geniès, G. Bidan, A.F. Diaz, *J. Electroanal. Chem.* 149 (1983) 101.
[79] P. Wang, Y. Li, *J. Electroanal. Chem.* 408 (1996) 77.
[80] S. Dong, W. Jin, *J. Electroanal. Chem.* 354 (1993) 87.
[81] S. Dong, M. Liu, *Electrochim. Acta* 39 (1994) 947.
[82] H. Sung, H. So, W. Paik, *Electrochim. Acta* 39 (1994) 645.
[83] P. Gómez-Romero, M. Lira-Cantu, *Adv. Mater.* 9 (1997) 144.
[84] T. F. Otero, S. A. Cheng, D. Alonso, F. Huerta, *J. Phys. Chem. B* 104 (2000) 10528.
[85] T. F. Otero, S. A. Cheng, F. Huerta, *J. Phys. Chem. B* 104 (2000) 10522.
[86] H. X. Guo, Y. Q. Li, L. F. Fan, X. Q. Wu, M. D. Guo, *Electrochim. Acta* 51 (2006) 6230.
[87] M. D. Guo, H. X. Guo, *J. Electroanal. Chem.* 585 (2005) 28.
[88] X. L. Wang, H. Zhang, E. B. Wang, Z. B. Han, C. W. Hu, *Mater. Lett.* 58 (2004) 1661.
[89] L. M. Abrantes, C. M. Cordas, E. Vieil, *Electrochim. Acta* 47 (2002) 1481.
[90] P. Gomez-Romero, O. Ayyad, J. Suàrez-Guevara, D. Muñoz-Rojas, *J. Solid State Electrochem.* 14 (2010) 1939.
[91] E. Nguema, V. Vigneras, J. L. Miane, P. Mounaix, *Eur. Polymer J.* 44 (2008) 124.
[92] P. Gomez-Romero, N. Casan-Pastor, M. Lira-Cantu, *Solid State Ionics* 101 (1997) 875.
[93] G. Siné, C. C. Hui, A. Kuhn, P. J. Kulesza, K. Miecznikowski, M. Chojak, A. Paderewska, A. Lewera, *J. Electrochem. Soc.* 150 (2003) C351.
[94] P. C. Lekha, S. Subramanian, D. P. Padiyan, *Journal of Materials Science* 44 (2009) 6040.
[95] D. G. Shuchukin, D. V. Suiridov, *Electrochem. Commun.* 4 (2002) 402.
[96] M. Barth, M. Lapkowski, S. Lefrant, *Electrochim. Acta* 44 (1999) 2117.
[97] P. C. Lekha, E. Subramanian, D. P. Padiyan, *Sensors Actuator B Chem*. 122 (2007) 274.

[98] A. Mahmoud, B. Keita, L. Nadjo, O. Oung, R. Contant, S. Brown, Y. Kouchkovsky, *J. Electroanal. Chem.* 463 (1999) 129.

[99] B. Fabre, G. Bidan, *Electrochim. Acta* 42 (1997) 2587.

[100] I. Perepichka, D. Perepichka, H. Meng, F. Wudl, *Adv. Mater.* 17 (2005) 2281.

[101] L. Groenendaal, J. Dhaen, J. Manca, J. Van Luppen, E. Verdonck,; F. Louwet, L. Leenders, *Synth. Met.* 115 (2003) 135.

[102] T. Yamamoto, *Asia Mater.* 2 (2010) 54.

[103] A. F. Diaz, J. Bagon, Handbook of Conducting Polymers; Stotheim, T. A. Ed, 1 (1986).

[104] E. Genies, G. Bidan, A. F. Diaz, *J. Electroanal. Chem.* 149 (1983) 113.

[105] Y. Wei, C. Chan, J. Tian, G. Jang, K. F. Hsueh, *Chem. Mater.* 3 (1991) 888.

[106] G. Bidan, E. M. Genies, M. Lapkowski, *Synth. Met.* 31 (1989) 327.

[107] G. Bidan, M. Lapkowski, J. P. Travers, *Synth. Met.* 28 (1989) C113.

[108] M. Lapkowski, G. Bidan, M. Fournier, *Synth. Met.* 41 (1991) 407.

[109] B. Fabre, G. Bidan, *Adv. Mater.* 5 (1993) 646.

[110] M. Lapkowski, G. Bidan, M. Fournier, *Synth. Met.* 41 (1991) 411.

[111] M. Lapkowski, G. Bidan, M. Fournier, *Pol. J. Chem.* 65 (1991) 1547.

[112] A. M. White, R. C. T. Slade, *Electrochim. Acta* 49 (2004) 861.

[113] L. Adamczyk, P. J. Kulesza, K. Miecznikowski, B. Palys, M. Chojak, D. Krawczyk. *J. Electrochem. Soc.* 152 (2005) E98.

[114] G. Decher, *Science* 277 (1997) 1232.

[115] S.T. Dubas, J.B. Schlenoff, *Macromolecules* 32 (1999) 8153.

[116] P. Bertrand, A. Jonas, A. Laschewsky, R. Legras, *Macromol. Rapid Commun.* 21 (2000) 319.

[117] F.N. Crespilho, V. Zucolotto, O.N. Oliveira Jr, F.C. Nart, *Int. J. Electrochem. Sci.* 1 (2006) 194.

[118] N. G. Hoogeveen, M. A. C. Stuart, G. J. Fleer, M. R. Böhmer, *Langmuir* 12 (1996) 3675.

[119] N. G. Hoogeveen, M. A. C. Stuart, G. J. Fleer, *J. Colloid Interface Sci.* 182 (1996) 133.

[120] L Kolarik, D. F. Furlong, H. Joy, C. Struijk, R. Rowe, *Langmuir* 15 (1999) 8265.

[121] D. Cochim, M. Paßmann, G. Wilbert, R Zentel, E. Wischerhoff, A. Laschewsky, *Macromolecules* 30 (1997) 4775.

[122] M. Paßmann, G. Wilbert, D. Cochim, R Zentel, *Macromol. Chem. Phys.* 199 (1998) 179.

[123] P. Fisher, A. Laschewsky, E. Wischerhoff, X. Arys, A. Jonas, R. Legras, *Macromol. Symp.* 137 (1999) 1.

[124] S. Liu, D.G. Kurth, B. Bredenkotter, D. Volkmer, *J. Am. Chem. Soc.* 124 (2002) 12279.

[125] Y. Wang, C. Guo, Y. Chen, C. Hu, W. Yu, *J. Colloid Interface Sci.* 264 (2003) 176.

[126] Y. Feng, Z. Han, J. Peng, J. Lu, B. Xue, L. Li, H. Ma, E. Wang, *Mater. Lett.* 60 (2006) 1588.

[127] S. Li, E. Wang, C. Tian, B. Mao, Y. Song, C. Wang, L. Xu, *Mater. Res. Bull.* 43 (2008) 2880.

[128] L. Cheng, J. Liu, S. Dong, *Anal. Chim. Acta* 417 (2000) 133.

[129] S. Zhai, Y. Chen, S. Wang, J. Jiang, *Talanta* 63 (2004) 927.

[130] L. Cheng, S. Dong, *J. Electroanal. Chem.* 481 (2000) 168.

[131] J. Liu, L. Cheng, S. Dong, *Electroanalysis* 14 (2002) 569.
[132] S. Gao, T. Li, X. Li, R. Cao, *Mater. Lett.* 60 (2006) 3622.
[133] C. Li, X. Wang, H. Ma, F. Wang, Y. Gu, *Electroanalysis* 20 (2008) 1110.
[134] D. Martel, M. Gross, *J Solid State Electrochem.* 11 (2007) 421.
[135] G. Bazzan, W. Smith, L.C. Francesconi, Drain C.M. *Langmuir* 24 (2008) 3244.
[136] K. Shiu, F.C. Anson, *J. Electroanal. Chem.* 309 (1991) 115.
[137] K. Kalcher, *Electroanalysis* 2 (1990) 419.
[138] J. Lindquist, *J. Electroanal. Chem.* 52 (1974) 37.
[139] Y. Zhang, J. B. Zheng, *Electrochim. Acta* 52 (2007) 7210.
[140] G. Shul, J. Sirieix-Plenet, L. Gaillon, M. Opallo, *Electrochem. Commun.* 8 (2006) 1111.
[141] H. Liu, P. He, Z. Li, C. Sun, L. Shi, Y. Liu, G. Zhu, J. Li, *Electrochem. Commun.* 7 (2005) 1357.
[142] M.M. Barsan, E.M. Pinto, M. Florescu, C.M.A. Brett, *Anal. Chim. Acta* 635 (2009) 71.
[143] F. Abertús, A. Llerena, J. Alpízar, V. Cerdá, M. Luque, A. Ríos, M. Valcárcel, *Anal. Chim. Acta* 355 (1997) 23.
[144] M. Luque, A. Ríos, M. Valcárcel, *Anal. Chim. Acta* 395 (1999) 217.
[145] Ü.A. Kirgöz, D. Odaci, S. Timur, A. Merkoçi, S. Alegret, N. Besün, A.Telefoncu, *Anal. Chim. Acta* 570 (2006) 165.
[146] Z. Han, Y. Zhao, J. Peng, A. Tian, Y. Feng, Q. Liu, *J. Solid State Chem.* 178 (2005) 1386.
[147] H. Hamidi, E. Shams, B. Yadollahi, F. K. Esfahani, *Talanta* 74 (2008) 909.
[148] L. Li, W. Li, C. Sun, L. Li, *Electroanal.* 14 (2002) 368.
[149] Z. Han, Y. Zhao, J. Peng, Y. Feng, J. Yin, Q. Liu, *Electroanalysis* 17 (2005) 1097.
[150] Z. Han, Y. Zhao, J. Peng, Q. Liu, E. Wang, *Electrochim. Acta* 51 (2005) 218.
[151] X. Wang, E. Wang, Y. Lan, C. Hu, *Electroanalysis* 14 (2002) 1116.
[152] X. Wang, Z. Kang, E. Wang, C. Hu, *Mater. Lett.* 56 (2002) 393.
[153] Y. Liang, P. He, Y. Ha, Y. Zhou, C. Pei, X. Li, *Electrochem. Commun.* 11 (2009) 1018.
[154] B. Haghighi, H. Hamidi, *Electroanalysis* 21 (2009) 1057.
[155] H. Hamidi, E. Shams, B. Yadollahi, F. K. Esfahani, *Electrochim. Acta* 54 (2009) 3495.
[156] X. L. Wang, H. Y. Lin, G. C. Liu, B. K. Chen, Y. F. Bi, *Chem. Res. Chin. Univ.* 24 (2008) 129.
[157] A. J. Bard, L. R. Faulkner, Electrochemical Methods, Wiley, 2001
[158] C. M. A. Brett, A. M. Oliveira Brett, Electroanalysis, Oxford Chemistry Primers, 1998.
[159] A. M. O. Brett, C. M. A. Brett, Electrochemistry: Principles, Methods and Aplications, Oxford University Press, 1993.
[160] R. Greef, R. Peat, L. M. Peter, D. Pletcher, J. Robinson, Instrumental methods in Electrochemistry, Ellis Horwood Limited, Chichester, 1985.
[161] C. M. A. Brett, ECS Transactions 13 (2008) 67.
[162] J. Ross Macdonald, W. B. Johnson in: E. Barsoukov, J. R. Macdonalds (Eds), Impedance Spectroscopy, Theory, Experiment and Applications, 2nd Edition, John Wiley and Sons, New York, 2005.

[163] A. Lasia in B. E. Conway, J. O´M. Bocknis, R. E. White (Eds), EIS-Modern Aspects of Electrochemistry nº 32, Kluwer, 2002.

CHAPTER 2

POLYOXOMETALATES:
SYNTHESIS AND CHARACTERIZATION

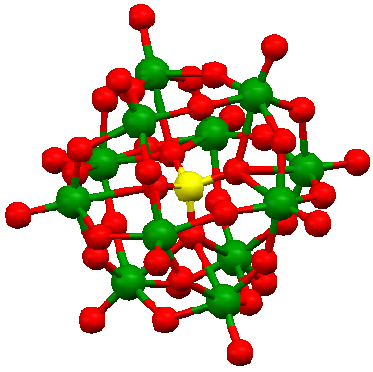

2.1. Introduction

The first polyoxometalate dates from 1826 when Berzelius described the yellow precipitate that is produced when ammonium molybdate is added to phosphoric acid and which is now known to be the ammonium phosphomolybdate $(NH_4)_3[PMo_{12}O_{40}]\cdot nH_2O$. However, it was not until the discovery of the silicotungstic acids and their salts by Marignac in 1862 that the analytical compositions of such heteropoly acids were precisely determined [1]. Thereafter, the field developed rapidly through the twentieth century and the synthesis of new salts was greatly improved. However, given the dimensions and structural complexity of these anions, their characterization presented difficulties until recently. Nowadays, with the development of new instrumental techniques such as nuclear magnetic resonance (NMR), X-ray powder diffraction, amongst others, it is possible to obtain more precise information about these compounds.

Generally, POMs preparation is based on reactions in aqueous solutions or in organic solvents (or a mixture of solvents). The α-Keggin polyoxotungstates are prepared by controlled acidification of aqueous solutions that contain the simple oxoanion (WO_4^{2-}) and species with the primary heteroatom (for example, HPO_4^{2-}, SiO_4^{2-}, amongst others) (equation 2.1) [1,2].

The lacunary species of the Keggin anions can be obtained by the addition of alkaline solutions to aqueous solutions containing these parent anions (equation 2.2), or by acidification of aqueous solutions of sodium tungstate and oxoanions that contain the

required heteroatom, at defined pH values (equation 2.3), whenever the heteroatom is non-metallic [1,2]. If the heteroatom is a metal, a salt of this metal is used instead of the oxoanion. Frequently, the lacunary anion can be changed into the Keggin anion if the pH values of the solution are acid enough. For example, the lacunary $[PW_{11}O_{39}]^{7-}$ is stable between pH values of 2 and 6, its conversion into the Keggin anion $[PW_{12}O_{40}]^{3-}$ occurring by acidification.

$$12\ WO_4^{2-} + HPO_4^{2-} + 23\ H^+ \rightarrow [PW_{12}O_{40}]^{3-} + 12\ H_2O \quad (2.1)$$

$$[PW_{12}O_{40}]^{3-} + (5-x)\ OH^- \rightarrow [H_xW_{11}O_{39}]^{(7-x)-} + HWO_4^{2-} + (2-x)\ H_2O \quad (2.2)$$

$$11\ WO_4^{2-}(aq) + HPO_4^{2-}(aq) + 17\ H^+(aq) \rightarrow [PW_{11}O_{39}]^{7-}(aq) + 9\ H_2O(l) \quad (2.3)$$

The first mono-substituted polyanions $[XW_{11}M(H_2O)O_{39}]^{m-}$ ($[XW_{11}M]$) were known in the middle of the nineteen sixties, with the pioneering work of Baker [3]. He proposed that the anions with X = Si^{IV}, $Co^{II,III}$, $(H_2)^{2+}$ and M = $Co^{II,III}$, Ga^{III} belonged to a new category of heteropolyelectrolytes, with an analogous structure to the Keggin anion [3]. Initially, the majority of the work reported on mono-substituted polyanions involved the potassium salts. In the literature, three different general methods can be found for the preparation of the mono-substituted anions $[XW_{11}M]$ [4-6]:

- Method 1: After isolation of the potassium salt of $[XW_{11}O_{39}]^{(n+4)-}$, this is reacted, in hot aqueous solution or in suspension, with a solution containing the desired metal cation, in a ratio slightly higher than the stoichiometric value for the cation.

- Method 2: To an aqueous solution containing the $[XW_{12}O_{40}]^{n-}$ anion and the desired metal cation, boiling $KHCO_3$ or KCH_3COO, is slowly added, until a pH value compatible with the total conversion of XW_{12} to XW_{11} and compatible with the stability of the formed complex. For X = P, pH = 5.0 – 5.5; X = Si, Ge, pH = 6.0 – 6.7.

- Method 3 (direct method): Acidification of an aqueous solution containing a salt of the element X (disodium hydrogenophosphate when the heteroatom is phosphor,

and sodium metassilicate when it is silicon [4,7,8]) and tungstate, in a molar proportion of 1:11, respectively. The values of pH are 4.7 – 5.0 for X = P, and 6.0 – 6.7 for X = Si. Finally, an aqueous solution of the desired metal substituent is added.

The stability of $[XW_{11}M(H_2O)O_{39}]^{m-}$ species, in aqueous solution, depends on the pH value. Commonly, at lower pH values (pH<2) the decomposition of $[XW_{11}M(H_2O)O_{39}]^{m-}$ into $[XW_{12}O_{40}]^{n-}$ can occur, with release of the metal M from the lacuna (sped up by the presence of WO_4^{2-}), while for higher pH values (pH>9) total destruction of the substituted anion structure occurs, with formation of its basic units: WO_4^{2-}, $X_aO_b^{n-}$, or $M(OH)_c$ [4,5]. On the other hand, the pH range within which the anions are stable depends on X and M and on the oxidation state of M. Mono-substituted anions by transition metal cations M^{3+} are, in general, more stable at lower pH values than those substituted by M^{2+}. The production of polyoxometalate salts is done, in general, through precipitation/crystallization with alkali metal cations (Li^+, K^+, Na^+, Cs^+) or with alkylammonium cations (for example, tetra-butylammonium, TBA). Alternatively, the anions may be transferred into an organic solution with the help of a chosen cationic phase transfer agent (alkylammonium or other) and the salt recovered from this media. The salts of alkylammonium cations, or of similar cations with larger size, are generally insoluble in water, being recrystallized in organic solvents. The use of the appropriate counter-cation can be determinant in the isolation of a particular type of polyoxometalate and for the attainment of suitable crystals for structural characterization by X-ray powder diffraction. The interest for the tetra-butylammonium salts emerged from the need to obtain the anions as soluble compounds in organic solvents, especially for catalytic applications.

In this chapter the synthesis and characterization of the several polyoxometalates used in the next chapters are presented. The compounds were characterized by different techniques such as infrared and UV-visible absorption spectroscopy, elemental analysis and thermogravimetry.

2.2. Experimental

2.2.1. Reagents

All reagents used in the synthesis of all the compounds were used as received.

2.2.2. Instrumentation and methods

The infrared spectra were acquired using KBr pellets of the prepared polyoxotungstates. These were analysed in the range of wavenumbers from 500 to 4000 cm^{-1}, with resolution of 2 cm^{-1} and 32 accumulations. The equipment used was a Fourier transform spectrometer, Mattson 7000.

UV–vis absorption spectroscopy was performed in a Jasco V-560 UV-visible spectrophotometer, using a quartz cell with 0.4 cm path length.

Thermogravimetric analyses were performed in air between 20° and 800℃, using a Mettler M3 balance, coupled to a TC 10 A processor. The heating speed used was 5 K/minute.

The elemental analysis of C, N and H were obtained, for all tetra-butylammonium salts, in a Leco CHNS-932 equipment.

The elemental analyses of inorganic elements, by inductively coupled plasma spectrometry (ICP), were conducted in a Jobin Yvon JY70 plus, in the Central Laboratory of Analysis of University of Aveiro. The TBA samples were attacked with an alkaline solution of the dissodium salt of EDTA, in order to analyse the elements P and W, or with HF/HNO_3 for the analysis of the transition metals.

2.2.3. Synthesis

Several polyoxotungstate salts were prepared following the described procedures, as indicated in Table 2.1. Some abbreviations used in this work are also shown in Table 2.1. In this section only the procedures used in the synthesis adapted from those in the literature will be described.

Table 2.1. List of the polyoxotungstates produced by published methods.

Compounds	Reference
$K_8[SiW_{11}O_{39}]\cdot 13H_2O$ (K-SiW_{11})	9
$K_5[SiW_{11}Fe(H_2O)O_{39}]\cdot 13H_2O$ (K-$SiW_{11}Fe$)	10
$K_6[SiW_{11}Co(H_2O)O_{39}]\cdot 12H_2O$ (K-$SiW_{11}Co$)	11
$K_7[PW_{11}O_{39}]\cdot 8H_2O$ (K-PW_{11})	12
$K_4[PW_{11}Fe(H_2O)O_{39}]\cdot 15H_2O$ (K-$PW_{11}Fe$)	10
$TBA_4H_3[PW_{11}O_{39}]$ (TBA-PW_{11})	13
$TBA_4H_x[PW_{11}M(H_2O)O_{39}]\cdot nH_2O$	13,14,15
$M = Co^{II}$, Fe^{III} (TBA-$PW_{11}Co$, TBA-$PW_{11}Co$)	

2.2.3.1. Synthesis of $TBA_4H_4[SiW_{11}O_{39}]$

The synthesis of $TBA_4H_4[SiW_{11}O_{39}]$ is described in the literature [16] and was carried out using the phase transfer method, by putting into contact, in a separation funnel, an aqueous solution of $K_8[SiW_{11}O_{39}]\cdot 13H_2O$ (0.5 mmol in 30 mL) and a TBABr solution in 1,2-dicloroethane (4 mmol in 45 mL). The solutions were vigorously stirred and, after some resting for some minutes, the organic phase of 1,2-dicloroetane was removed and dried in a rotary evaporator, until an oil was formed. This oil was then dissolved in approximately 20 mL of acetonitrile and precipitation of the TBA salt was achieved by adding a minimal quantity of water. After stirring this solution for a while, the TBA salt was filtered and dried in an oven.

Analytical Found (calculated) : $TBA_4H_4[SiW_{11}O_{39}]$ (TBA-SiW_{11}) (%): W = 54.5 (55.4), C = 19.87 (21.07), N = 1.43 (1.53), H = 3.74 (4.09).

2.2.3.2. Synthesis of $TBA_4H_x[SiW_{11}M(H_2O)O_{39}]\cdot nH_2O$, $M = Co^{II}$, Fe^{III}

These compounds were prepared by phase transfer from the corresponding potassium salts, synthesized above, following the same procedure as previously described for the lacunary TBA salt.

Analytical Found (calculated):

$TBA_4H[SiW_{11}Fe(H_2O)O_{39}]$ (TBA-$SiW_{11}Fe$) (%): W = 53.6 (54.4), C = 20.60 (20.67), N = 1.45 (1.51), H = 3.85 (3.98), Fe = 1.48 (1.50).

$TBA_4H_2[SiW_{11}Co(H_2O)O_{39}]\cdot H_2O$ (TBA-$SiW_{11}Co$) (%): W = 52.2 (54.0), C = 20.55 (20.55), N = 1.56 (1.50), H = 4.05 (4.04), Co = 1.39 (1.57).

2.3. Potassium salts of lacunary and mono-substituted anions

The preparation of the lacunary Keggin-type anions where X = Si or P can be carried out by one of the methods referred to in 2.1. The preparative method used consists in the acidification, with heating (80-90 ℃) and stirring, of aqueous solutions of sodium tungstate dihydrate and of an oxoanion that contains the required heteroatom, in stoichiometric ratios [12]. The anions are isolated, from the aqueous solution, in the form of potassium salts by the addition of an excess of potassium chloride, being recrystallized with hot distilled water (60 ℃).

Many potassium salts of the mono-substituted anions $[XW_{11}M(H_2O)O_{39}]^{n-}$, X = Si, P and others with transition metal cations, in different oxidation states were described in the 1970s [1,3,5,11,17]. Several authors published the preparative methods and characterization of these compounds, having used electrochemical and spectroscopic techniques among others [3-5,8,10,18-20].

In this work, the potassium salts of anions with general formula $[XW_{11}M(H_2O)O_{39}]^{m-}$, X = Si and P and M` = Co(II) and Fe(III) were prepared. The method used to prepare $[XW_{11}Fe(H_2O)O_{39}]^{m-}$, where X = Si and P, is described in the literature [10]. For the $[SiW_{11}Co(H_2O)O_{39}]^{6-}$ synthesis, an already described method was also used [11].

The infrared adsorption spectra of Keggin-type polyoxotungstates present a set of intense bands in the region between 600 and 1200 cm^{-1}, that correspond to asymmetric vibrations $\nu_{as}(X\text{-}O_a)$, $\nu_{as}(W\text{-}O_d)$, $\nu_{as}(W\text{-}O_b\text{-}W)$ and $\nu_{as}(W\text{-}O_c\text{-}W)$. Figure 2.1 shows, as example, the infrared spectrum for $K_5[SiW_{11}Fe^{III}(H_2O)O_{39}]\cdot 13H_2O$ salt.

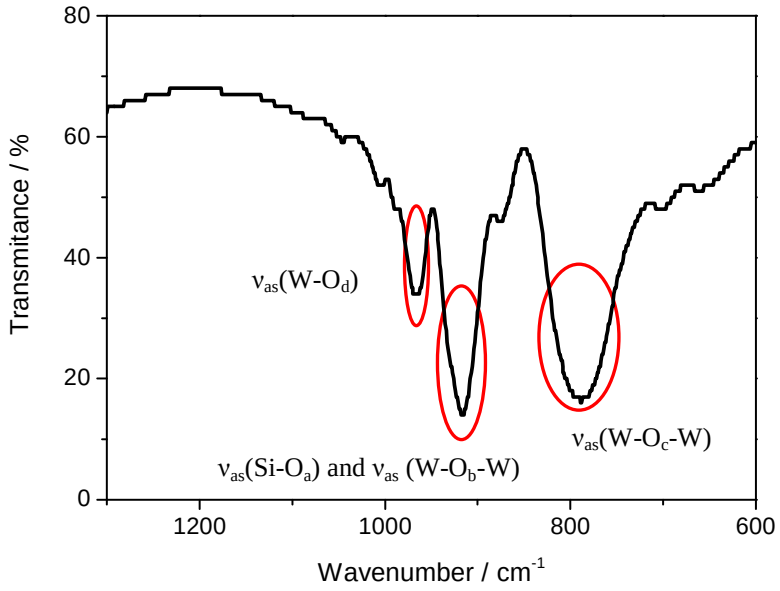

Figure 2.1. Infrared spectrum of the $K_5[SiW_{11}Fe^{III}(H_2O)O_{39}]\cdot 13H_2O$ salt.

In this anion, as for the other prepared silicon compounds, the band corresponding to the X-O_a vibration appears overlapped with the band due to the W-O_b-W bond, while in the spectra of the phosphor anions there is a splitting of the former. This splitting is important because it reflects the deviation from the extremely symmetric structure of the Keggin anion [10,21]. For the phosphotungstates, the splitting of the band attributed to the ν_{as}(X-O_a) vibration is lower for the metal substituted anion than for $[PW_{11}O_{39}]^{7-}$, which is due to the partial reestablishment of symmetry, due to the introduction of the transition metal cation that will fill the lacuna [1].

In all spectra, an intense and large band at 3500 cm^{-1} is observed which is characteristic of water present in the structure and is attributed to the antissymmetric elongation of the O-H bond. The band at 1600 cm^{-1} is attributed to the angular deformation of the H-O-H angle of structural water [22]. The water molecules that are possibly adsorbed at the surface of the compound may, in the same way, contribute to absorption in the same range of infrared as well as the molecules of the structure.

For a given X, the absorption infrared spectra of the compounds substituted by transition metal cations are very similar so that this technique by itself may not allow the distinction between them. Table 2.2 presents the wavenumbers for the prepared potassium salts of the polyoxotungstates and the respective assignment of the bands, based on the literature [18].

Table 2.2. Absorption infrared bands (cm^{-1}) in the spectra of potassium salts of the $[XW_{11}O_{39}]^{n-}$ and $[XW_{11}M(H_2O)O_{39}]^{m-}$ anions.

Compound	v_{as}(X-O_a)	v_{as}(W-O_d)	v_{as}(W-O_b-W)	v_{as}(W-O_c-W)
K-PW_{11}	1090	955	907	813
	1049		858	745
K-PW_{11}Fe	1086	969	892	813
	1064			740 (o)
K-SiW_{11}	890	955	890	800
				740
K-SiW_{11}Fe	917	968	917	794
	882 (oh)		882 (oh)	705
K-SiW_{11}Co	907	963	907	806
				759 (oh)
				699

The electronic absorption spectra of Keggin polyanions and their derivatives (lacunary and mono-substituted) are similar and they present, two absorption bands in the UV region in aqueous solution. The typical band that appeared close to 250 nm (table 2.3) is characteristic of all heteropolyanions with the Keggin structure, and was attributed to charge transfer from the bridging oxygen atoms (O_b and O_c) to W^{VI} atoms [23,24]. As can be seen in Table 2.3, this band is shifted to higher wavelengths for the metal substituted anions in comparison to that of the lacunary anions. The shift is attributed to the lower density of negative charge of the metal substituted anions [25]. In the lower limit of the UV-visible spectra, near 190 nm, appears, in all spectra, a second band which is attributed to the charge transfer of terminal oxygen atoms to the tungsten atoms, $O_d \rightarrow W^{VI}$ [23,26].

For the iron substituted phosphotungstate potassium salts a charge transfer shoulder ($O \rightarrow Fe^{III}$) was observed at 376 nm. A shoulder at 366 nm was also observed for K-SiW_{11}Fe. For K-SiW_{11}Co, besides the O→W charge transfer bands, the spectra present another band at 539 nm with a shoulder at 498 nm, corresponding to a $^4T_{1g}$ (F) → $^4T_{1g}$ (P) *d-d* transition split by spin-orbit coupling [27], and another at 369 nm corresponding to a O → Co charge transfer band [27].

Table 2.3. Values of wavelength obtained for charge transfer across bridge bonds W-O-W.

Anion	λ ($O_{b/c} \rightarrow W^{VI}$) / nm
K-PW_{11}	250
K-$PW_{11}Fe$	260
K-SiW_{11}	248
K-$SiW_{11}Fe$	258
K-$SiW_{11}Co$	254

Thermogravimetry (TG) studies were conducted in order to study the thermal stability of the prepared compounds and to determine the amount of hydration water molecules in each. The range of temperatures used was between 40 and 800 ℃. Figure 2.2 shows a thermogram for the $K_8[SiW_{11}O_{39}]\cdot 13H_2O$ salt, which is representative of the behaviour of the other prepared polyoxotungstates.

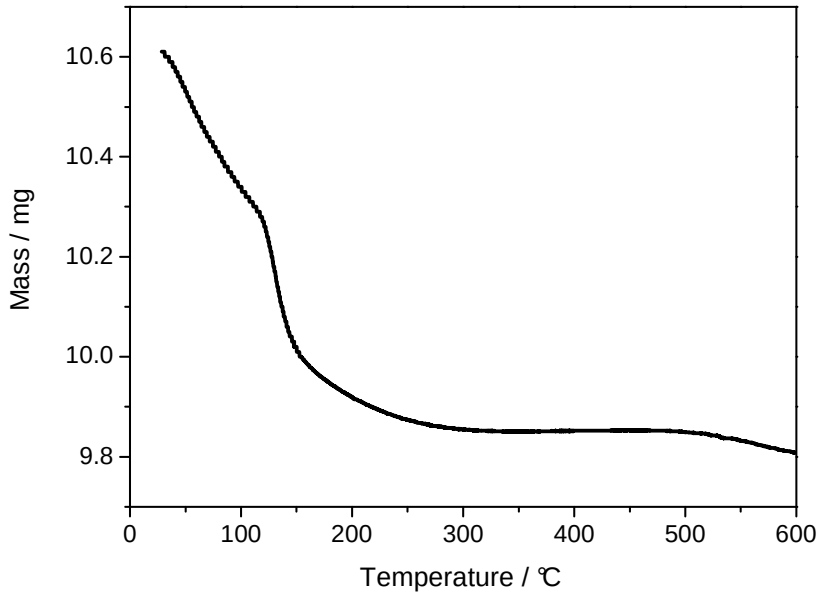

Figure 2.2. Thermogram of the $K_8[SiW_{11}O_{39}]\cdot 13H_2O$ salt.

Thermogravimetric curves, generally, show two steps that occur in the temperature range of 40 to approximately 100 ℃, and 110 to 200 ℃. These weight losses correspond to the loss of crystallization water and/or adsorbed water, leading to the anhydrous polyoxotungstate. The decomposition of the polyanion occurs at higher temperatures and

the end result is a mixture of oxides. Table 2.4 presents the number of water molecules present for each POM.

Table 2.4. Number of water molecules present in the prepared polyoxotungstates

Anion	n(H_2O)
K-PW_{11}	8
K-$PW_{11}Fe$	15
K-SiW_{11}	13
K-$SiW_{11}Fe$	13
K-$SiW_{11}Co$	12

2.4. Tetra-butylammonium salts of lacunary and mono-substituted anions

The method used for the preparation of $TBA_4H_3[PW_{11}O_{39}]$ (TBA-PW_{11}) can be found in the literature [13]. It is precipitation and involves the addition of an aqueous solution of TBABr to the reaction mixture of the X oxoanion and tungstate, in stoichiometric ratio and after the pH is adjusted to 4.8. The preparation of the $TBA_4H_4[SiW_{11}O_{39}]$ (TBA-SiW_{11}) salt was carried out from its potassium salt, $K_8[SiW_{11}O_{39}]\cdot 13H_2O$, following an adapted method from the literature [16]. This method is a phase transfer method where the aqueous solution of the potassium salt is placed in contact with a solution of TBABr in 1,2-dicloroethane. After vigorously stirring the two solutions, the organic part is separated and the 1,2-dicloroethane is evaporated. Following evaporation, an oil is obtained, that is then dissolved in acetonitrile. Precipitation of the tetra-butylammonium salt is achieved by addition of a minimum quantity of water to the previous acetonitrile solution.

The TBA salts of the mono-substituted polyanions $[PW_{11}M(H_2O)O_{39}]^{m-}$ where M = Co^{II} and Fe^{III} , were prepared following procedures already performed in our laboratory [13-15]. The compounds obtained were $TBA_4[PW_{11}Fe(H_2O)O_{39}]\cdot 2H_2O$ and $TBA_4H[PW_{11}Co(H_2O)O_{39}]\cdot H_2O$. The TBA salts of the mono-substituted polyanions $[SiW_{11}M(H_2O)O_{39}]^{m-}$, where M = Co^{II} and Fe^{III}, were prepared by the phase transfer method, following an procedure adapted from the literature, using the respective

potassium salts as precursors [16]. The compounds obtained were $TBA_4H[SiW_{11}Fe(H_2O)O_{39}]$ and $TBA_4H_2[SiW_{11}Co(H_2O)O_{39}]\cdot H_2O$. The recrystallization of the metal substituted TBA salts was performed in acetonitrile, in the same way as for the lacunary polyoxotungstates. All TBA salts were characterized by elemental analysis (C, N, H, W, P, Si, M), thermogravimetry and IV absorption spectroscopy.

The infrared absorption spectra of Keggin-type polyoxotungstates present the characteristic bands of the polyanions and also the bands of the tetra-butylammonium cation. The spectra present a set of intense bands in the region between 600 and 1200 cm^{-1} that correspond to the asymmetric vibrations as referred to previously. Figure 2.3 shows, as example, the infrared spectrum for TBA-SiW_{11} in this region.

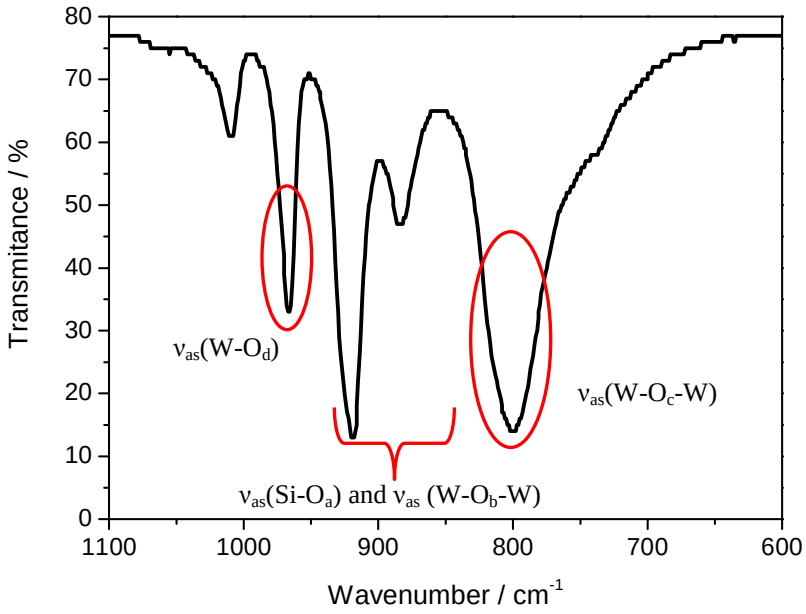

Figure 2.3. Infrared spectrum of the $TBA_4H_4[SiW_{11}O_{39}]$ salt.

The wave numbers of the bands in Fig. 2.3, for the TBA salts, are similar to those obtained for the potassium salts except for the $\nu_{as}(W\text{-}O_d)$. The potassium salts of the lacunary anion present this band at 955 cm^{-1} while, in the TBA salts, this band is at 969 cm^{-1}. This behaviour was already observed by Rocchiccioli-Deltcheff *et al*., when they studied the TBA and potassium salts of the Keggin anions $[XW_{12}O_{40}]^{n-}$ by infrared spectroscopy [28]. When comparing the spectra for TBA and potassium salts, there was a shift to higher wavenumbers of the $\nu_{as}(W\text{-}O_d)$ band. The lower value observed for the potassium salt was attributed to interactions between the polyanions. These interactions

may arise from the repelling of negative charge densities of the terminal oxygens O_d. In the presence of larger cations, like TBA, the interactions between polyanions are smaller because the distance between the terminal oxygens of different polyanions is greater. Rocchiccioli-Deltcheff *et al*., reported that the true value of wavenumber of the $v_{as}(W\text{-}O_d)$ bond is found in the presence of larger cations, like TBA [28].

Table 2.5 presents the absorption infrared spectroscopy results for all the prepared polyoxotungstates. The attribution of the bands was performed taking into account the available data in the literature [17,28,29]

For the TBA-SiW_{11} anion, the band corresponding to the $X\text{-}O_a$ vibration appears overlapped with that due to the $W\text{-}O_b\text{-}W$ bond, while in the TBA-PW_{11} anion there is a splitting of the same band.

Table 2.5. Absorption infrared bands (cm^{-1}) in the spectra of TBA salts of the lacunary and metal substituted polyoxotungstates prepared.

Compound	$v_{as}(X\text{-}O_a)$	$v_{as}(W\text{-}O_d)$	$v_{as}(W\text{-}O_b\text{-}W)$	$v_{as}(W\text{-}O_c\text{-}W)$
TBA-PW_{11}	1110 1059	960	894	809
TBA-$PW_{11}Fe$	1072	963	887	807
TBA-$PW_{11}Co$	1062	956	889	820
TBA-SiW_{11}	921	969	886	802
TBA-$SiW_{11}Fe$	910 879	958	910 879	798
TBA-$SiW_{11}Co$	908 882 (o)	960	908 882(o)	810 788(o)

In acetonitrile solution, the lacunary polyanion $[PW_{11}O_{39}]^{7-}$, presents a charge transfer band at 258 nm, corresponding to a O → W transition [27]. The electronic spectra in the visible region of $[PW_{11}Co(H_2O)O_{39}]^{5-}$, in acetonitrile solution, present an absorption band at 480 nm, a shoulder at 513 nm and another peak of lower intensity at 568 nm. These are the *d-d* bands and correspond to high spin Co(II) with symmetry close to octahedral [6,30] The $PW_{11}Fe$ polyanion presents, a charge transfer band O → Fe in the visible region, that is in agreement with a d^5 high spin configuration. The position of the

λ_{max} of the charge transfer band depends on the charge and size of the central heteroatom [10].

The lacunary $[SiW_{11}O_{39}]^{8-}$ presents a charge transfer band O → W at 258 nm. The mono-substituted polyanion $[SiW_{11}Co(H_2O)O_{39}]^{6-}$, presents two adsorption bands at 479 nm and 516 nm and the $[SiW_{11}Fe(H_2O)O_{39}]^{5-}$ polyanion presents, like $PW_{11}Fe$, a charge transfer band O → Fe in the visible region, that is in agreement with the d^5 high spin configuration.

Figure 2.4 shows the thermogram for $TBA_4H_3[PW_{11}O_{39}]$, as an example, and it is representative of the other TBA salts of the prepared polyanions.

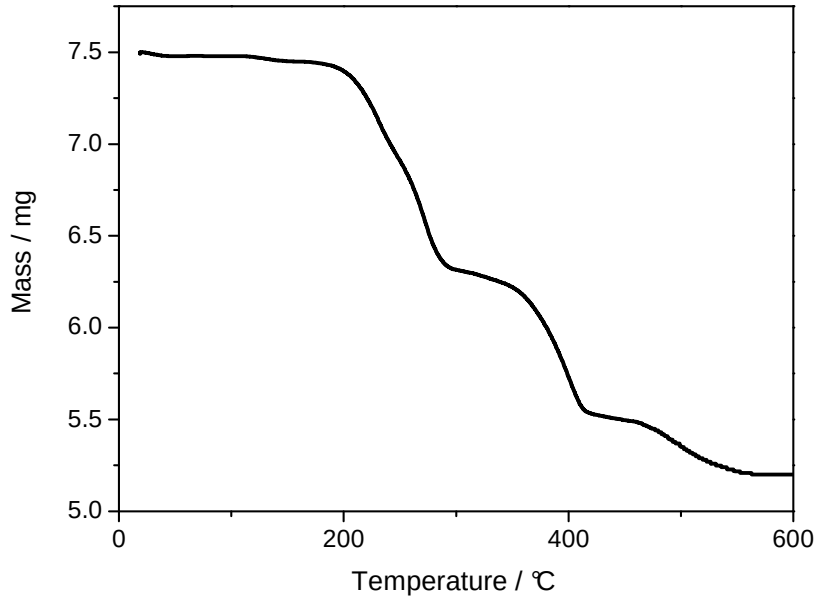

Figure 2.4. Thermogram of the $TBA_4H_3[PW_{11}O_{39}]$ salt.

The thermogravimetry curves may show several steps. The first one occurring at temperatures lower than about 150 ℃ corresponds to the loss of crystallization water leading to the anhydrous compound. Other steps, occurring at temperatures always higher than 200 ℃ (temperatures varying according to X, M and the counterion), correspond to the decomposition of the compound, involving the loss of organic material and destruction of the heteropolyanion. The results from thermogravimetry of the TBA-salts of the lacunary anions indicate the absence of hydration water because there was no mass loss between 40 and 150 ℃. The decompo sition of the salt occurs between 200 and 600 ℃, with a mass loss of 28.28 and 30.59 % for TBA-SiW_{11} and TBA-PW_{11}, respectively.

In the $PW_{11}Fe$ and $PW_{11}Co$ anions the loss of two and one hydration waters, respectively, was observed. The TBA salts of the $SiW_{11}Fe$ and $SiW_{11}Co$ polyanions presented no and one hydration water, respectively. The quantification of these water molecules was calculated as previously for the other polyoxotungstates. The quantity of TBA and coordination waters was determined taking into account the value of weight loss between 200 and, approximately, 500 ℃. These values of 30.0% for $SiW_{11}Co$ and of 28.1% for $SiW_{11}Fe$ show the presence of four TBA ions for each polyanion. The values of 28.3% for $PW_{11}Fe$ and 27.7% for $PW_{11}Co$ also indicate the presence of the same number of TBA ions for these polyanions.

From previous work carried out in our laboratory on the potassium and tetra-butylammonium salts of these anions it is known that the thermal decomposition of TBA salts occurs between, approximately, 150 and 650 ℃ [14]. The release of the metal M from the substituted polyanions accompanies the initial degradation of the organic cations, and the parent Keggin anion $[PW_{12}O_{40}]^{3-}$ is formed at approximately 300 ℃ as an intermediate in the decomposition of the TBA salts. The decomposition of the $[PW_{12}O_{40}]^{3-}$ then occurs at temperatures higher than 450 ℃.

2.5. Conclusions

In this chapter, the preparation of the polyoxotungstates used in the studies developed in the next chapters, was described. The tetra-butylammonium salt synthesis was explained in more detail than that of the potassium salts, and especially the silicotungstates because they are not so well described in the literature as the phosphotungstates.

All the compounds were characterized by several techniques and the obtained results are in good agreement with the data found in the literature.

2.6. References

[1] M. T. Pope, Heteropoly and Isopoly Oxometalates, Springer Verlag, 1983.

[2] W. Klemperer, *Inorg. Synth.* 27 (1990) 71.

[3] L. C. W. Baker, V. S. Baker, K. Eriks, M. T. Pope, M. Shibata, O. W. Rollins, J. H. Fang, L. L. Koh, *J. Am. Chem. Soc.* 88 (1966) 2329.

[4] C. M. Tourné, G. F. Tourné, *Bull. Soc. Chim. Fr.* 4 (1969) 1124.;

[5] C. M. Tourné, G. F. Tourné, S. A. Malik, T. J. R. Weakley, *J. Inorg. Nucl. Chem.* 32 (1979) 3875.

[6] T. J. R. Weakley, *J. Chem. Soc., Dalton Trans.* (1973) 341.

[7] A. Tezé, G. Hervé, *Inorg. Synth.* 27 (1990) 85.

[8] A. Tezé, G. Hervé, *J. Inorg. Nucl. Chem.* 29 (1977) 999.

[9] A. Tezé, G. Hervé, *Inorg. Synth.* 27 (1990) 89.

[10] F. Zonnevijlle, C. M. Tourné, G. F. Tourné, *Inorg. Chem.* 21 (1982) 2751.

[11] T. J. R. Weakly, S. A. Malik, *J. Inorg. Nucl. Chem.* 29 (1967) 2935.

[12] C. Brevard, R. Schimpf, G. Tourne, C. M. Tourne, *J. Am. Chem. Soc.* 105 (1983) 7059.

[13] M. M. Q. Simões, C. M. M. Conceição, J. A. F. Gamelas, P. M. D. N. Domingues, A. M. V. Cavaleiro, J. A. S. Cavaleiro, A. J. V. Ferrer-Correia, R. A. W. Johnstone, *J. Mol. Catal. A* 144 (1999) 461.

[14] J. A. F. Gamelas, F. A. S. Couto, M. C. N. Trovão, A. M. V. Cavaleiro, J. A. S. Cavaleiro, J. D. Pedrosa de Jesus, *Thermochim. Acta* 326 (1999) 165.

[15] J. A. F. Gamelas, M. R. Soares, A. Ferreira, A. M. V. Cavaleiro, *Inorg. Chim. Acta* 342 (2003) 16.

[16] M. S. Balula, J. A. Gamelas, H. M. Carapuça, A. M. V. Cavaleiro, W. Schlindwein, *Eur. J. Inorg. Chem* (2004) 619.

[17] L. C. W. Baker, J. S. Figgis, *J. Am. Chem. Soc.* 92 (1970) 3794.

[18] C. Rocchiccioli-Deltcheff, R. Thouvenot, *J. Chem. Research (S)* (1977) 46, *(M)* (1977) 549.

[19] C. M. Tourné, G. F. Tourné, *C. R. Acad. Sc. Paris, Série C* 266 (1968) 1363.

[20] C. M. Tourné, G. F. Tourné, *C. R. Acad. Sc. Paris, Série C* 266 (1968) 702.

[21] F. Zonnevijlle, C. M. Tourné, G. F. Tourné, *Inorg. Chem.* 21 (1982) 2742.

[22] K. Nakamoto, Infrared Spectra of Inorganic and Coordination compounds, 2ª Ed, Wiley-Interscience, John Wiley & Sons, New York (1963).

[23] K. Nomiya, Y. Sugie, K. Amimoto, M. Miwa, *Polyhedron* 6 (1987) 519.

[24] M. Fournier, R. Massart, *C. R. Acad. Sc. Paris, Série C* 276 (1973) 1517.

[25] E. Wang, Q. Wu, B. Zhang, R. Huang, *Transt. Met. Chem.* 16 (1991) 478.

[26] H. So, M. T. Pope, *Inorg. Chem.* 11 (1972) 1441.

[27] F. Couto, Master Thesis, University of Porto, 1994.

[28] C. Rocchiccioli-Deltcheff, M. Fournier, R. Franck, R. Thouvenot, *Inorg. Chem.* 22 (1983) 207.

[29] X. Zang, M. T. Pope, M. R. Chance, G. B. Jameson, *Polyhedron*, 14 (1995) 1381.
[30] S. Balula, PhD Thesis, University of Aveiro, 2003.

CHAPTER 3

FUNCIONALISATION OF GLASSY CARBON ELECTRODES WITH TETRA-BUTYLAMMONIUM SALTS OF KEGGIN-TYPE SILICOTUNGSTATES

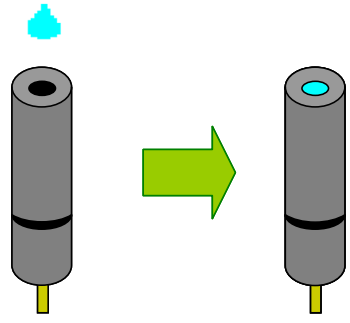

3.1. Introduction

The production of new devices for specific applications has been, in recent years, a rapidly growing area. Several approaches involve the immobilization of inorganic-organic hybrids. One of these approaches is based on the surface deposition of water-insoluble tetra-butylammonium POM salts onto carbon electrodes [1,2]. This procedure consists in the deposition of a small quantity of solution containing the POM over the electrode surface and subsequent solvent evaporation. An adsorbed single-layer is established as a non-organized and relatively thick deposit, as opposed to self-assembled-monolayer structures or to layer-by-layer assemblies. The main advantage of this method relies on the fact that it is possible to know the quantity of POM on the electrode surface.

The present chapter concerns the functionalisation of glassy carbon electrodes by deposition of tetra-butylammonium (TBA) salts of the lacunary (SiW_{11}) and of the mono-substituted anions ($SiW_{11}Co$ and $SiW_{11}Fe$). The deposited layer of TBA-POM was prepared by the simple method of solvent evaporation from acetonitrile solutions. The electrochemical behaviour of the immobilized polyanions in the TBA inorganic-organic hybrid microenvironment was examined and compared with their behaviour in aqueous solution (potassium salts), as well as with other related POMs, such as the phosphotungstate anions.

As far as we know, this is the first attempt to immobilize the Fe^{III} and Co^{II} substituted silicotungstate anions in this type of environment, producing a coating of crystallites by deposition through a one-step solvent evaporation process. The effect of solution pH on the voltammetric behaviour of the modified electrodes was evaluated. The morphological

features of the immobilized TBA-POM salts, on glassy carbon, were assessed by scanning electron microscopy.

Possible application of the $TBA_4H[SiW_{11}Fe(H_2O)O_{39}]$ modified electrode to the mediation of nitrite reduction was also tested.

3.2. Experimental

3.2.1. Reagents and solutions

Sodium sulphate (Riedel de Häen), sulfuric acid (Fluka), acetic acid (Pronalab) sodium acetate (Carlo Erba) and acetonitrile (Panreac, for instrumental analysis) were used as received). The tetra-butylammonium salts of the α-Keggin silicotungstates $[(C_4H_9)_4N]_4H_4[SiW_{11}O_{39}]$ (TBA-SiW_{11}), $[(C_4H_9)_4N]_4H_2[SiW_{11}Co^{II}(H_2O)O_{39}]\cdot H_2O$, (TBA-$SiW_{11}Co$) and $[(C_4H_9)_4N]_4H[SiW_{11}Fe^{III}(H_2O)O_{39}]$ (TBA-$SiW_{11}Fe$) were prepared as referred in the Chapter 2. The potassium salts $K_8[SiW_{11}O_{39}]\cdot 13H_2O$ (K-SiW_{11}), $K_6[SiW_{11}Co^{II}(H_2O)O_{39}]\cdot 12H_2O$, (K-$SiW_{11}Co$) and $K_5[SiW_{11}Fe^{III}(H_2O)O_{39}]\cdot 13H_2O$ (K-$SiW_{11}Fe$), were also prepared as described in Chapter 2.

Electrolyte solutions, for voltammetry, were prepared using ultra-pure water (18.2 mΩ cm at 25°C, Direct-Q 3 UV system, Millipore). Solutions within pH region 2.0-4.5 were prepared by mixing appropriate amounts of the H_2SO_4 (0.01 M) solution with a 0.10 M CH_3COOH/NH_4CH_3COO buffer (pH = 4.6). To test if there were effects due to changes of the ionic strength, $NaNO_3$ (0.50 M) was added to electrolyte solutions of different pH. No differences were observed in the voltammograms.

3.2.2. Instrumentation and methods

Cyclic voltammetry experiments were carried out using a computer controlled potentiostat (PGSTAT-12 /GPES software from Autolab/Ecochemie, Netherlands) in a conventional three-electrode compartment cell. The auxiliary and reference electrodes were a platinum wire (7.5 cm, BAS, MW-1032) and Ag/AgCl (sat. KCl) (BAS, MF-2052), respectively. The working electrode was a glassy carbon disc, GCE, (3 mm diameter, BAS, MF-2012), either modified with the POM salts or used as a bare surface.

A combined glass electrode (Hanna Instruments HI 1230), connected to an Inolab pH level 1 pH meter, was used for the pH measurements.

A Zeiss optical inverted microscope, connected to a Canon digital camera, was used for optical microscopy. Scanning electron microscopy was conducted on an Analytical FE-SEM SU-70 Hitachi, UHR 1.0 nm/15 kV (1.6 nm/1 kV).

3.2.3. Preparation of the modified electrodes and voltammetric procedures

The unmodified glassy carbon electrode was calibrated regularly using $[Fe(CN)_6]^{3-/4-}$ redox couple (ca. 1.01 mM) as the electroactive probe. In 0.50 M KCl solution, $[Fe(CN)_6]^{3-/4-}$ presented the expected reversible characteristics and the mid wave potential ($E_{1/2}$) was +267 mV vs. Ag/AgCl, with a peak-to-peak separation (ΔE_p) of 70 of $\pm$ 4 mV.

Prior to coating, the GCE was conditioned by a polishing/cleaning procedure using aluminium oxide, grain size 0.05 μm (Buehler-Masterprep), on a microcloth polishing pad (BAS Bioanalytical System Inc). The electrode was then rinsed with ultra-pure water and put in an ultrasonic bath cleaner for a final cleaning step by sonication, for 60 s.

The modified electrodes were prepared as follows: a 3 μL micro-drop of the selected TBA-POM acetonitrile solution (3 mM) was placed onto the surface of the glassy carbon electrode and the solvent was allowed to evaporate for about 15 min at room temperature. Studies using other concentrations of TBA-silicotungstate acetonitrile solutions (1 and 6 mM), were performed and higher microdrop volumes, by successive deposition (3+3 μL and 3+3+3 μL), were also tested.

An activation step was done by performing a 60 multicycle scan between –0.85 V and +0.4 V, in 0.01 M H_2SO_4. Thereafter, the modified working electrode was ready to use.

After preparation, the modified electrodes were examined by optical microscopy. In some cases, the modified electrodes were also checked at the end of the voltammetric experiments.

The electrocatalytic nitrite reduction experiments were carried out in pH 2.0 H_2SO_4 solutions with successive addition of nitrite.

Voltammetric measurements were made at room temperature (~ 20 ºC). Solutions were degassed with pure nitrogen for 5 minutes before the measurements and blanketed with N_2 during the measurements.

3.3. Voltammetric behaviour of lacunary and metal-substituted silicotungstate anions in aqueous media

The majority of the voltammetric studies reported for lacunary SiW_{11} and transition metal substituted $SiW_{11}M$ anions were performed in aqueous acidic media, generally for pH < 6 [3-8]. In these conditions, all compounds presented two reversible or quasi-reversible 2-electron consecutive waves at negative potentials, corresponding to the reduction of W^{VI} [4-6,8]. Most of these reductions involve the uptake of protons to prevent negative charge buildup [9].

In the present work, the electrochemical behaviour of the potassium salts (SiW_{11} and its mono-substituted Fe and Co derivatives), was studied in a systematic way in aqueous solution in the pH range of 2.0 to 4.5 (in the same experimental conditions used for the modified electrodes described in the next section). In this way, a proper comparison between the results obtained for the deposited TBA polyoxotungstates with those for the K^+ salts in solution may be carried out.

Figure 3.1 shows cyclic voltammograms for the water soluble K^+ salts of SiW_{11}, $SiW_{11}Fe$, and $SiW_{11}Co$, at pH 2.0, for a scan rate of 50 mV s^{-1}.

Table 3.1 resumes the data obtained for the corresponding anions, where E_{pc} is the cathodic peak potential, $\partial E_{pc}/\partial pH$ is the slope over the pH range from 2.0 to 4.5 at 50 mV s^{-1} and $|\Delta E_p| = |E_{pc}-E_{pa}|$).

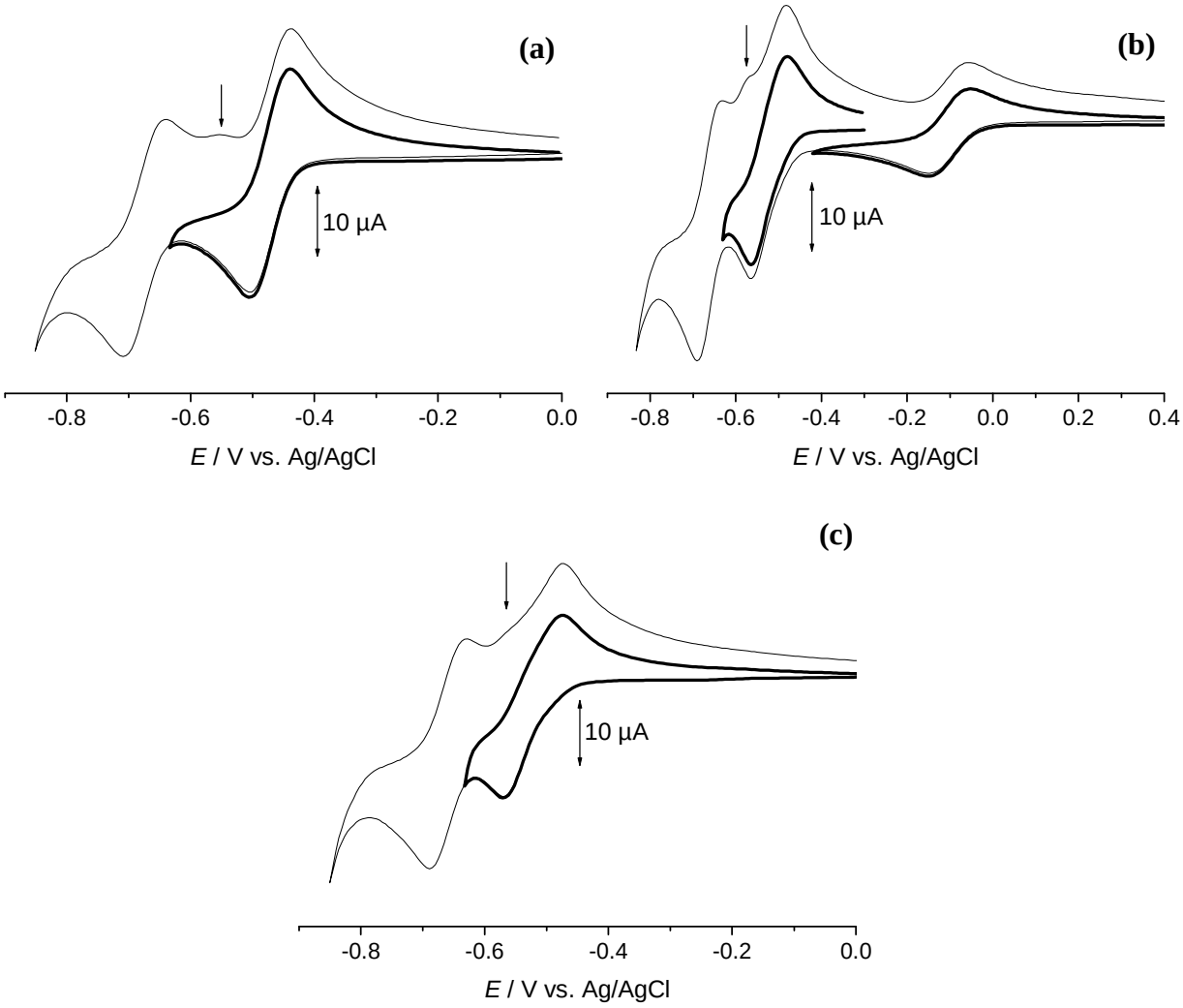

Figure 3.1. Cyclic voltammograms of K^+ salts (1 mM), in pH 2.0 buffer solution (H_2SO_4/HAc/NaAc), ν = 50 mV s^{-1}: (a) SiW_{11}, (b) $SiW_{11}Fe$ and (c) $SiW_{11}Co$. Also shown are the partial voltammograms for the first pair of W peaks and for the iron pair in $SiW_{11}Fe$ (bold lines). Arrows show the oxidation peaks for β-isomers.

Table 3.1. Cyclic voltammetric data for the two W redox processes and for the iron redox process of the K^+ silicotungstate salts at 50 mV s^{-1} and pH=2.0 buffer solution (H_2SO_4/HAc/NaAc).

		SiW_{11}	$SiW_{11}Fe$	$SiW_{11}Co$
First $W^{VI/V}$ process	E_{pc} / mV	- 501	-563	-566
	$E_{1/2}$ / mV	-471	-523	-519
	$\|\Delta E_p\|$ / mV	61	81	94
	$\|E_{pc}-E_{p/2}\|$ / mV	37	42	38
	$\partial E_{pc}/\partial$pH	-67	-99	-84
Second $W^{VI/V}$ process	E_{pc} / mV	-705	-690	-688
	$E_{1/2}$ / mV	-674	-663	-659
	$\|\Delta E_p\|$ / mV	62	57	58
	$\|E_{pc}-E_{p/2}\|$ / mV	33	32	33
	$\partial E_{pc}/\partial$pH	-68	-99	-90
$M^{III/II}$ process	$E_{1/2}$ / mV	---	-97	---
	$\|\Delta E_p\|$ / mV	---	80	---
	$\|E_p-E_{p/2}\|$ / mV	---	53	---
	$\partial E_{pc}/\partial$pH	---	---	---

For the cobalt-substituted species no Co-metal reduction/oxidation peaks were seen within the potential range studied. For all anions the values of $E_{1/2}$ were similar to published values using other electrolyte solutions [6-8]. In the experimental timescale used (scan rates in the range 20 to 750 mV s^{-1}), the values of $E_{1/2}$ did not change significantly (< 4%) with the scan rate and the ratio of anodic to cathodic peak currents was ca. 1. Furthermore, the first W cathodic and anodic peak currents were diffusion controlled and slopes log I_p vs. log v were ca. 0.5 (Fig. 3.2a).

The W peak potentials varied linearly with pH, with slopes E_p vs. pH of -67 and -68 mV/pH unit for the SiW_{11} anion and ca. -84 to -99 mV/pH unit for the metal-substituted anions. Figure 3.2b shows the relationship between peak potential (E_{pc}) and pH for the first W reduction process.

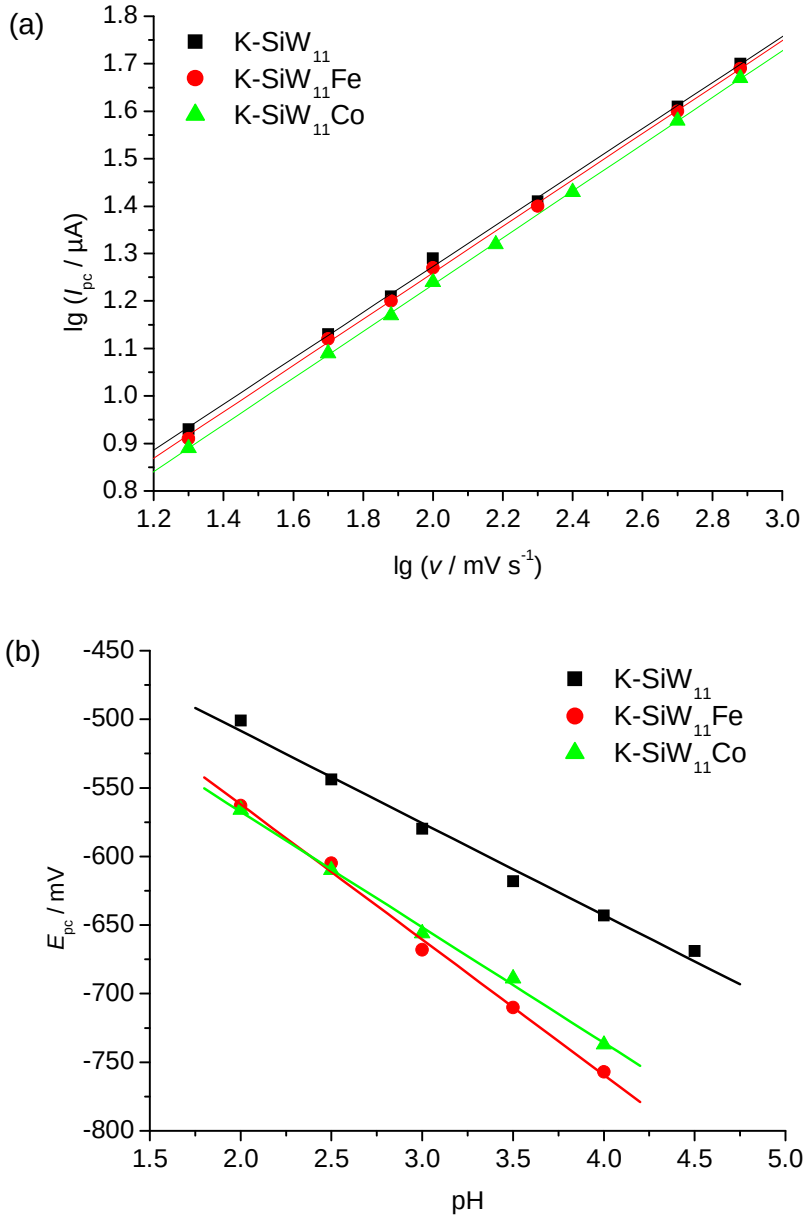

Figure 3.2. Plots of: (a) lg I_{pc} versus lg ν in pH = 2.0 buffer solution (H_2SO_4/HAc/NaAc) and (b) E_{pc} versus pH in buffer solutions, ν = 50 mV s^{-1}.

Thus, in the present experimental conditions, assuming a Nernstian behaviour, the first and second W reductions in SiW_{11} constitutes two two-electron/two-proton global processes (i.e. four W^{VI} are reduced within the oxo-W cage). For $SiW_{11}Fe$ and $SiW_{11}Co$, the slopes were slightly higher and the two-electron reduction is accompanied by addition of two to three protons. For $SiW_{11}Co$, at pH ca. 4, the first W wave was attributed to a two-

electron/two-proton process [4]. However, for $SiW_{11}Fe$, there was evidence of a higher protonation requirement [8].

Therefore, for the first W process, one might expect the protonated-reduced species to be reoxidized at more positive potentials, leading to larger ΔE_p (apparent) values than those predicted for the same process in the absence of protonation. Actually, for all soluble polyoxotungstates, although the $|E_p-E_{p/2}|$ parameter for the first W wave pointed to the occurrence of a two-electron process, the ΔE_p values were all above 60 mV. This fact indicated that the W ($2e^-$) process cannot be viewed as a simple EE reaction with the simultaneous transfer of $2e^-$ [10]. The large values of ΔE_p may suggest kinetic constraints.

For the metal-substituted species, the half-wave potentials of the first W peaks were shifted towards more negative values, compared with those of the lacunary anion. This is in agreement with the reported data [6,11]. For the $SiW_{11}Co$, anion the shape of the reduction/oxidation W peaks was slightly different and may indicate kinetic complications, which is also consistent with the relatively high ΔE_p values.

Furthermore, for all polyanions, a small oxidation peak was detected whenever the voltammogram was extended up to the second W reduction process (arrows in Fig. 3.1). The intensity of these peaks was dependent on the scan rate and they could only be seen for values lower than 100 mV s^{-1}. The appearance of those peaks may be attributed to the formation of β isomers that are oxidised at more positive potentials than the corresponding α isomers, as referred to in Chapter 2 [9]. A similar behaviour, described first for SiW_{11} [8], was also observed for $PW_{11}Ni$, $SiW_{11}Co(II)$, $SiW_{11}Co(III)$ and $SiW_{11}Mn(II)$ [5,6].

The redox process of the $Fe^{III/II}$ metal centre was clearly seen but the reversibility criteria point to the occurrence of a quasi-reversible one-electron process. There was no evidence of the influence of protons on the $Fe^{III/II}$ redox process.

3.4. Voltammetric behaviour of the hybrid TBA-silicotungstate modified electrodes in acidic media

Three different concentrations of TBA-silicotungstate solutions (1, 3 and 6 mM) were used to prepare the modified electrodes, using always the same drop volume (3 µL). The one that showed better results was the solution with 3 mM concentration. There was an increase in peak current with increasing concentration. However when a 6 mM concentration solution was used, the peaks were not as well defined as for 1 and 3 mM

concentrations. So, a 3 mM solution was chosen for the drop volume test. Here, three volumes were tested by successive deposition and by a single deposition. The results showed a decrease in the peak currents in the order 3, 3+3 and 3+3+3 µL. The deposition of a single 6 and 9 µL volume was also carried out and where drop spread over the whole surface, not just the glassy carbon. Thus, the conditions chosen for all future studies were 3 µL of a 3 mM TBA-silicotungstates acetonitrile solution.

An electrochemical pre-treatment, consisting of multi-cycle scanning (cf. Experimental), was also performed and led to a better definition of the CVs. This is indicative of reorganization and/or wetting of the deposited layer of the TBA-silicotungstate salts leading to an increase of the electron transfer rate from the electrode surface to the redox sites in the polyanion, which is in a TBA microenvironment.

3.4.1. Effect of scan rate and pH

The voltammetric features of the TBA-silicotungstate salts immobilized at the GCE surface were similar, in terms of the number of voltammetric waves, to those observed in aqueous solution for the corresponding soluble polyanions, at identical pH.

The voltammograms of the TBA-silicotungstate salts immobilized on the GCE presented two pairs of peaks for potentials lower than ca. -0.3 V (Fig. 3.3) assignable to the reduction/oxidation of the W atoms, *i.e*., corresponding to the expected four-electron global reduction process as seen for the same POM salts in aqueous solutions. The first pair was always well defined but the resolution of the second one was worse for higher pH values.

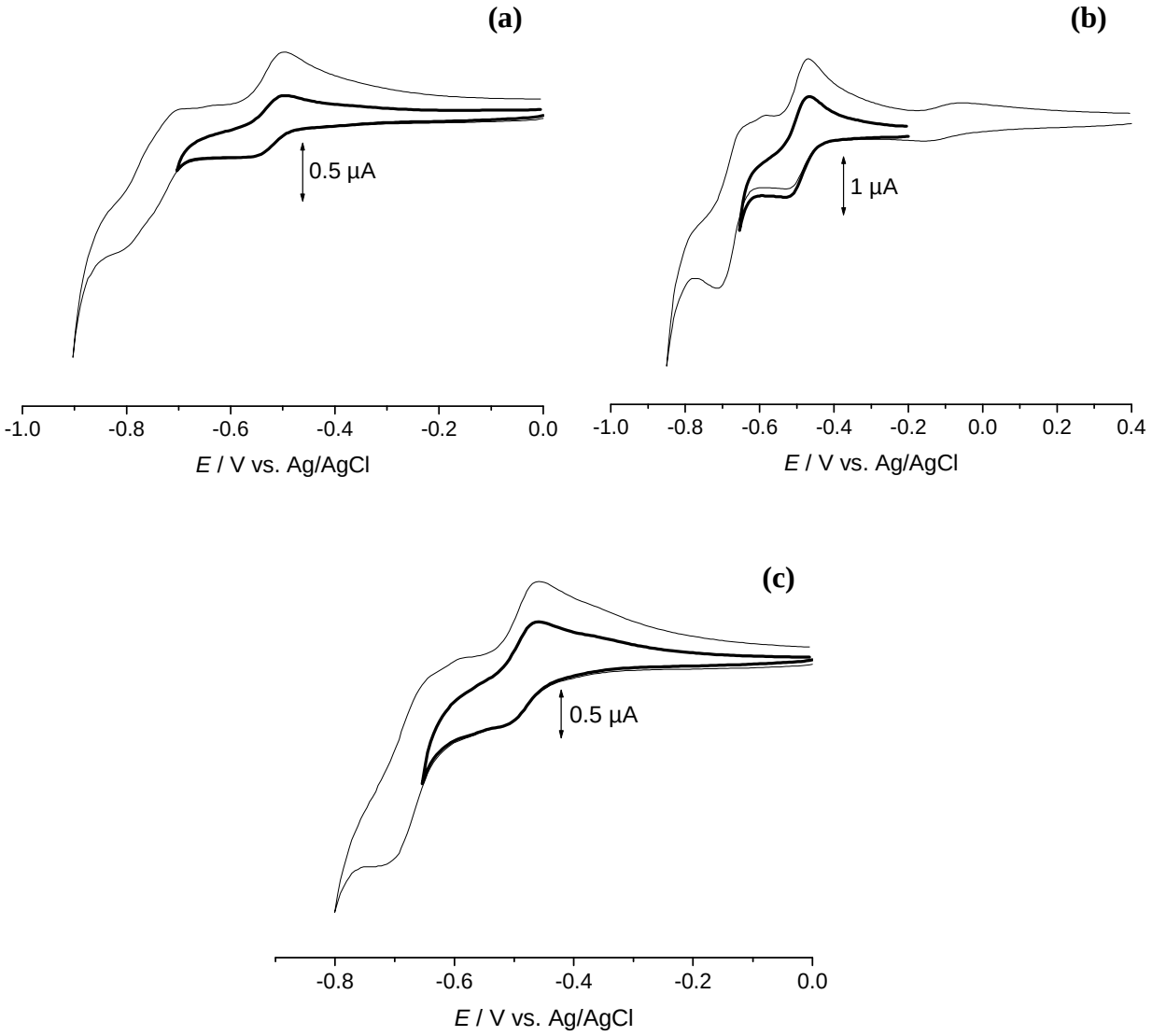

Figure 3.3. Cyclic voltammograms for immobilized TBA-polyanions on GCE immersed in pH 2.0 buffer solution (H_2SO_4/HAc/NaAc), ν = 50 mV s^{-1}: (a) SiW_{11}, (b) $SiW_{11}Fe$ and (c) $SiW_{11}Co$. Also shown are the partial voltammograms for the first pair of W peaks (bold lines).

Figure 3.4 shows typical cyclic voltammograms for the TBA-$SiW_{11}Fe$ electrode for different scan rates at pH 2.0. The signals for reduction/oxidation of the substituting metal ($Fe^{III/II}$) were observed only for this TBA-silicotungstate, at ca. -0.1 V. Co(II) is not electroactive within the working potential window.

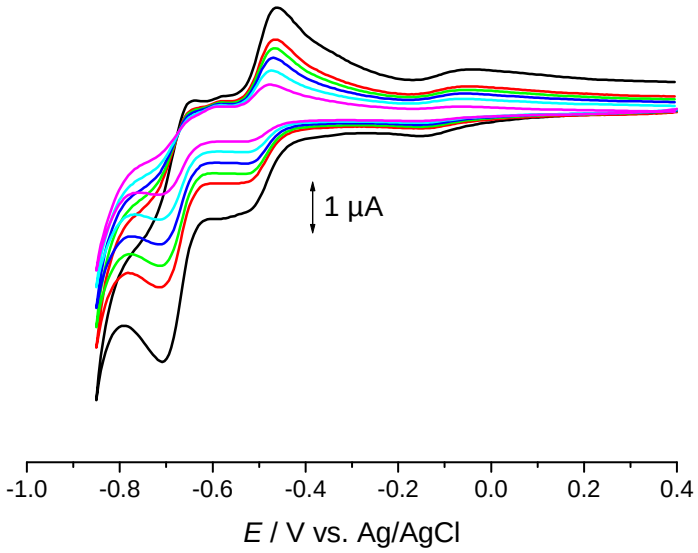

Figure 3.4. Cyclic voltammograms for TBA-$SiW_{11}Fe$ modified electrode in pH 2.0 buffer solution (H_2SO_4/HAc/NaAc) at different scan rates (10, 25, 50, 75, 100 and 250 mV s^{-1}).

The peak-to-peak separations of all pairs of peaks (W and Fe) were not close to zero (Table 3.2), as would be expected for a reversible redox process confined to an immobilized species. In fact, the representation of lg I_p vs. lg ν gave slopes close to 0.5. The expected behaviour (I_p proportional to ν) for a surface-confined redox process was not observed for any of the immobilized TBA-silicotungstates. The same trend was observed for other POM modified electrodes [2,12,13].

The potentials for the W reduction processes of the TBA-POM functionalised electrodes were less negative than the values for the corresponding aqueous anions (cf. Table 3.1 and 3.2). This might indicate thermodynamic facilitation of the reduction of the immobilized polyanions. Comparing with the potassium salts in solution, this effect was more obvious for the metal-substituted TBA salts in comparison with the lacunary anion. Taking into consideration the TBA-polyanion formula, (four TBA cations, protons and polyanion) one possibility is that protonated anions with a (-4) global charge are present in the immobilised phase. Therefore, no net charge differences are expected for the three TBA salts and this could account for the similarity of peak potentials in contrast with the data for the K^+ salts in solution. Similar results were obtained with TBA phosphotungstates immobilized on glassy carbon electrodes [2].

Table 3.2. Cyclic voltammetric data for the adsorbed TBA-silicotungstates on the GCE at 50 mV s^{-1} and pH=2.0 buffer solution (H_2SO_4/HAc/NaAc).

		SiW_{11}	$SiW_{11}Fe$	$SiW_{11}Co$
First $W^{VI/V}$ process	E_{pc} / mV	-498	-503	-498
	$E_{1/2}$ / mV	-476	-489	-479
	$\|\Delta E_p\|$ / mV	44	29	39
	$\|E_{pc}-E_{p/2}\|$ / mV	27	23	28
	$\partial E_{pc}/\partial$pH [a]	-67	-122	-105
Second $W^{VI/V}$ process	E_{pc} / mV	-698	-704	-702
	$E_{1/2}$ / mV	-669	-675	-676
	$\|\Delta E_p\|$ / mV	58	58	52
	$\|E_{pc}-E_{p/2}\|$ / mV	35	32	33
	$\partial E_{pc}/\partial$pH [b]	---	---	---
$M^{III/II}$ process	$E_{1/2}$ / mV	---	-116	---
	$\|\Delta E_p\|$ / mV	---	90	---
	$\|E_p-E_{p/2}\|$ / mV	---	73	---
	$\partial E_{pc}/\partial$pH [a]	---	---	---

[a] slope for the pH range 2.0 to 4.5 at 50 mV s^{-1}.
[b] not possible due to lower resolution of peaks with increasing pH values.

There was a marked linear dependence of pH on the first W peak potentials, with slopes of -67 mV/pH unit for TBA-SiW_{11} and -105 to -122 mV/pH unit for the metal substituted TBA-POM species (Co- and Fe-substituted, respectively). These data show that the redox mechanism at the W atoms immobilized as their TBA salts requires the involvement of protons. So, for the TBA-SiW_{11} electrode a $2e^-/2H^+$ redox process occurs at the first W wave. For both TBA-$SiW_{11}Fe$ and TBA-$SiW_{11}Co$ electrodes data points to $2e^-/4H^+$ redox processes. In these cases, it seems that the W redox processes is accompanied by the uptake of a larger number of protons than for the corresponding anions in aqueous solution. Similar behaviour was observed for a series of phosphotungstates (lacunary and metal substituted species) also immobilized on glassy carbon by the present methodology [2].

As was seen for soluble $SiW_{11}Fe$ there were no effects of pH on the iron process. The electron process at the iron centre ($E_{1/2}$ = - 116 mV) was now less reversible than in solution, with ΔE_p ca. 90 mV for v = 50 mV s^{-1}. This parameter was independent of pH

within the range 2.0 - 4.0. Comparing also with $PW_{11}Fe$ immobilized by the same method (ΔE_p ca. 83 mV for v = 50 mV s^{-1}) [2] the iron process on the silicotungstate modified electrode was less reversible.

3.4.2. Morphological aspects

The morphology of the TBA-POM deposits was examined by optical microscopy to confirm that the prepared electrodes were suitably covered with the TBA-POM salt (higher magnification × 100). In general, all electrodes appeared non-homogeneous with higher deposition densities at the edges, certainly due to the solvent evaporation procedure. Additionally, the electrode surface appeared as a tri-dimensional structure with high "apparent" roughness. Among all of these, the TBA-SiW_{11} modified electrode appeared to show higher roughness and crystal size. Figure 3.5 shows typical images for a TBA-SiW_{11} modified electrode at × 5 and x 50 of magnification, respectively. It can be seen that the surface is fully covered and with large crystallites can be seen, especially in the central zone.

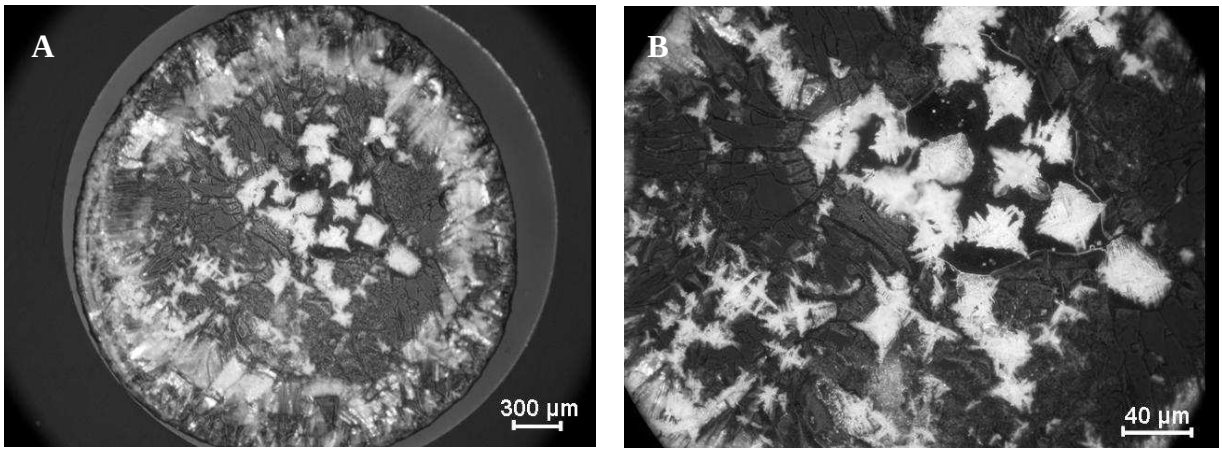

Figure 3.5. Typical optical micrographs for a TBA-SiW_{11}-GCE. (A) General view of the electrode surface: × 5 magnification. (B) Crystallites on the electrode surface: × 50 magnification.

Figure 3.6 shows typical images of a TBA-$SiW_{11}Fe$ modified electrode taken at two different magnifications. At × 5 (Fig. 3.6A), the surface shows several circular domains with different dimensions (the crystallites correspond to the darker parts) seen in the

figure. Amplification of the image, either at the circular border domains or at any site of the electrode centre revealed the presence of highly populated crystallite regions (Fig 3.6B). For this latter magnification, the image was taken under polarized light for better resolution (the microcrystallites are now seen in white).

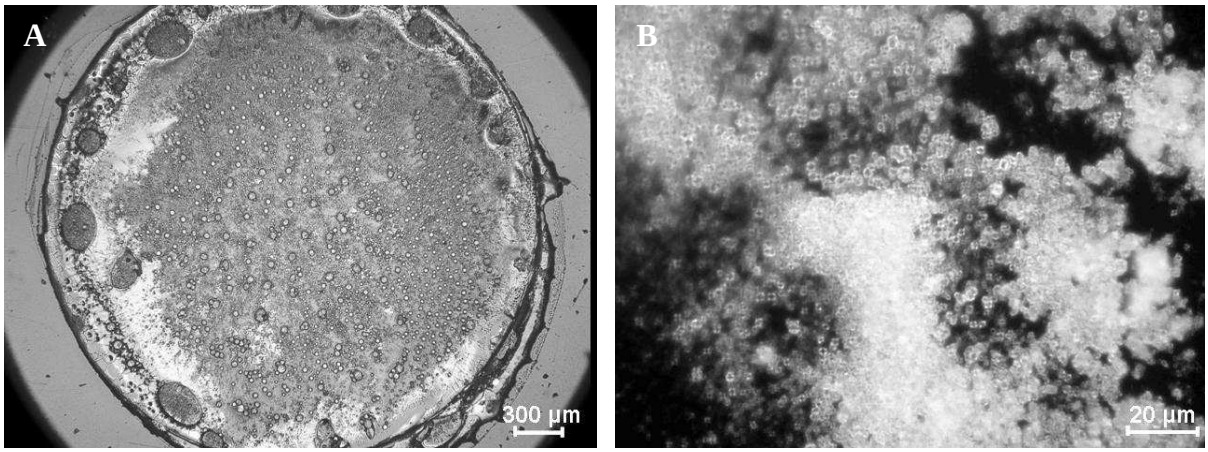

Figure 3.6. Typical optical micrographs for a TBA-SiW_{11}Fe-GCE. (A) General view of the electrode surface: × 5 magnification. (B) Crystallites on the electrode surface: × 100 magnification (under polarized light).

To gather more information on the morphology of the electrodes, scanning electron microscopy (SEM) was used. Figure 3.7 (A–C) presents the SEM micrographs for the three TBA-POM modified electrodes, acquired at the same magnification. The electrode surfaces were non-regular, with areas pointing to fast growth of the crystals and/or to the development of low crystallinity. Generally, the TBA-SiW_{11}Co deposits showed lower roughness.

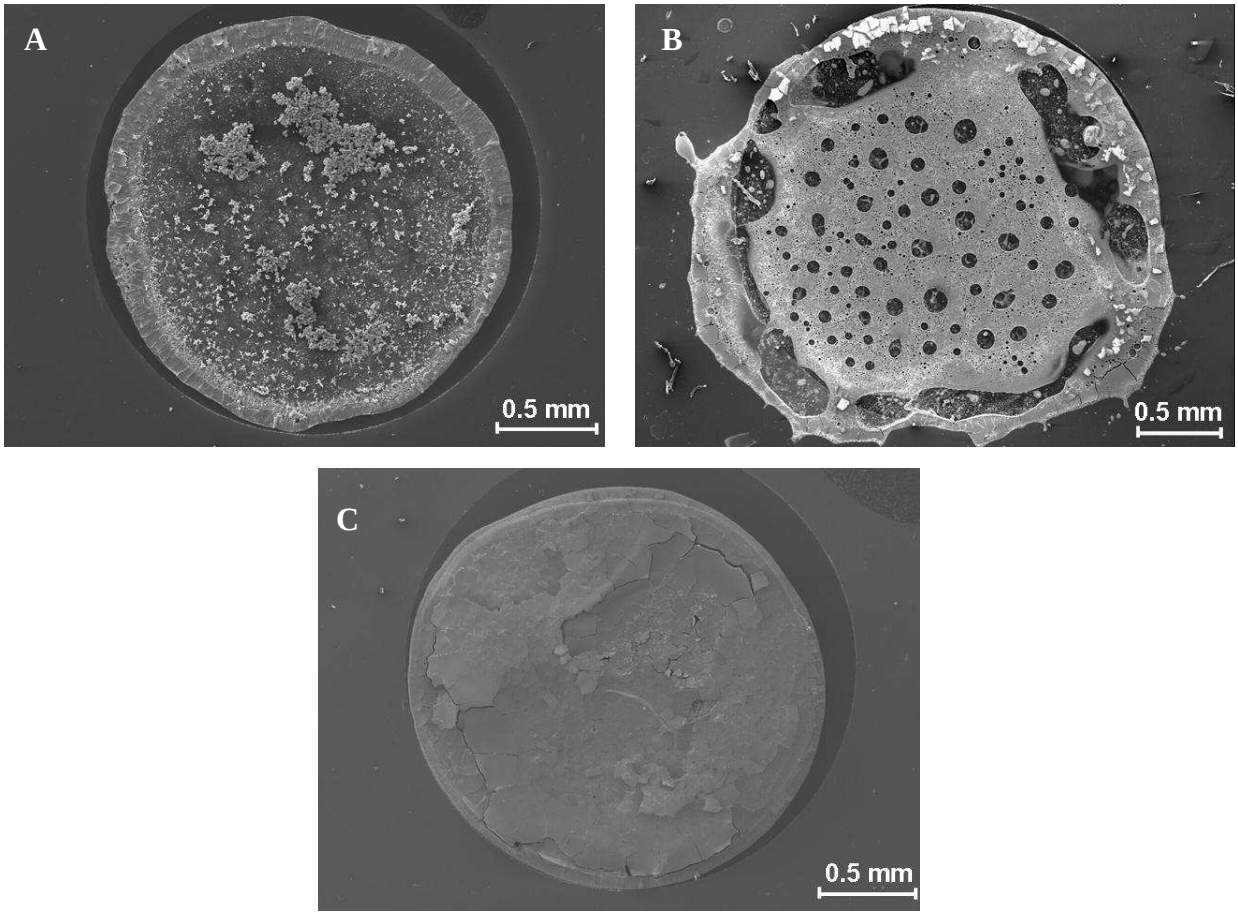

Figure 3.7. Typical SEM micrographs for a: (A) TBA-SiW_{11}-GCE, (B) TBA-SiW_{11}Fe-GCE and (C) TBA-SiW_{11}Co-GCE salts (all micrographs were acquired at the same x30 magnification).

For the TBA-SiW_{11} deposit (Fig. 3.8A), it seems that the solvent evaporation process leads to the development of relatively large cubic crystals (<15 μm), especially in the central zones. Near the border, the formation of small size cubic crystals and dendrites, was also observed (Fig. 3.8B).

For the TBA-SiW11Co deposits, at magnifications below x1000, mainly a compact surface with apparently low crystallinity was seen. There were cracks on the surface which revealed the presence of very small crystallites underneath. A dense population of microcrystallites of very low micrometer dimensions, i. e. smaller than 5 μm (Fig. 3.8E and F), could only be detected at higher magnification.

For comparison, the SEM images of the TBA-POM salts in powder form were also recorded and can be seen in Fig. 3.9.

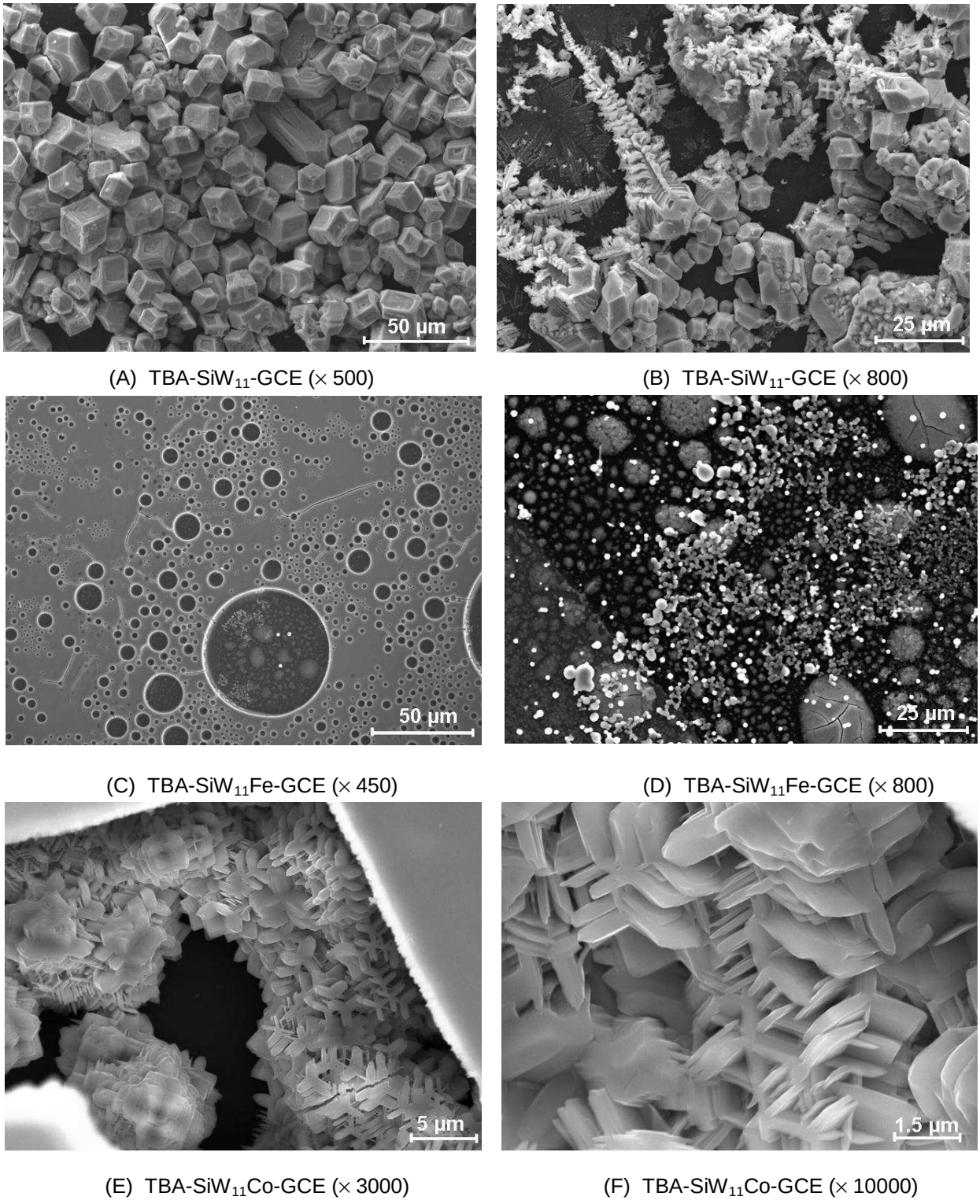

(A) TBA-SiW_{11}-GCE (× 500)

(B) TBA-SiW_{11}-GCE (× 800)

(C) TBA-$SiW_{11}Fe$-GCE (× 450)

(D) TBA-$SiW_{11}Fe$-GCE (× 800)

(E) TBA-$SiW_{11}Co$-GCE (× 3000)

(F) TBA-$SiW_{11}Co$-GCE (× 10000)

Figure 3.8. Typical SEM micrographs for TBA-POM salts deposited on GCE.

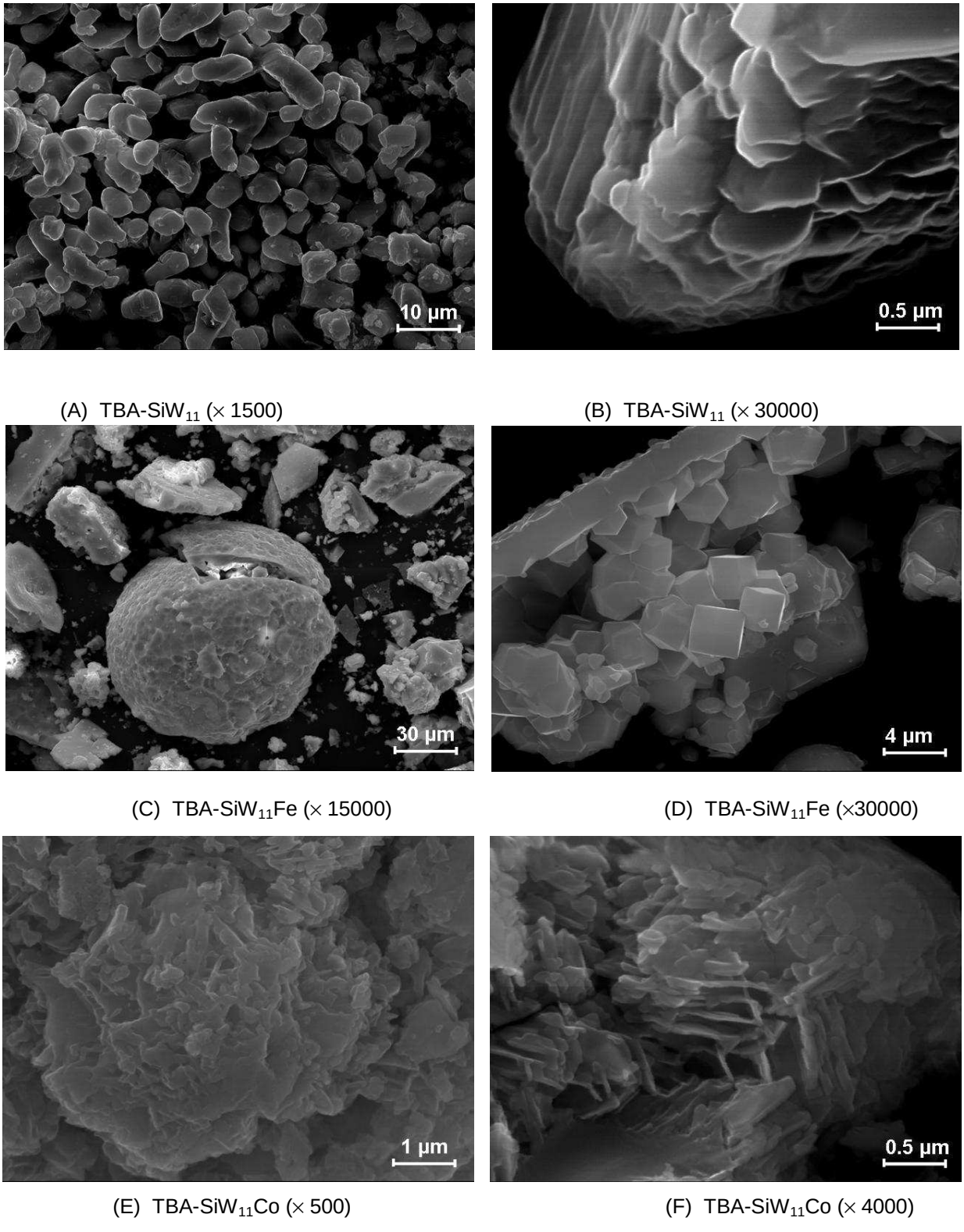

(A) TBA-SiW_{11} (× 1500)

(B) TBA-SiW_{11} (× 30000)

(C) TBA-$SiW_{11}Fe$ (× 15000)

(D) TBA-$SiW_{11}Fe$ (×30000)

(E) TBA-$SiW_{11}Co$ (× 500)

(F) TBA-$SiW_{11}Co$ (× 4000)

Figure 3.9. Typical SEM micrographs for solid TBA-POM salts.

The morphologies of the powder compounds and of the TBA-POM deposits are similar. The TBA salts of mono-substituted silicotungstates are isomorphs and crystallize in the cubic system [14]. Figure 3.9 C shows the presence of circular accumulations for the TBA-$SiW_{11}Fe$ powder that could also be seen for the TBA-POM deposits (Fig. 3.8 D). Increasing magnification in this area (Fig. 3.9 D) reveals that the TBA-$SiW_{11}Fe$ powder that is obtained at the end of the synthesis process (also recrystallised from acetonitrile) gave cubic-like crystals. Similarities between powder and deposit could also be observed for the TBA-$SiW_{11}Co$ salts.

An important question is whether the morphological characteristics influence the voltammetric properties of the TBA-POM immobilized salts. Since the ΔE_p values did not approach zero (cf. Table 3.2), one might assume that the diffusion of protons from solution to the deposited TBA-POM crystallites is rate determining. One also has to consider that these types of modified electrode suffer from heterogeneity of the crystallites and exposure of different crystal faces to the solution. In fact, the present method, although a very simple and fast procedure, produces heterogeneous micrometer-thick deposits of TBA-POM salts. Nevertheless, the glassy carbon surface becomes fully covered with micro-aggregates of the corresponding salts. Some other kinetic restrictions might also be occurring through out the whole process.

In order to evaluate how the heterogeneity of the deposits and the reproducibility of the preparation method influenced the reproducibility of the electrochemical measurements, eight different electrodes (prepared by the same methodology), for each of the salts TBA-$SiW_{11}Co$ and the TBA-$SiW_{11}Fe$, were used to measure the peak current corresponding to the first W reduction. The relative standard deviations of the values obtained were 3% for the TBA-$SiW_{11}Fe$ electrode and 16% for the cobalt polyoxotungstate TBA salt. Peak potentials were unchanged (within an experimental error of $\pm$ 5mV). At first glance, the TBA-$SiW_{11}Co$ electrodes were less reproducible and/or more susceptible to kinetic constraints that could influence peak currents. This is consistent with the general morphological aspect of those electrodes, where diffusion of protons might be more difficult, as well as with the voltammetric data (low reversibility).

The medium term stability was determined for a single TBA-$SiW_{11}Fe$ electrode. After it had been used for a time working day, it was kept overnight in its protection case. On the second day it was used again in similar experiments, such as scan rate effect in pH 2.0 buffer solution (H_2SO_4/HAc/NaAc), and the results were identical. The response then began to diminish and after 6 working days the peak currents decreased to ca. 30% of the original values (Fig. 3.10), although peak potentials remained unchanged.

Conversely, the TBA-SiW_{11} modified electrode was fragile and, after one day, the W peak currents began to decrease, pointing to a faster depletion of the adsorbed lacunary-TBA salt from the electrode surface. This may be related to the observed higher crystal size for TBA- SiW_{11}, leading to greater mechanical fragility or to a lower stability of this anion in the pH conditions used, in comparison with the metal substituted anions.

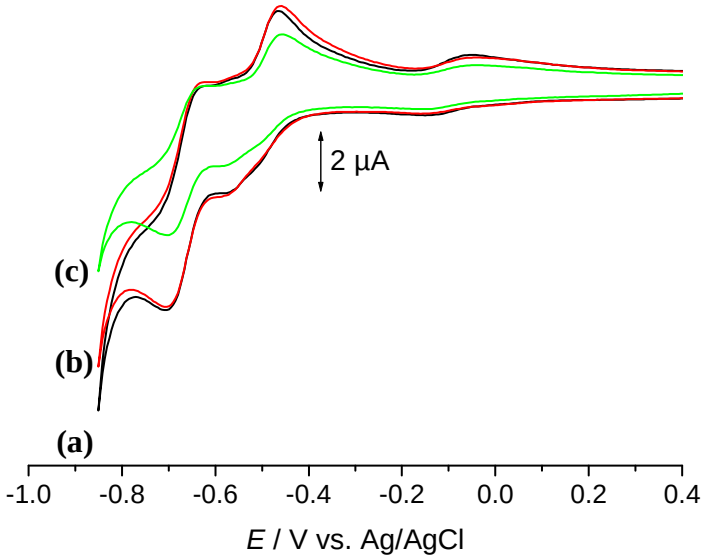

Figure 3.10. Cyclic voltammograms for immobilized TBA- $SiW_{11}Fe$ on the GCE (same conditions as in Fig. 3.3), (a) first; (b) second and (c) sixth working day.

3.3.2.3. Application of the TBA-$SiW_{11}Fe$ modified electrode in the reduction of nitrite

Concerning the applicability of a POM species as reduction electrocatalyst, it is convenient that the reduced form, which is the catalytic mediator, can provide a large number of electrons at a suitable potential and not too negative because of interference from H_2 evolution. As was seen previously for the functionalised electrodes, there was no significant difference between the $E_{1/2}$ values for the first W reduction process of the lacunary and its metal substituted species. More interesting is the fact that the potentials for the metal-substituted TBA-POM modified electrodes were less negative than the values for the corresponding aqueous soluble anions (cf. Tables 3.1 and 3.2). Therefore, the mediation of a reaction such as the reduction of nitrite might be favoured for the metal-substituted TBA-POM modified electrodes. Consequently, the TBA-$SiW_{11}Fe$ electrode was chosen for preliminary tests as a mediator for the electroreduction of nitrite in pH 2.0 H_2SO_4 solutions.

For nitrite, one difficulty that comes up is which are the actual reactive species in acidic solution. Equations (1) and (2) suggest that HNO_2 and/or NO should be the reactive species, at least up to pH 3.3 [15,16]. HNO_2 disproportionates in fairly acidic solutions, even though the rate of this process is known to be low [15,16]. It has been claimed that nitrous acid should be the reactive form of nitrite between pH 2 and 8 in the case of the iron-substituted polyoxotungstates [17].

$$HNO_2 \rightleftharpoons H^+ + NO_2^- \quad (3.1)$$

$$3HNO_2 \rightleftharpoons H^+ + NO_3^- + 2NO + H_2O \quad (3.2)$$

Figure 3.11 presents voltammograms for the TBA-$SiW_{11}Fe$ modified electrode, in the absence and in the presence of increasing concentrations of nitrite, in the interval [0 - 0.09 mM], at 20 mV s^{-1}.

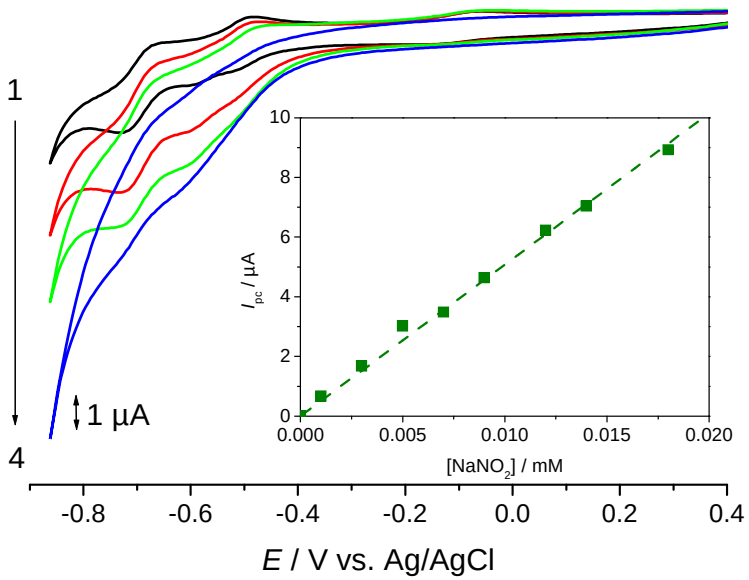

Figure 3.11. Catalytic activity of immobilised TBA-$SiW_{11}Fe$ in the presence of different amounts of nitrite. Cyclic voltammograms obtained in the absence and in the presence of increasing concentrations of nitrite, in the interval [0 - 0.09 mM]: a) 0; b) 0.01; c) 0.04 and d) 0.09 mM. Inset: plot of the catalytic peak current at -0.6 V vs. the concentration of nitrite. Experimental conditions: pH 2.0 buffer solution (H_2SO_4/HAc/NaAc), ν = 20 mV s^{-1}.

A solution of nitrite with the same concentrations does not present any reduction signals. As Fig. 3.11 depicts, for increasing concentrations of nitrite in solution the peak

current of the first W reduction process (ca.-0.6V) increased whereas the corresponding oxidation current decreased. This is typical for a reduction process mediated by a reduction catalyst. The following equations present the possible overall process [16].

$$SiW_{11}{}^{VI}Fe(H_2O)O_{39}{}^{5-} + 2e^- + 4H^+ \rightarrow H_4SiW_2{}^{V}W_9{}^{VI}Fe(H_2O)O_{39}{}^{3-} \quad (3.3)$$

$$H_4SiW_2{}^{V}W_9{}^{VI}Fe(H_2O)O_{39}{}^{3-} + n\ HNO_2 \rightarrow SiW_{11}{}^{VI}Fe(H_2O)O_{39}{}^{5-} + n\ N\ products \quad (3.4)$$

The inset in Fig. 3.11 shows a plot of the catalytic peak current at -0.6 V vs. the concentration of nitrite. A linear range could only be defined for a nitrite concentration below 0.02 mM. These results show that TBA-$SiW_{11}Fe$ salts immobilised on a GCE is a mediator for the reduction of nitrite, as reported for this anion in aqueous solution (e.g. [17,18]).

A similar behaviour was observed for $SiW_{11}Fe$ in aqueous solution. Curves (a-d) in Figure 3.12 show the electrochemical responses for an NO_2^- concentration of 0, 1.00, 2.00 and 3.00 mM, obtained in H_2SO_4 aqueous solution (pH 2.0), at the scan rate of 20 mV s^{-1}.

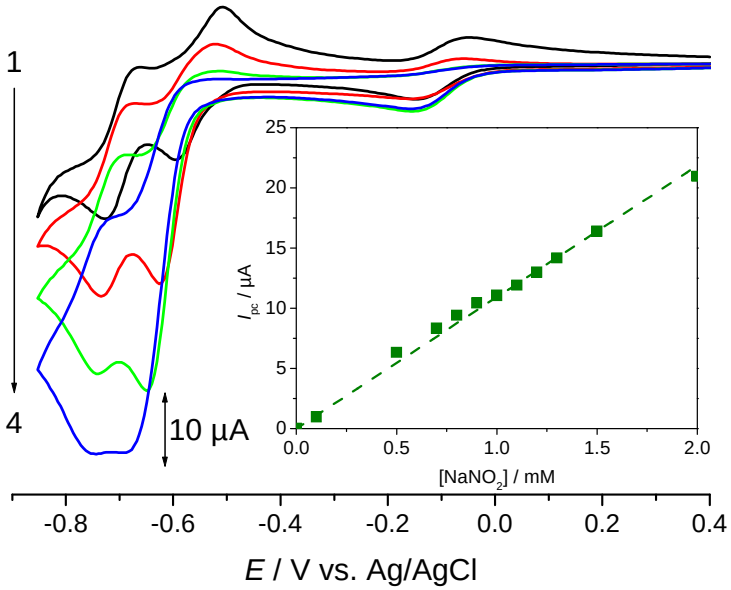

Figure 3.12. Catalytic activity of the water soluble K-$SiW_{11}Fe$ anion in the presence of different amounts of nitrite in aqueous solution. Cyclic voltammograms obtained in the absence and in the presence of increasing concentrations of nitrite, in the interval [0 – 3.00 mM]: a) 0; b) 1.00; c) 2.00 and d) 3.00 mM. Inset: plot of the catalytic peak current at -0.6 V vs. the concentration of nitrite. Experimental conditions: pH 2.0 buffer solution (H_2SO_4/HAc/NaAc), ν = 20 mV s^{-1}.

At pH 2.0, the catalytic currents increased with increase of nitrite concentration, as shown in the inset. The linear range could be observed for a concentration of nitrite up to 2.0 mM. This shows that the reduced forms of the heteropolyanion react with the added nitrite.

However, for some TBA-$SiW_{11}Fe$ modified electrodes, the total recovery of the initial electrode condition was not possible. At the final of the electrocatalysis experiments the electrode surface became partially depleted in microcrystallites (optical examination) and the original voltammogram could not be restored.

In the present experimental conditions, nitrite reduction is not mediated by the lacunary SiW_{11} (homogeneous reduction) [17]. It appears that the presence of the iron substituting metal in the polyanion structure is essential for catalysis. However, there are studies of the catalytic response of $SiW_{11}Fe$, towards the reduction of nitrite pointing to the extreme sensitivity, either in solution or immobilized on several electrodes, to supporting electrolyte and pH. [15,16].

The electrocatalytic properties of the TBA-$SiW_{11}Co$ modified electrodes were also tested for the reduction of nitrite. However, no effect was observed on the cyclic voltammograms of this modified electrode although $SiW_{11}Co$ presents the tungsten reduction and oxidation peaks at almost the same potential as the $SiW_{11}Fe$.

3.5. Conclusions

The preparation of glassy carbon electrodes modified by the adsorbed hybrid salts TBA-SiW_{11}, TBA-$SiW_{11}Fe$ and TBA-$SiW_{11}Co$, using solvent evaporation, was proved to be simple and fast. Reproducible and stable electrodes were produced and their voltammetric characteristics could be studied in different experimental conditions.

The results highlighted that:

- All modified electrodes consisted of a rather thick layer (ca. micrometer thick) of the TBA-silicotungstate and could be produced by the single-drop solvent evaporation method, from acetonitrile solutions. The salts deposited on the functionalised hybrid electrodes showed a relatively high crystallinity.
- For all immobilized TBA-silicotungstates the W redox processes were diffusion-controlled and, in fact, the first W reduction process was accompanied by the uptake of protons diffusing from the acidic solution into the adsorbed hybrid layer. Further, the first

W reduction process, for all modified electrodes, was thermodynamically favoured compared to what occurs with the corresponding water soluble polyanions.

- For future applications of the TBA-silicotungstate modified electrodes, namely in electrocatalysis, two aspects may be of relevance: i) the specific role of the substituting metals, either the potential of the W waves or on the electrocatalysis of nitrite, or other species, ii) improvement of the mechanical stability of the modified electrodes under catalysis working conditions.

3.6. References

[1] M. I. Prodromidis, P. G. Veltsistas, C. E. Efstathiou, M. I. Karayannis, *Electroanalysis* 13 (2001) 960.

[2] H. M. Carapuça, M. S. Balula, A. P. Fonseca, A. M. V. Cavaleiro, *J. Solid State Electrochem*. 10 (2006) 10.

[3] M. Sadakane M, E. Steckhan, *Chem. Rev.* 98 (1998) 219.

[4] A. Muller, L. Dloczick, E. Diemann, M. T. Pope, *Inorg. Chim. Acta* 257 (1997) 231.

[5] M. Sadakane, E. Stechan, *J. Mol. Catal. A: Chem.* 114 (1996) 221.

[6] F. A. R. S. Couto, A. M. V. Cavaleiro, J. D. Pedrosa de Jesus, J. E. J. Simão, *Inorg. Chim.Acta* 281 (1998) 225.

[7] J. Kim, A. A. Gewirth, *Langmuir* 19 (2003) 8934.

[8] J. E. Toth, F. C. Anson, *J. Electroanal. Chem.* 256 (1988) 361.

[9] M. T. Pope, Heteropoly and Isopoly Oxometalates, Spring Verlag, 1983.

[10] A. J. Bard, L. R. Faulkner, Electrochemical Methods, Wiley, 2001.

[11] L.Cheng, H. Sun, B.Liu, J.Liu, S.Dong, *J.Chem. Soc. Dalton Trans.* (1999) 2619.

[12] X. L. Wang, E. B. Wang, Y. Lan, C. W. Hu, *Electroanalysis* 14 (2002) 1116.

[13] P. Wang, X. Wang, X. Jing, G. Zhu, *Anal. Chim. Acta* 424 (2000) 51.

[14] S. Balula, PhD Thesis, University of Aveiro, 2003.

[15] B. Keita, F. Girard, L. Nadjo, R. Contant, R. Belghiche, M. Abbessi, *J. Electroanal. Chem.* 508 (2001) 70.

[16] S. Dong, X. Xi, M. Tian, *J. Electroanal. Chem.* 385 (1995) 227.

[17] J. E. Toth, F. C. Anson, *J. Am. Chem. Soc.* 111 (1989) 2444.

[18] C. Rong, F. C. Anson, *Inorg. Chim. Acta* 242 (1996) 11.

CHAPTER 4

NOVEL POLY(HEXYLMETHACRYLATE) COMPOSITE CARBON ELECTRODES MODIFIED WITH TBA SALTS OF KEGGIN PHOSPHOTUNGSTATES

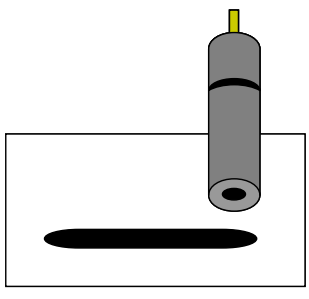

4.1. Introduction

Over recent decades, carbon paste, i.e., a mixture of carbon (graphite) powder and a binder (pasting liquid), has become one of the most popular electrode materials used for electrode preparation. Such a position can be attributed to the gathering of many physicochemical and electrochemical properties of this carbon-like substrate and its easy of preparation [1-3]. Carbon paste electrodes (CPE) are composite electrodes because they result from the combination of two or more materials and they have been widely applied in electrochemistry owing to their many advantages. Besides being easy to prepare and handle they are inexpensive, have low background currents and surface renewal is rapid [3,4].

A number of reviews have been exclusively devoted to CPEs [1-6]. Presently, CPEs represent one of the most frequent types of working electrodes. The large majority of CPEs involve pastes made with insulating liquids (paraffin oil, silicon oil, and others). The basic requirements for a pasting liquid are its lack of solubility in the solution under measurement, a low vapour pressure to ensure both mechanical stability and long lifetime, and in the case of voltammetric and amperometric applications, its electrochemical inactivity in the potential window of interest. In contrast to the relatively complicated modifications of solid substrates, carbon pastes can be modified simply to obtain quantitatively new sensors with desired, often predefined, properties [2,3].

The present work concerns novel carbon composite electrodes modified with tetra-butylammonium salts of $[PW_{11}O_{39}]^{7-}$ and $[PW_{11}Co^{II}(H_2O)O_{39}]^{5-}$, and a new easy way to

immobilize these POMs by bulk or surface film modification. Bulk modification was done by mixing the POM salts directly with the carbon paste (classified as CPE_1). For surface modification, a drop of a mixture of graphite and poly(hexylmethacrylate) binder, with or without tetra-butylammonium salts of lacunary and mono-substituted POM anions is deposited on the top of the surface of a normal carbon-paste electrode (graphite/mineral oil). These modified electrodes will be referred to in this chapter as CPE_2.Comparison with the electrochemical behaviour of the polyoxoanion in the electrodes and in aqueous solution was also carried out. To our knowledge, this is the first report of fabrication of a surface-modified carbon composite electrode using poly(hexylmethacrylate) binder.

4.2. Experimental

4.2.1. Reagents and solutions

Sulphuric acid (Fluka), acetic acid (Pronalab), sodium acetate (Carlo Erba), poly(hexylmethacrylate) solution (MW 400,000 in toluene - Aldrich), mineral oil (Fluka), potassium hexacyanoferrate (III) (Merck), potassium chloride (Merck) and graphite powder (Sigma Aldrich) were used as received. The tetra-butylammonium salts of the α-Keggin phosphotungstates $[(C_4H_9)_4N]_4H_3[PW_{11}O_{39}]$ (TBA-PW_{11}) and $[(C_4H_9)_4N]_4H[PW_{11}Co^{II}(H_2O)O_{39}]\cdot H_2O$, (TBA-$PW_{11}$Co) were prepared as described in Chapter 2. Electrolyte solutions for voltammetry were prepared using ultra-pure water (resistivity 18.2 MΩ cm at 25°C, Direct-Q 3 UV system, Millipore). Solutions within the pH range 2.0-3.0 were prepared by mixing appropriate amounts of a 0.01 M H_2SO_4 solution with a 0.10 M $CH_3COOH/NaCH_3COO$ buffer (pH = 4.6). Potassium hexacyanoferrate (III) solutions (1.0 mM) were prepared dissolving the appropriate amount of $K_3[Fe(CN)_6]$ in 1.0 M KCl.

4.2.2. Instrumentation and methods

Electrochemical experiments were carried out as referred to in Chapter 3,using a carbon paste electrode, CPE, inserted into a CPE cavity of diameter 3 mm (BAS, MF-

2010). For pH measurements the same instrument was used as referred previously in Chapter 3.

4.2.3. Preparation of the unmodified and modified CPEs

Figure 4.1 shows a schematic representation of electrode preparation. The carbon paste electrode without bulk modification (CPE_1) was fabricated as follows. A mass of 1.0 g of graphite powder and 0.5 mL of mineral oil were mixed in an agate mortar and pestle to achieve a homogeneous mixture. A portion of this paste was then packed into the cavity of the carbon paste electrode body and the surface was smoothed on a piece of a weighing paper. POM bulk-modified carbon paste electrodes (POM-CPE_1) were prepared by substituting a corresponding amount of the graphite powder (10% mass ratio of the modifier relative to the carbon powder) by TBA-PW_{11} (PW_{11}-CPE_1) or TBA-$PW_{11}Co$ ($PW_{11}Co$-CPE_1).

For the poly(hexylmethacrylate) surface-modified carbon composite electrodes (CPE_2), two mixtures were prepared: (a) 0.75 g of graphite powder and 1.50 g of poly(hexylmethacrylate) solution; (b) 0.75 g of graphite powder, 0.10 g of POM and 1.50 g of poly(hexylmethacrylate) solution. A drop of 5 µL of each slurry was placed onto the surface of an unmodified CPE prepared as described above and the solvent was allowed to evaporate for about 20 min. If the drop spread outside the circular area of the carbon paste the electrode assembly was rejected; thus, all electrodes employed had the same surface area. Electrodes with film composition (a), abbreviated as CPE_2, were used for the characterization of the electrode in the absence of POMs. The POMs used for case (b) were TBA-PW_{11} (PW_{11}-CPE_2) or TBA-$PW_{11}Co$ ($PW_{11}Co$-CPE_2).

An electrode surface activation step was done by cycling the potential 60 times, between 0.0 V and -0.85 V, in 0.01 M H_2SO_4 at a scan rate of 100 mV s^{-1}. This step was needed to stabilise the electrodes and to obtain reproducible results, after which they were ready to use.

Measurements were made at room temperature (~ 20 ºC). Solutions were degassed with pure nitrogen for 5 minutes before the measurements and nitrogen-blanketed during the measurements.

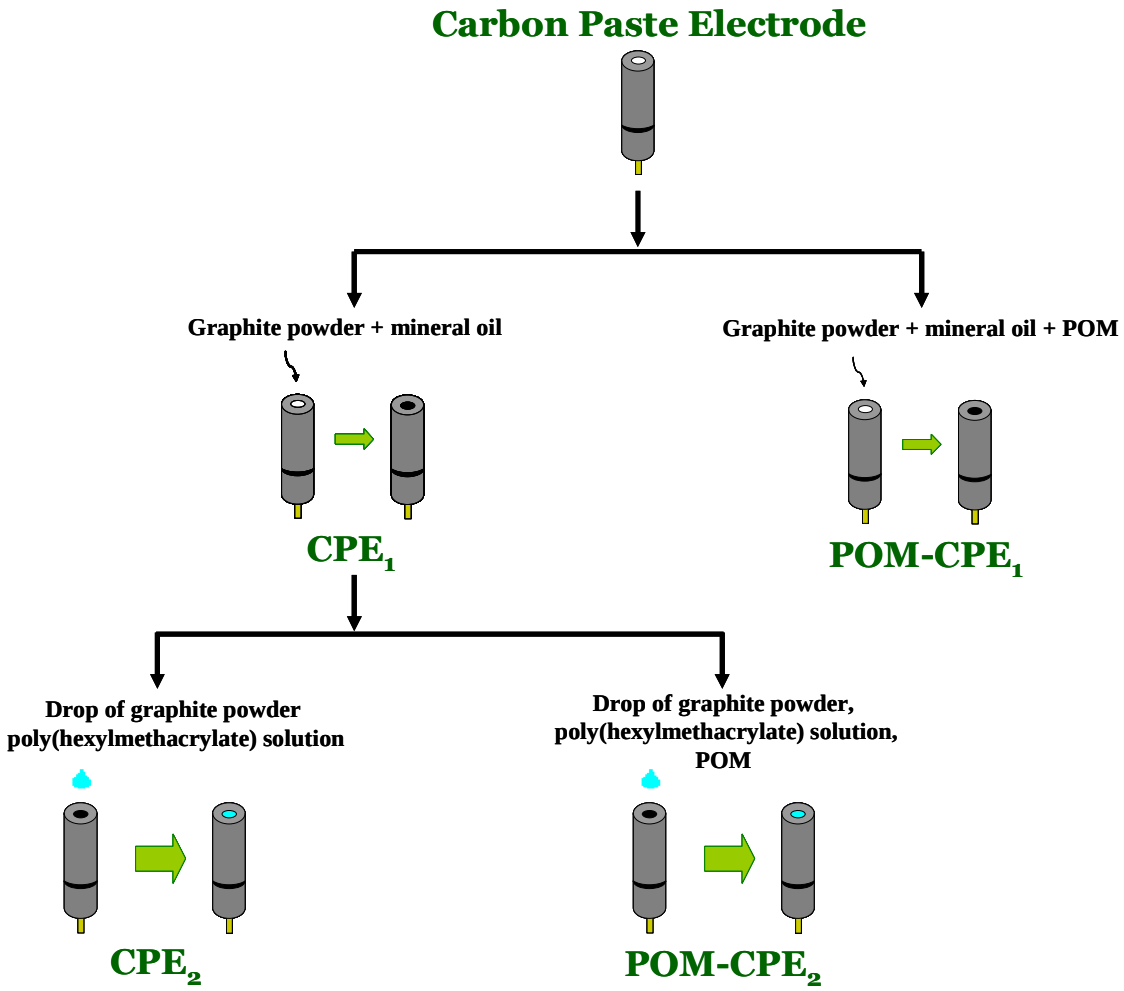

Figure 4.1. Schematic representation indicating the components used in electrode preparation.

4.3. Characterization of carbon paste electrodes CPE_1 and CPE_2

Hexacyanoferrate electroactive species were selected to evaluate the performance of the prepared carbon paste electrodes CPE_1 and CPE_2. A more reversible voltammogram indicates faster electrode kinetics and better access to the electrode and a greater available surface area should result in higher peak currents. Fig. 4.2 shows the electrochemical response of CPE_1 and CPE_2 in 1.0 mM $K_3[Fe(CN)_6]$ + 1.0 M KCl solution. A slight increase in the background current response at CPE_2 is visible with respect to CPE_1. On the other hand, the peak current for the $[Fe(CN)_6]^{3-/4-}$ redox couple is significantly higher (increase >115%) at CPE_2. The poly(hexylmethacrylate)-graphite

electrode surface may have more exposed graphite particles, and possibly additional porosity or roughness, leading to a higher available area for electrode reaction. The peak-to-peak separations (ΔE_p) were 76 mV for the CPE_1 and 170 mV for CPE_2, indicating quasi-reversible electron transfer processes, the increase for CPE_2 attributed to slower kinetics.

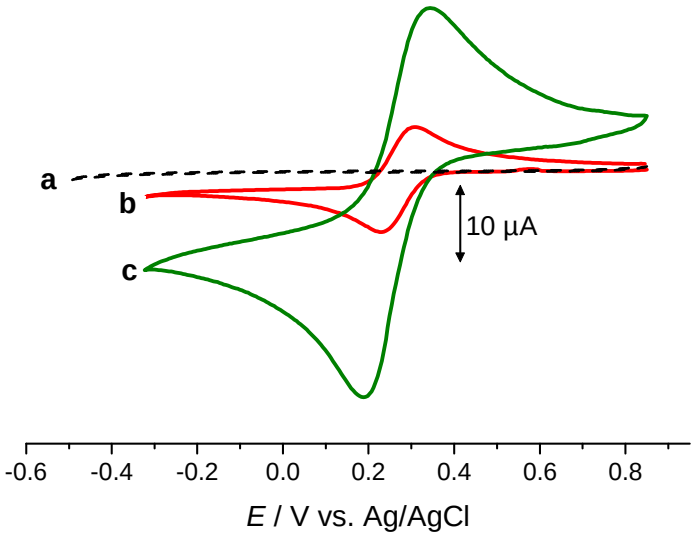

Figure 4.2. Cyclic voltammograms of (a) CPE_1 and CPE_2 in 1 M KCl electrolyte and, (b) CPE_1 and (c) CPE_2 in a solution of 1 mM $K_3[Fe(CN)_6]$ + 1 M KCl. Scan rate 20 mV s^{-1}.

The relationship between I_p and ν, seen in Fig. 4.3 as lg (I_p/A) versus lg (ν/V s^{-1}), gave slopes close to 0.50 for both CPE_1 and CPE_2, the square root relationship between cathodic peak current and scan rate indicating that the redox processes at CPE_1 and CPE_2 are diffusion-controlled. In the timescale used (scan rates between 20-1000 mV s^{-1}) the values of $E_{1/2}$ did not change significantly (<10%) with scan rate and the ratio of anodic and cathodic peak currents was ca. 1.

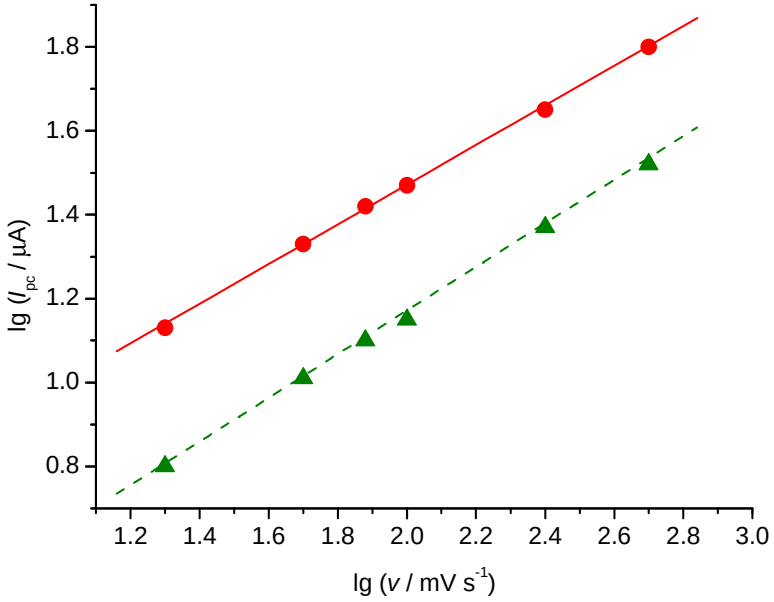

Figure 4.3. Plot of lg I_{pc} versus lg ν for (▲) CPE_1 and (●) CPE_2 in a solution of 1 mM $K_3[Fe(CN)_6]$ + 1 M KCl.

4.4. Voltammetric behaviour of POM-CPE_1 and POM-CPE_2

Generally, Keggin phosphotungstates are unstable in neutral and basic solutions [7]. Therefore, all studies with the electrodes modified with the TBA salts of the phosphotungstates PW_{11} and $PW_{11}Co$ were performed in acidic aqueous solution.

Cyclic voltammograms of the dissolved lacunary PW_{11} anion and of the metal-substituted $PW_{11}Co$ in acidic solutions show two reversible or quasi-reversible two-electron waves at negative potentials, corresponding to the reduction of the tungsten atoms [8,9]. In these anions, the tungsten reduction processes are accompanied by the addition of protons to counterbalance the increase in the negative charge and, therefore, the half-wave potentials of the W waves are pH-dependent.

The voltammetric features of the TBA-phosphotungstates immobilized in the carbon paste electrode were similar to those observed in aqueous solution for the corresponding anions in terms of the numbers of electrons transferred. However, the shape of the cyclic voltammograms is a little different from those obtained for aqueous dissolved POMs, but similar to those obtained for the TBA-silicotungstates immobilized by the droplet methodology described in Chapter 3. Fig. 4.4 shows cyclic voltammograms for $PW_{11}Co$-CPE_2 immersed in pH 2.0 aqueous solution (H_2SO_4/HAc/NaAc).

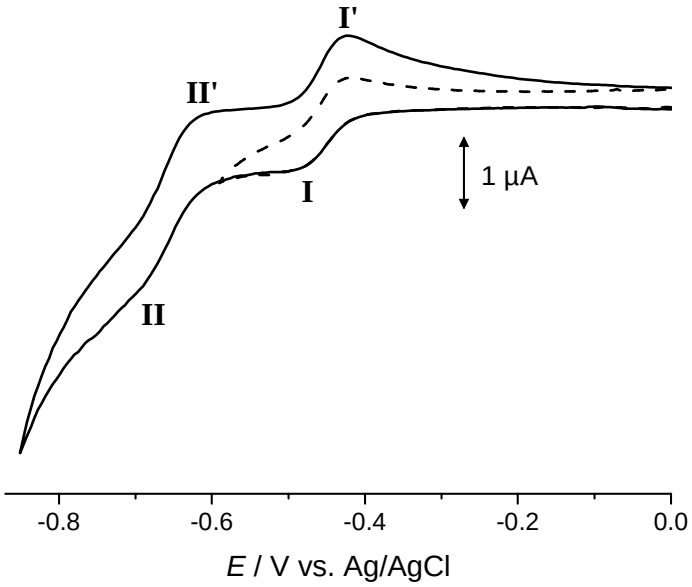

Figure 4.4. Cyclic voltammograms for $PW_{11}Co$-CPE_2 immersed in pH 2.0 H_2SO_4/HAc/NaAc aqueous solution at ν=50 mV s^{-1}, inverting the scan direction after the first reduction peak (---) and after the second reduction peak (—).

In the conditions used, two reversible or quasi-reversible two-electron waves were observed with reduction peak potentials at – 482 and – 685 mV vs Ag/AgCl for $PW_{11}Co$. In the same conditions PW_{11} presented peaks at – 487 and – 685 mV. Redox peaks I-I' and II-II' are attributed to two consecutive two-electron reduction processes of the tungsten atoms, i.e. corresponding to the expected four-electron global reduction process, as was obtained for these anions immobilized on GCEs by droplet evaporation [10] and for the corresponding silicotungstates in previous work [8,11,12]. The first pair was always well-defined but the resolution of the second couple was worse for higher pH values. The reduction/oxidation peak of the substituting metal ($Co^{III/II}$) was not observed because Co(II) is generally not electroactive within the potential window used from -0.85 to 0.0 V.

Electrochemical pre-treatment, consisting of scanning for 60 cycles, led to a better definition of the cyclic voltammograms. This suggests that cycling leads to reorganization and/or wetting of the layer containing the TBA-phosphotungstate salts, resulting in an increase of the electron transfer rate from the electrode surface to the redox sites of the polyanion.

Cyclic voltammograms at PW_{11}-CPE_1 and PW_{11}-CPE_2 in pH 2.0 H_2SO_4/HAc/NaAc aqueous solution at scan rates from 20 to 1000 mV s^{-1} are shown in Fig. 4.5.

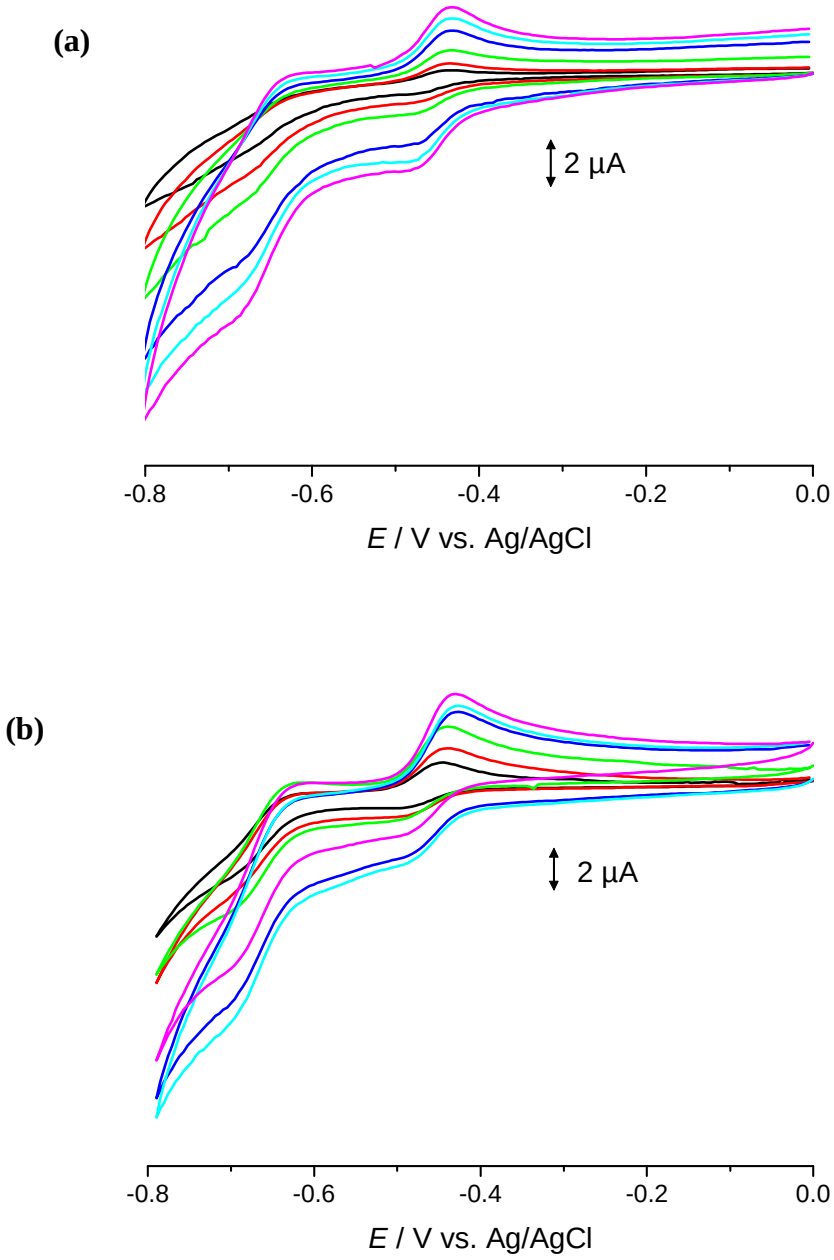

Figure 4.5. Cyclic voltammograms for (a) PW_{11}-CPE_1, and (b) PW_{11}-CPE_2, immersed in pH 2.0 buffer solution (H_2SO_4/HAc/NaAc) at scan rates 20, 50, 100, 500, 750 and 1000 mV s^{-1}.

Cathodic and anodic peak currents were proportional to the square root of scan rate which means that the process is controlled by counter-ion diffusion (see below).

The same behaviour was observed for the modified electrodes with TBA silicotungstates salts adsorbed on GCE by droplet evaporation (see Chapter 3). The same occurred for other electrodes modified with Keggin-type anions, such as with $H_3[PMo_{12}O_{40}]\cdot nH_2O$ for higher scan rates ($\nu \geq 100$ mV s^{-1}) [13] in a ceramic-carbon electrode, for hexadecylpyridium phosphomolybdate hybrid material in a carbon paste electrode [14], and for lacunary and Fe and Co metal substituted phosphotungstate TBA salts adsorbed on GCE by droplet evaporation [10].

Table 4.1 presents voltammetric data for the first tungsten reduction process for the immobilized TBA phosphotungstates. The results concerning the second reduction process were not included due to the fact that peaks were not always well resolved. The potentials for the first tungsten process at the $PW_{11}Co$ carbon paste electrodes were almost 70 mV less negative than the corresponding polyoxoanion in aqueous solution. This may demonstrate that the electron transfer at the tungsten – oxide cage structure is thermodynamically favoured for this POM when it is immobilized in the carbon paste. For the PW_{11}, no significant changes were observed. Also, as a consequence of immobilization, there were no substantial differences between the potential of the first tungsten process upon metal substitution, in contrast to aqueous solutions [9]. A similar behaviour was observed for these phosphotungstates immobilized by the droplet evaporation method [10] and for the corresponding silicotungstates immobilized by the same procedure in Chapter 3.

The cathodic peak potentials shifted slightly in the negative direction and the corresponding anodic peak potentials to the positive direction with increasing scan rates, leading to an increase of peak-to-peak separation (ΔE_p). The fact that ΔE_p for the first W reduction wave has a value of 29 mV for CPE_1 (see Table 4.1), together with the linear relation between peak currents and square root of scan rate alluded to above indicates a 2-electron counter-ion diffusion-controlled process (57/*n* mV for a reversible process). The values of $|E_p\text{-}E_{p/2}|$ are in agreement with this hypothesis. The values of ΔE_p for CPE_2 are larger which suggests kinetic constraints in the presence of the polymer in the matrix. This could be due to a very thin film of the polymer remaining on top of parts of the graphite particles, which reduces the ease of reduction or oxidation [15]. The mechanism will involve successive additions of electrons and protons (for reduction), as has been observed in non-aqueous solution and where it was also pointed out that there are pronounced medium effects on the observed voltammetry [16].

Table 4.1. Cyclic voltammetric data for the first W reduction processes in pH 2.0 buffer solution (H_2SO_4/HAc/NaAc) at 50 mV s^{-1}.

Electrode	E_{pc} *	E_{pa} *	$\lvert \Delta E_p \rvert$ *	$\lvert E_{pc} - E_{p/2} \rvert$ *	I_{pc} (μA)	E_{pc} # (aq)
PW_{11}-CPE_1	-470	-441	29	28	-0.40	-486
$PW_{11}Co$-CPE_1	-487	-458	29	29	-0.45	-548
PW_{11}-CPE_2	-487	-449	38	32	-0.72	-486
$PW_{11}Co$-CPE_2	-482	-425	57	34	-0.53	-548

* mV vs. Ag/AgCl; # E_{pc} values for polyoxoanions in aqueous solution of pH 2.2, ν=100 mV s^{-1} [9]

Initial pre-treatment led to activation of the modified electrode in terms of electron transfer between the electrode and the active redox sites of the TBA-phosphotungstates, so it may be assumed that diffusion of H^+(aq) from the solution to the immobilized phosphotungstates is rate-determining.

The pH of the supporting electrolyte has an influence on the electrochemical behaviour of POM-CPE. With increasing pH, the cathodic and anodic peak potentials are shifted in the negative direction by 99 mV for $PW_{11}Co$ and by 62 mV per pH unit for PW_{11}, suggesting $2e^-/3H^+$ (as noted before in [11]), and $2e^-/2H^+$ processes, respectively, the protons diffusing from the solution to the surface of the electrode to maintain charge neutrality. For surface-confined processes, the amount of POM that is accessible for reaction at an electrode surface can be determined, as in [17], but to do so in this case would require knowledge of the diffusion coefficient of the counterion which it is not feasible to ascertain with meaningful accuracy, particularly given the non-uniformity of composite electrode surfaces.

4.5. Stability and surface renewal of POM modified CPEs

Compared with polyoxometalate-modified electrodes fabricated by other methods, POM-CPEs have certain advantages. One of the main attractions of using CPEs is that the surface of the electrodes can be renewed after each use. Another is that the resulting carbon paste electrode possesses high stability. Figure 4.6 shows, as an example, the cyclic voltammograms for the PW_{11}-CPE_2 electrodes. When the potential range was

maintained in the range 0.0 to -0.9 V, POM-CPEs were stable for over 150 cycles at a scan rate of 100 mV s^{-1} and the current response remained almost unchanged. After use during a full working day, these modified CPEs were kept overnight in a protecting case and were stored at room temperature (~20ºC); on testing the next day the results were practically identical. After storing again for one week at room temperature there was negligible change in the shape and height of the redox waves. The decrease of peak current values compared with the original ones was less than 5%. Peak potentials were constant throughout.

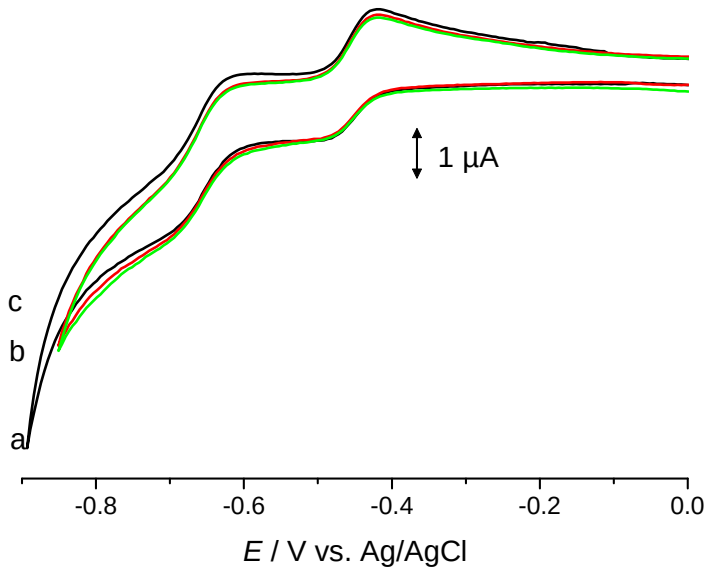

Figure 4.6. Cyclic voltammograms for PW_{11}-CPE_2 immersed in pH 2.0 buffer solution (H_2SO_4/ HAc/NaAc), ν = 50 mV s^{-1}: (a) first (b) second working day; (c) after one week.

4.6. Conclusions

A new chemically modified carbon paste electrode (CPE_2) has been developed, modifying the surface of a traditional carbon paste electrode with a coating of a mixture of graphite, poly(hexylmethacrylate) and the polyoxometalates (TBA-PW_{11} and TBA-PW_{11}Co) and the electrodes proved to be stable. The electrochemical behaviour of the modified electrodes was studied by cyclic voltammetry. For the two immobilized TBA-phosphotungstates, the first tungsten redox processes were diffusion-controlled, and were accompanied by the uptake of protons diffusing from the acidic solution into the mixture

containing the POMs. Compared with other types of POM-modified electrode, CPEs present the advantages of high stability due to the insolubility of the organic-inorganic hybrid salts of POMs in aqueous solution and the affinity of the organic part ($((C_4H_9)_4N)^+$) toward the paste which is important for practical applications. Modification using poly(hexylmethacrylate) also slightly improves the electrode sensitivity for the same amount of POMs.

4.7. References

[1] I. Švancara, A. Walcarius, K. Kalcher, K. Vytřas, *Cent. Eur. J. Chem.* 7 (2009) 598.

[2] K. Kalcher, I. Švancara, R. Metelka, K. Vytřas, A. Walcarius, The Encyclopedia of Sensors, Vol. 4, American Scientific, Stevenson Ranch, 2006, 283 – 430.

[3] I. Švancara, K. Vytřas, K. Kalcher, A. Walcarius, J. Wang, *Electroanalysis* 21 (2009) 7.

[4] K. Kalcher, *Electroanalysis* 2 (1990) 419.

[5] K. Kalcher, J. M. Kauffmann, J. Wang, I. Švancara, K. Vytřas, C. Neuhold, Z. P. Yang *Electroanalysis* 7 (1995) 5.

[6] K. Vytřas, K. Kalcher, I. Švancara, K. Schachl, E. Khaled, J. Ježková, J. Konvalina, R. Metelka *Electrochem. Soc. Proc.* 18 (2001) 277.

[7] M.T. Pope, Heteropoly and Isopoly Oxometalates, Springer-Verlag, Berlin, 1983.

[8] B. Keita, L. Nadjo, *J. Electroanal. Chem.* 243 (1988) 87.

[9] F.A.R.S. Couto, A.M.V. Cavaleiro, J.D. Pedrosa de Jesus, J.E.J. Simão, *Inorg. Chim. Acta* 281 (1998) 225.

[10] H.M. Carapuça, M.S. Balula, A.P. Fonseca, A.M.V. Cavaleiro, *J. Solid State Electrochem.* 10 (2006) 10.

[11] D.M. Fernandes, S.M.N. Simões, H.M. Carapuça, A.M.V. Cavaleiro, *Electrochim. Acta* 53 (2008) 6580.

[12] J.E. Toth, F.C. Anson, *J. Electroanal. Chem.* 256 (1988) 361.

[13] P. Wang, X. Wang, X. Jing, G. Zhu, *Anal. Chim. Acta* 424 (2000) 51.

[14] X.L. Wang, E.B. Wang, Y. Lan, C.W. Hu, *Electroanalysis* 14 (2002) 1116.

[15] M.M. Barsan, E.M. Pinto, M. Florescu, C.M.A. Brett, *Anal. Chim. Acta* 635 (2009) 71.

[16] S.X. Guo, A.W.A. Mariotti, C. Schlipf, A.M. Bond, A.G. Wedd, *Inorg. Chem.* 45 (2006) 8563.

[17] A. Balamurugan, S.M. Chen, *J. Solid State Electrochem.* 11 (2007) 1679.

CHAPTER 5

SELF-ASSEMBLY MULTILAYER FILMS BASED ON KEGGIN-TYPE POLYOXOTUNGSTATES AND POLY(ETHYLENIMINE)

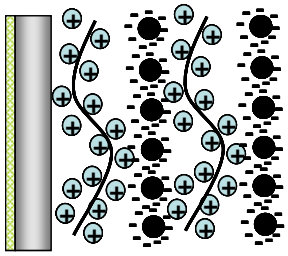

SELF-ASSEMBLY MULTILAYER FILMS BASED ON KEGGIN-TYPE POLYOXOTUNGSTATES AND POLY(ETHYLENIMINE) 101

5.1. Introduction

In recent years, many techniques have been developed to fabricate composite films since they can be used to design and build different types of molecular architecture. Layer-by-layer (LbL) assembly has proven to be a promising technique for fabricating uniform and ultrathin film devices by the alternate immersion of a substrate into solutions containing the chosen oppositely-charged species [1,2].

Multilayers based on POMs, polyelectrolytes and conducting polymers have been widely used, as already referred to in Chapter 1 [3-15]. However, there are only a few reports using poly(ethylenimine) (PEI) as the polycation [16,17]. In most studies it is used as the anchorage layer together with PSS [18,19]. Although they are extensively used, only some reports can be found in the literature concerning the characterization of the structure and charge transfer processes in these multilayer films.

Electrochemical impedance spectroscopy (EIS) has been successfully used to study interfacial processes, in order to obtain information about the structure and changes that may occur at the electrode-electrolyte interface, and about reaction mechanisms and electrode kinetics [20]. It is an effective method to investigate the interfacial properties of modified electrodes [21-23]. It is complementary to cyclic voltammetry that often allows quantitative determination of kinetic and diffusion parameters [24]. Modification of electrode substrates alters the features of the impedance spectra. Impedance methods are also attractive because of the small sinusoidal potentials that are used, rather than the wide potential window used in cyclic voltammetry. Thus, EIS has unique benefits for

monitoring the formation processes of multilayer films and in the characterisation of the films and their interfacial properties.

The present chapter concerns the fabrication of stable ultrathin films of lacunary SiW_{11} and mono-substituted polyoxometalates $PW_{11}Fe$, $SiW_{11}Fe$ and $SiW_{11}Co$, with poly(ethylenimine) (PEI) by the layer-by-layer self-assembly method. Growth of the multilayer films adsorbed on a quartz slide was monitored by UV–Vis absorption spectroscopy and the surface morphology of the thin films on a glassy carbon electrode was examined by scanning electron microscopy (SEM). The electrochemical behaviour of the immobilized polyanions and electron transfer to $[Fe(CN)_6]^{3-/4-}$ and $[Ru(NH_3)_6]^{3+/2+}$ as electrochemical probes was investigated by cyclic voltammetry. Additionally, the possible application of some of the modified electrodes as a sensor for nitrite, iodate and/or bromate reduction was tested.

Electrochemical impedance spectroscopy was used to characterize glassy carbon electrodes modified with hybrid films composed of PEI and Keggin-type $SiW_{11}Fe$ using $K_3[Fe(CN)_6]$ and $Cl_3[Ru(NH_3)_6]$ as redox probes. ITO modified electrodes were also used for comparison. Impedance spectra were analysed by fitting to equivalent electrical circuits and the effect of the number of layers, and of the two redox probes used on the spectra and on the charge transfer processes are discussed.

5.2. Experimental

5.2.1. Reagents and solutions

The potassium salts $K_8[SiW_{11}O_{39}]\cdot 13H_2O$, $K_5[SiW_{11}Fe^{III}(H_2O)O_{39}]\cdot 13H_2O$, $K_6[SiW_{11}Co^{II}(H_2O)O_{39}]\cdot 12H_2O$ and $K_4[PW_{11}Fe^{III}(H_2O)O_{39}]\cdot 6H_2O$ were prepared as described in Chapter 2.

Poly(ethylenimine) (MW = 50,000–100,000; 30 wt. % aqueous solution; branched, consisting of tertiary, secondary and primary amino groups in the ratio of 25/50/25, respectively) was purchased from Polysciences Europe GmbH and was used without further treatment. Sodium chloride (Merck), potassium chloride (Merck), acetic acid (Pronalab), sodium acetate (Carlo Erba), potassium ferricyanide (Merck), hexaammineruthenium (III) chloride (Aldrich), sodium nitrite (Merck), sodium bromate (Sigma-Aldrich), potassium iodate (Sigma-Aldrich), buffer solution pH 9 (0.05 M H_3BO_3,

0.05 M KCl, 0.022 M NaOH) (Merck) and other reagents were analytical grade and were used as received.

The electrolyte used for electrochemical studies was prepared by mixing appropriate amounts of the CH_3COOH (0.1 M) and $NaCH_3COO$ (0.1 M) solutions to give a pH 4.0 solution. Potassium ferricyanide and hexammineruthenium (III) chloride solutions (1.0 mM) were prepared dissolving the appropriate amount of $K_3[Fe(CN)_6]$ and $[Ru(NH_3)_6]Cl_3$ in 1M KCl. Electrolyte solutions for voltammetry were prepared using ultra-pure water (resistivity 18.2 MΩ cm at 25°C, Direct-Q 3 UV system, Millipore).

5.2.2. Instrumentation and methods

UV–vis absorption spectroscopy of the K-SiW_{11}, K-SiW_{11}Co, K-SiW_{11}Fe and K-PW_{11}Fe aqueous solutions was performed using a quartz cell with 0.4 cm path length in a Jasco V-560 UV-visible spectrophotometer. A set of 7 solutions of each compound (0.001-0.05 mM) in 0.1 M acetate buffer (pH 4.0) was used to determine the isotropic molar absorption coefficient. The absorbance of each solution was measured and a calibration curve was obtained by plotting the values of absorbance vs. concentration. As the path length is known (0.4 cm) the ε is determined using the slope and the Beer-Lambert law. The UV–Vis absorption spectra of the multilayer films were recorded on quartz slides.

Scanning electron microscopy was conducted on an Analytical FE-SEM SU-70 Hitachi, UHR 1.0 nm/15 kV (1.6 nm/1 kV). The film preparation for the SEM evaluation was performed on a glassy carbon electrode that was previously cut to fit the equipment.

A glassy carbon electrode, GCE, (3 mm diameter, BAS, MF-2012) was used as working electrode, on which the multilayer films were formed. Indium tin oxide (ITO) electrodes with geometric area of 0.50 cm^2 (ITO on quartz slides) were also used as substrate for comparison. The auxiliary and reference electrodes were a platinum wire (7.5 cm, BAS, MW-1032) and Ag/AgCl (sat. KCl) (BAS, MF-2052), respectively. Electrochemical experiments were carried out as described previously in Chapter 3.

Electrochemical impedance measurements were carried out using a Solartron 1250 Frequency Response Analyser, coupled to a Solartron 1286 Electrochemical Interface (UK) controlled by ZPlot Software. The voltage perturbation was 10 mV rms over a frequency range from 65 kHz to 0.01 Hz with 10 frequencies per decade, and integration time 60 s. Impedance spectra were analysed by fitting to equivalent electrical circuits using ZView Software (Scribner Associates, USA).

5.2.3. Preparation of self-assembly $(PEI/POM)_n$ films

Films were prepared on glassy carbon electrodes, ITO electrodes and quartz slides. Prior to coating, the GCE was conditioned by a polishing/cleaning procedure. The GCE was successively polished with 1.0 μm diamond polishing compound (Metadi II, Buehler) and aluminium oxide of particle size 0.3 μm (Buehler-Masterprep) on a microcloth polishing pad (BAS Bioanalytical Systems Inc), then the electrode was rinsed with ultra-pure water and finally sonicated, for 5 min, in an ultrasonic bath (Branson 2510). The quartz slides and ITO electrodes were cleaned by placing them in a H_2SO_4/H_2O_2 (3:1) (v/v) hot bath (~80º C) for 40 min and then in a $H_2O/H_2O_2/NH_3$ (5:1:1) (v/v/v) hot bath (~80º C) for another 40 min. The cleaned quartz slides and ITO electrodes were rinsed with ultra-pure water and dried under a flow of pure nitrogen.

After the cleaning step, the GCE, ITO electrodes or quartz slide were immersed in a 5 mg/mL (0,12 M) PEI solution (in pH = 9.0 buffer for $SiW_{11}Fe$ and $PW_{11}Fe$; in pH = 4.0 acetate buffer for SiW_{11}, $SiW_{11}Fe$ and $SiW_{11}Co$) for 20 min. The GCE was then immersed in a 0.3 mM POM solution (in pH = 4.0 acetate buffer) for 20 min. This process was repeated until the desired number of bilayers of PEI/POM was obtained. Water rinsing and nitrogen drying steps were performed after each immersion.

The solutions used for the film preparation were used immediately after their preparation and degassed with pure nitrogen for at least 10 min.

Additionally, the influence of different concentrations of POMs was tested. The effects of different deposition times was tested for the $(PEI/SiW_{11}Fe)_n$ multilayers. All measurements were made at room temperature (~20º C).

5.3. Film formation

Thin multilayer films of lacunary and mono-substituted Keggin-type polyoxometalates (SiW_{11}, $SiW_{11}Co$, $SiW_{11}Fe$ or $PW_{11}Fe$) and protonated poly(ethylenimine) prepared by layer-by-layer self-assembly were deposited on glassy carbon electrodes, ITO electrodes or on quartz slides, by alternate immersion in aqueous solutions of PEI and of the chosen polyoxoanion.

The formation of the multilayer structure via alternate adsorption of cationic PEI and anionic POM on a substrate is represented in Fig. 5.1. The influence of pH, concentration

and time of immersion were studied, in order to find the best deposition conditions and will be discussed in sections 5.4 and 5.6.

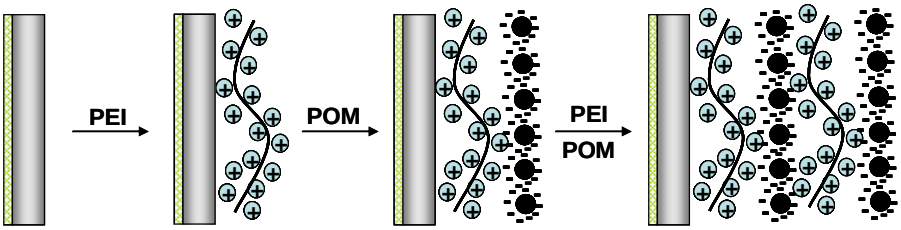

Figure 5.1. Schematic diagram of the formation of the multilayer structure via alternate adsorption of cationic PEI and anionic POM on a substrate.

5.4. Characterization of multilayer $(PEI/POM)_n$ films deposited on quartz slides

UV-Vis spectroscopy was used after the deposition of each bilayer to monitor the growth process of the multilayer films. Figures 5.2 and 5.3 show UV-Vis spectra of $(PEI/PW_{11}Fe)_n$ and $(PEI/SiW_{11}Fe)_n$ and of $(PEI/SiW_{11})_n$ and $(PEI/SiW_{11}Co)_n$, respectively, assembled on a quartz slide. The spectra are all similar, presenting three absorption bands for the iron compounds and two for the lacunary and cobalt-substituted POM; the band positions and shape did not change during multilayer construction. PEI does not absorb above 200 nm and the films exhibit the characteristic bands of these POMs. In Fig. 5.2 the bands appear near 195, 260 and 340 nm. The first two can also be seen in the UV-Vis spectra in Fig. 5.3 The bands near 195 and 260 nm correspond to charge transfer transitions from the terminal oxygen atoms to tungsten atoms ($O_d \rightarrow W$) and across bridge bonds W–O–W ($O_b \rightarrow W$ or $O_c \rightarrow W$), respectively [25,26]. The band near 340 nm in Fig. 5.2 corresponds to charge transfer transitions from oxygen to iron ($O \rightarrow Fe$). The low intensity *d-d* bands of cobalt (II), observed in aqueous solution around 540 nm [27], were not discernible. The absorption bands at 248 nm (SiW_{11}), 254 nm ($SiW_{11}Co$), 260 nm ($PW_{11}Fe$) and 258 nm ($SiW_{11}Fe$) were chosen to monitor film growth.

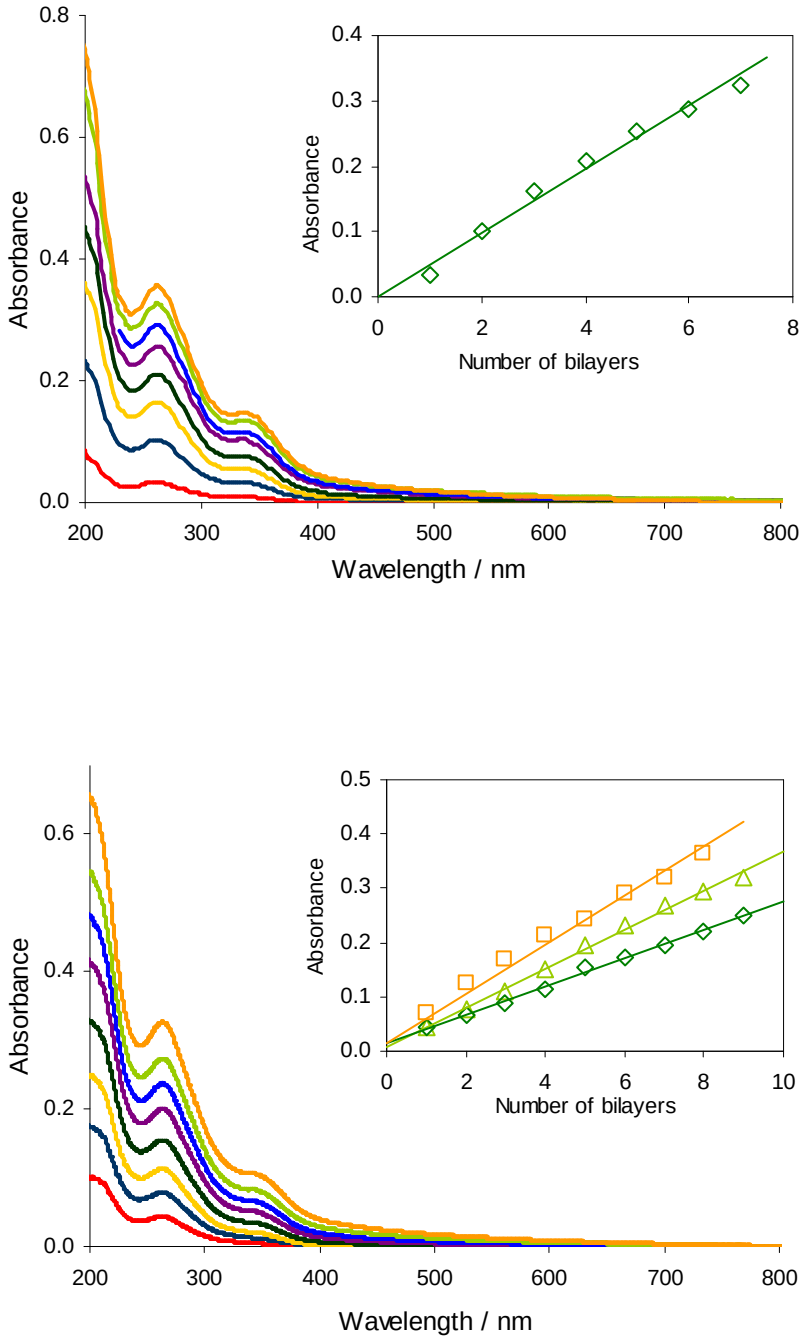

Figure 5.2. UV-Vis absorption spectra of (a) $(PEI/PW_{11}Fe)_n$ and (b) $(PEI/SiW_{11}Fe)_n$ multilayers for n = 0 – 8 adsorbed on a quartz slide. The insets in (a) and (b) show the absorbance at (a) 260 nm and (b) 258 nm, as a function of n. The inset in (b) also shows the absorbance as a function of n for different deposition times: (□) 20, (Δ) 10 and (◊) 5 min.

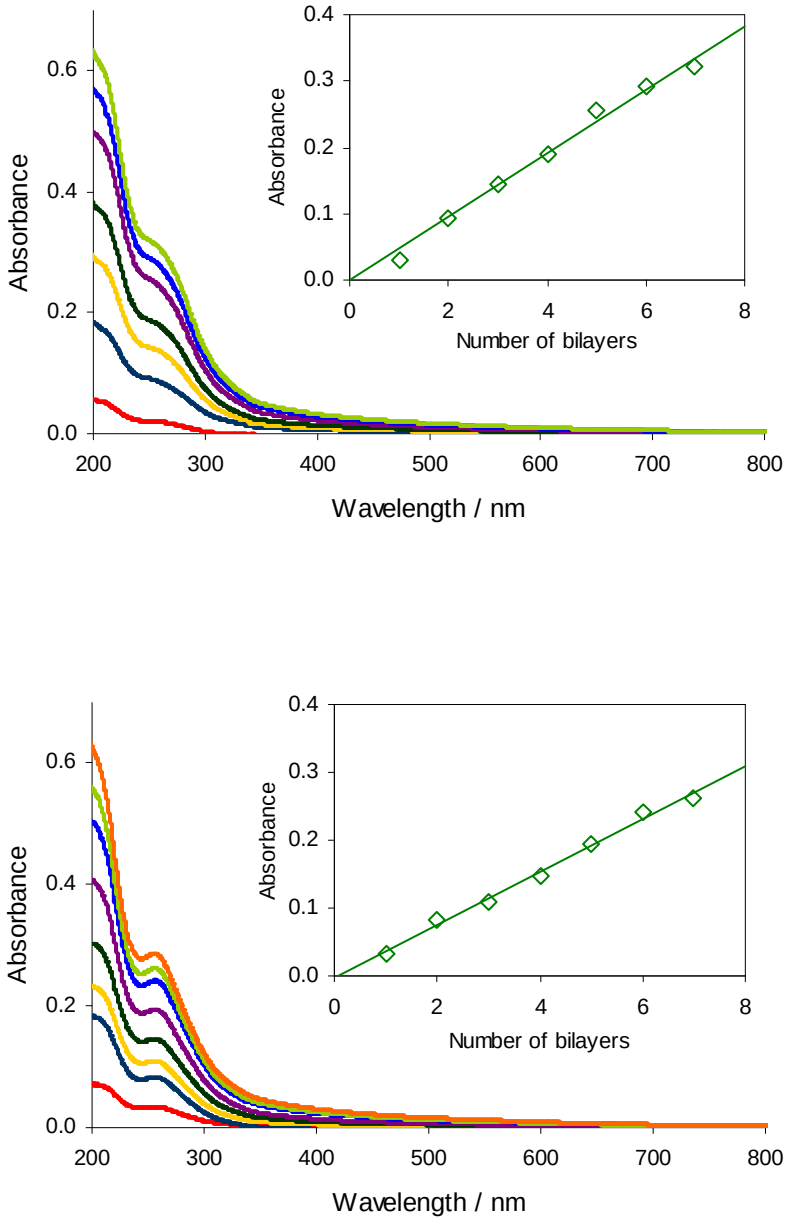

Figure 5.3. UV-Vis absorption spectra of (a) $(PEI/SiW_{11})_n$ and (b) $(PEI/SiW_{11}Co)_n$ multilayers for n = 0 – 7 adsorbed on a quartz slide. The insets in (a) and (b) show the absorbance at (a) 248 nm and (b) 254 nm, as a function of n.

The insets in Fig. 5.2 and Fig. 5.3 show that the absorbance increases almost linearly with the number of deposited layers, suggesting that the quantity of polyoxometalate deposited per bilayer was approximately the same up to seven bilayers

for SiW_{11}, $SiW_{11}Co$ and $PW_{11}Fe$ and up to eight for $SiW_{11}Fe$. With further increase in the number of multilayers the absorbance increases less reaching a plateau. The inset in Fig. 5.2b also shows the absorbance of $(PEI/SiW_{11}Fe)_n$ multilayers at 258 nm as a function of *n* for three different deposition times. It can be seen that there is a considerable difference between deposition times of 5, 10 or 20 min. Typically, in the literature, an adsorption time between 5 and 20 min for each polyion is used although, in most cases, the major amount of polyelectrolyte was in fact adsorbed within a few minutes [28-31]. Longer deposition times (30 and 60 min) were also evaluated, besides the ones referred to above. However, saturation was achieved after 20 min since the absorbance values at 258 nm did not increase further for longer deposition times. Cyclic voltammetry tests were in agreement with this, so, except when indicated, 20 min was the time used in the experiments described below.

The surface coverage per layer, Γ, can be estimated from the spectra of the multilayers, according to the Beer-Lambert law

$$\Gamma = A_\lambda / 2m\varepsilon_\lambda \qquad (5.1)$$

where A_λ is the absorbance at the specified wavelength, *m* is the number of layers and ε_λ is the isotropic molar absorption coefficient (M^{-1} cm^{-1}) [32]. In aqueous solution (acetate buffer, pH 4) the isotropic molar absorption coefficients for SiW_{11}, $SiW_{11}Co$, $SiW_{11}Fe$ and $PW_{11}Fe$ are ε_{248} = 7.66 x 10^4 M^{-1} cm^{-1}, ε_{254} = 7.27 x 10^4 M^{-1} cm^{-1}, ε_{258} = 8.84 x 10^4 M^{-1} cm^{-1} and ε_{260} = 9.87 x 10^4 M^{-1} cm^{-1}, respectively. Using eqn.(1), this leads to values of the surface coverage of 2.88 x 10^{-10} mol cm^{-2} for SiW_{11}, 2.63 x 10^{-10} mol cm^{-2} for $SiW_{11}Co$, 3.04 x 10^{-10} mol cm^{-2} for $SiW_{11}Fe$ and 2.72 x 10^{-10} mol cm^{-2} for $PW_{11}Fe$ for 20 min deposition time. In the case of $SiW_{11}Fe$, surface coverages of 2.15 x 10^{-10} mol cm^{-2} and 1.75 x 10^{-10} mol cm^{-2} were obtained for deposition times of 10 and 5 min. These values are somewhat higher than the 1.00 x 10^{-10} mol cm^{-2} obtained for $(PMo_{12}/PDDA)_n$ by Wang *et al* [33] which they attributed to monolayer coverage. A possible explanation for the values obtained being higher than expected may be the existence of diffuse scattering due to the heterogeneity of the surface. It is known that when a beam is passed through a thin layer of matter its intensity is generally diminished as a consequence of both absorption and scattering. These scattering losses would give rise to a lower intensity of the transmitted beam and thence higher calculated absorbance values and surface coverages.

5.5. Scanning electron microscopy characterization

SEM images provide information about the surface morphology and homogeneity of the PEI layer and $(PEI/POM)_n$ multilayer films. Figure 5.4 shows SEM images of the PEI layer on a glassy carbon electrode at two magnifications. In Fig. 5.4a it can be seen that after PEI adsorption the surface is fully covered with small white bead-shaped domains of different sizes. Amplification of the image reveals that the darker parts are also covered with PEI (Fig. 5.4b).

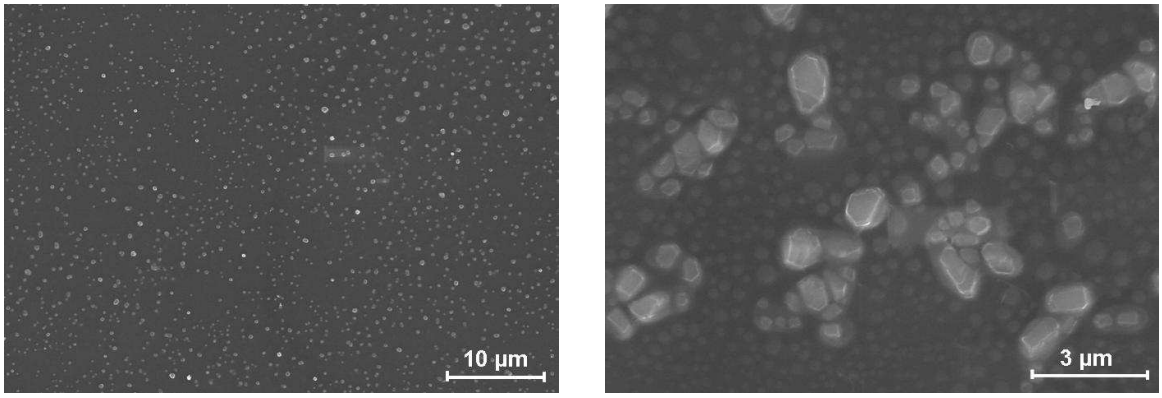

(a) PEI layer (× 2000) **(b) PEI layer (× 8000)**

Figure 5.4. Typical SEM micrographs for a PEI layer adsorbed on a glassy carbon electrode.

Figure 5.5 shows representative images upon adsorption of two bilayers of (PEI/$SiW_{11}Co$), (PEI/$PW_{11}Fe$) and (PEI/$SiW_{11}Fe$) at different magnifications. In the three cases, a completely-covered surface is observed but the deposited film presents a considerable number of cracks (Fig. 5.5 a, c and e). These may be due to the vacuum system used in the SEM chamber and also to the high-energy beam; in fact, it was possible to see the formation of cracks in places where they did not exist previously on increasing the magnification. Higher magnification (Fig. 5.5 b, d and f) reveals the presence of a high density of irregular shaped domains of small micrometric dimensions underneath these cracks. The features of the SEM images were the same for larger number of bilayers and the results for SiW_{11} were very similar. Although the pH values of the solutions of POMs were different, no significant changes are observed on the morphology of the deposited bilayers.

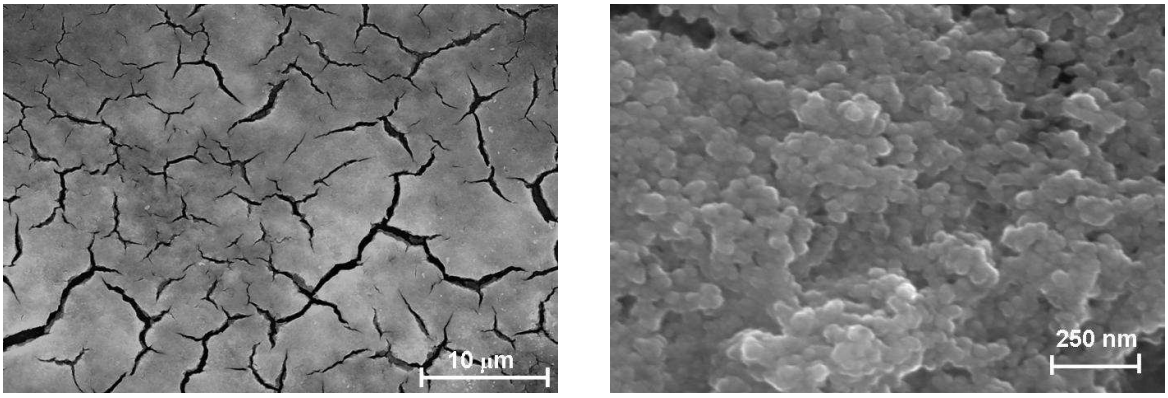

(a) $(PEI/SiW_{11}Co)_2$ (× 2500) (b) $(PEI/SiW_{11}Co)_2$ (× 80000)

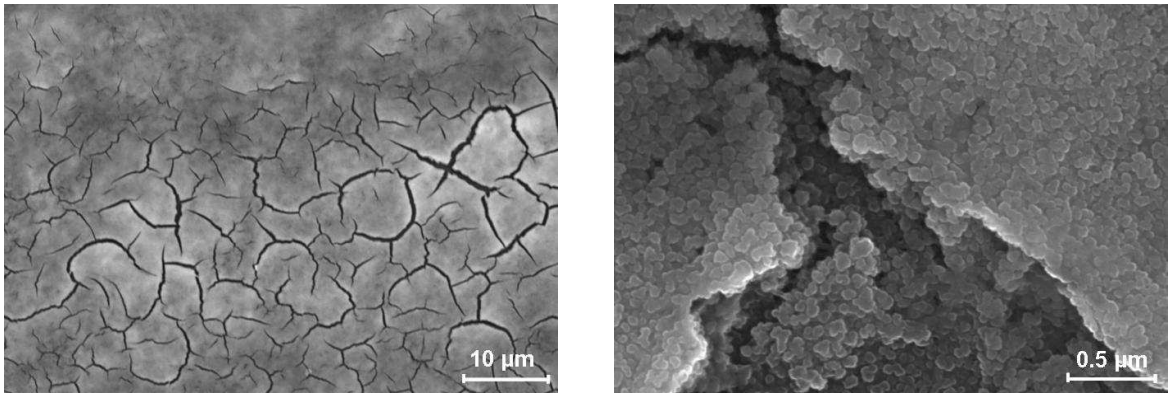

(c) $(PEI/PW_{11}Fe)_2$ (× 1800) (d) $(PEI/PW_{11}Fe)_2$ (× 35000)

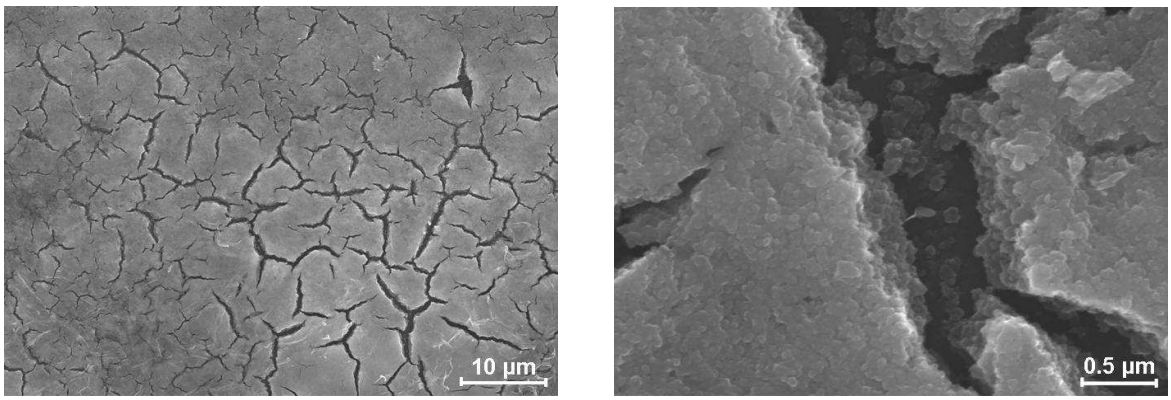

(e) $(PEI/SiW_{11}Fe)_2$ (× 1800) (f) $(PEI/SiW_{11}Fe)_2$ (× 30000)

Figure 5.5. Representative SEM micrographs of $(PEI/SiW_{11}Co)_2$, $(PEI/PW_{11}Fe)_2$ and $(PEI/SiW_{11}Fe)_2$ films on a glassy carbon electrode at different magnifications.

5.6. Voltammetric behaviour of multilayer films

All voltammetric results presented below were obtained using a concentration of 0.3 mM of POM for film preparation. Studies with electrodes obtained using 1 mM POM solutions ($SiW_{11}Fe$ and $PW_{11}Fe$) for the same deposition time did not show significant changes in the peak currents. This suggests that, in this concentration range, the concentration of POM has little effect on the amount of POM adsorbed in each layer and that in fact, the determinant factor for higher adsorption of POM may be the amount of available PEI rather than the POM concentration since higher concentrations of POM did not led to higher peak currents.

In order to ensure reproducible results and as mentioned in section 5.2.3 on film preparation, after each immersion the electrode was rinsed with ultra-pure water and dried under a flow of nitrogen. Rinsing removes weakly attached, physically adsorbed molecules, preparing the surface for the next adsorbed layer [31] and guarantees precise increments in the thickness of the layer-by-layer self-assembled films.

To understand the electrochemical behaviour of $(PEI/POM)_n$ films, comparison with the redox behaviour of the POMs in aqueous solution is important. The majority of the voltammetric studies reported for lacunary and transition metal substituted Keggin-type anions in aqueous solution have been performed in acidic media [34-37]. In these conditions, all anions studied in this work presented two consecutive reversible or quasi-reversible 2-electron waves at negative potentials, corresponding to the reduction of W^{VI} atoms as already observed in Chapter 3 and also referred in Chapter 1. The iron-substituted polyanions presented another wave at a less negative potential due to the redox process of $Fe^{III/II}$. The four polyoxotungstates studied in different acidic aqueous solutions, presented E_{pa} and E_{pc} values independent of scan rate, suggesting that the electrode reactions are reversible; peak currents were proportional to the square root of scan rate, indicating that the redox processes were controlled by diffusion, as referred previously in Chapter 3.

Figure 5.6 shows cyclic voltammograms for single (PEI/SiW_{11}) and ($PEI/SiW_{11}Co$) bilayers and Fig. 5.7 for single ($PEI/PW_{11}Fe$) and ($PEI/SiW_{11}Fe$) bilayers at different scan rates at pH 4.0, which demonstrate that the electrochemical properties of the four POMs studied are maintained in the multilayer films. Since PEI is not electroactive, its presence is not reflected in the cyclic voltammograms. Under the conditions used, the cyclic voltammograms of (PEI/SiW_{11}) and ($PEI/SiW_{11}Co$) bilayers only presented two quasi-reversible two-electron reduction peaks which were observed at -711 and -876 mV for

SiW_{11}, -714 and -885 mV for $SiW_{11}Co$ vs. Ag/AgCl. These redox peaks are attributed to two consecutive two-electron reduction processes of tungsten atoms, i. e. corresponding to the expected four-electron global reduction process. For ($PEI/PW_{11}Fe$) and ($PEI/SiW_{11}Fe$) bilayers, three reduction peaks were observed. The redox peaks corresponding to the tungsten reductions were observed at -750 and -905 mV for $SiW_{11}Fe$ and at -680 and -838 mV for $PW_{11}Fe$ vs. Ag/AgCl. The pair of peaks for the one-electron reduction/oxidation of $Fe^{III/II}$ is also observed in the cyclic voltammograms of $SiW_{11}Fe$ and $PW_{11}Fe$ at -163 and -171 mV, respectively. The reduction/oxidation peak of substituting metal $Co^{III/II}$ was not observed because Co(II) is not usually electroactive within the potential window used from -1.0 to 0.0 V.

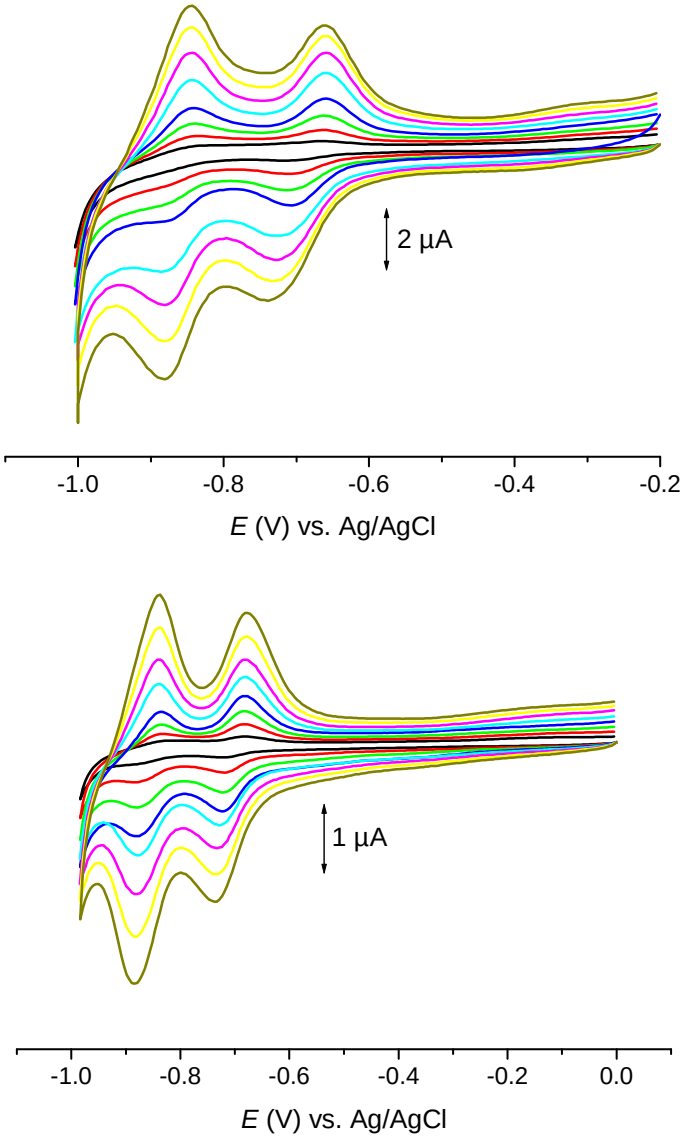

Figure 5.6. Cyclic voltammograms in $CH_3COOH/NaCH_3COO$ buffer solution (pH 4.0) at different scan rates: 25, 50, 75, 100, 125, 150, 200, 250 and 300 mV s^{-1} for (a) $(PEI/SiW_{11})_1$ and (b) $(PEI/SiW_{11}Co)_1$ bilayer films.

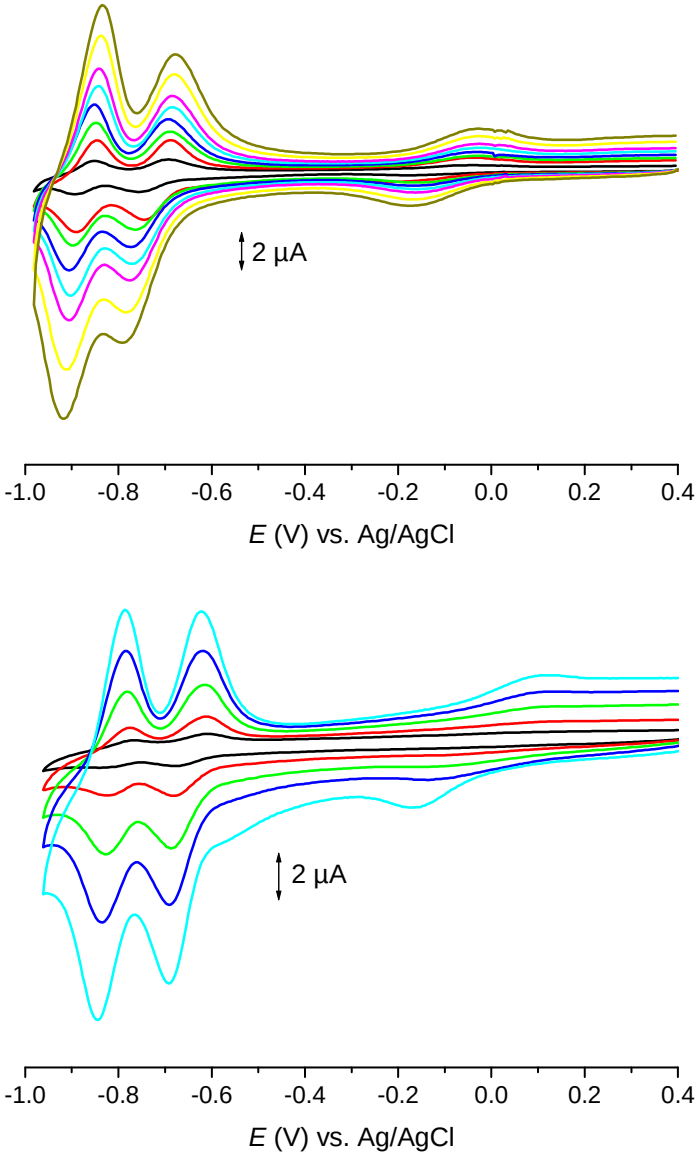

Figure 5.7. Cyclic voltammograms for (PEI/POM) bilayer films in $CH_3COOH/NaCH_3COO$ buffer solution (pH 4.0) at different scan rates: (a) 25, 50, 75, 100, 125, 150, 200 and 250 mV s^{-1} for ($PEI/SiW_{11}Fe$) and (b)10, 25, 50, 75 and 100 mV s^{-1} for ($PEI/PW_{11}Fe$).

In the experimental timescale employed (scan rates in the range 10 to 100 mV s^{-1} for ($PEI/PW_{11}Fe$), 25 to 250 mV s^{-1} for ($PEI/SiW_{11}Fe$) and 25 to 300 mV s^{-1} for (PEI/SiW_{11}) and ($PEI/SiW_{11}Co$) the values of peak potential changed only slightly with scan rate, and the ratio of anodic to cathodic peak currents was close to 1.

It was found that the cathodic and anodic peak currents of the first W wave were directly proportional to the scan rate, which indicates a surface-confined process [38]. This behaviour has also been observed by S. Liu et al. for $[Co_4(H_2O)_2P_4W_{30}O_{112}]^{16-}$,

$[Eu(H_2O)P_5W_{30}O_{110}]^{12-}$ and $[Na(H_2O)P_5W_{30}O_{110}]^{14-}$ [2] and by B. Xu *et al.* for $K_6[P_2W_{18}O_{62}]\cdot 14H_2O$ [6] using the LbL methodology. Similar behaviour was also observed for the Keggin type $[SiW_{11}Ni(H_2O)O_{39}]^{6-}$ [39] deposited on the electrode by electrodeposition with cysteamine. The number of electrons transferred in the tungsten redox processes is obtained by comparison of the peak currents for the $Fe^{III/II}$ couple with those of the first tungsten reduction process and indicates a 2-electron process (i.e. two coincident one-electron $W^{VI/V}$ reductions). Note that the peak currents for the $Fe^{III/II}$ couple are influenced by the slow kinetics of this process (the peak-to-peak separation is substantially higher than for the first W wave), thus the I_p for the $Fe^{III/II}$ reduction is certainly less than for a fully reversible process. In addition, the anodic/cathodic peak-to-peak separation (ΔE_p) for the tungsten waves was ca. 30–60 mV instead of zero, which would have been expected for a reversible surface process. These higher values of ΔE_p suggest kinetic constraints.

Comparison of the electrochemical behaviour of the multilayer (PEI/$SiW_{11}Fe$) film with that of the potassium salt of $SiW_{11}Fe$ in pH 4.0 aqueous solution (see Chapter 3) shows that there are no significant differences in the peak potentials, but the peaks are broader than in solution. This broadening may be related to the large coulombic repulsion between the negative sites of highly-charged polyanions in the same layer, as suggested in reference [40]. It also demonstrates that the PEI layers do not block electron transfers between the immobilized anions of $SiW_{11}Fe$. The potentials for the first tungsten process at the SiW_{11} modified electrode are almost 70 mV more negative than the corresponding polyoxoanion in aqueous solution (E_{pc} = -643 mV at pH = 4.0). However, for $SiW_{11}Co$ the potentials are similar (E_{pc} = -730 mV in solution at pH = 4.0). This difference in both modified electrodes is due to the fact that in aqueous solution there are substantial differences between the potentials of the first tungsten process upon metal substitution as seen in Chapter 3 and in reference [38], in contrast to what happens when POM are immobilized, where the potentials of lacunary and mono-substituted POMs are practically the same (see Chapter 3 and 4).

Cyclic voltammograms for $(PEI/SiW_{11}Co)_n$, $(PEI/SiW_{11})_n$, $(PEI/PW_{11}Fe)_n$ and $(PEI/SiW_{11}Fe)_n$ multilayer films with different numbers of layers are presented in Figures 5.8 and 5.9. In all cases, the cathodic peak potentials shift to more negative values by approximately 10 to 30 mV and the anodic peak potentials shift to slightly more positive values with an increase in the number of layers. Plots of peak current vs. the number of bilayers (n), show linear growth up to n = 7 for both $SiW_{11}Co$ and SiW_{11}, n = 5 for $PW_{11}Fe$ and n = 6 for $SiW_{11}Fe$. Above these numbers of bilayers, peak currents begin to show a

negative deviation from linearity, which can be ascribed to effects of film resistance, i.e. difficulty of transferring electrons through the film to the electrode substrate. Although the peaks for $(PEI/SiW_{11})_n$ multilayer films are not so well defined as for $(PEI/SiW_{11}Co)_n$, they appear at the expected potentials and the system exhibits the same characteristics.

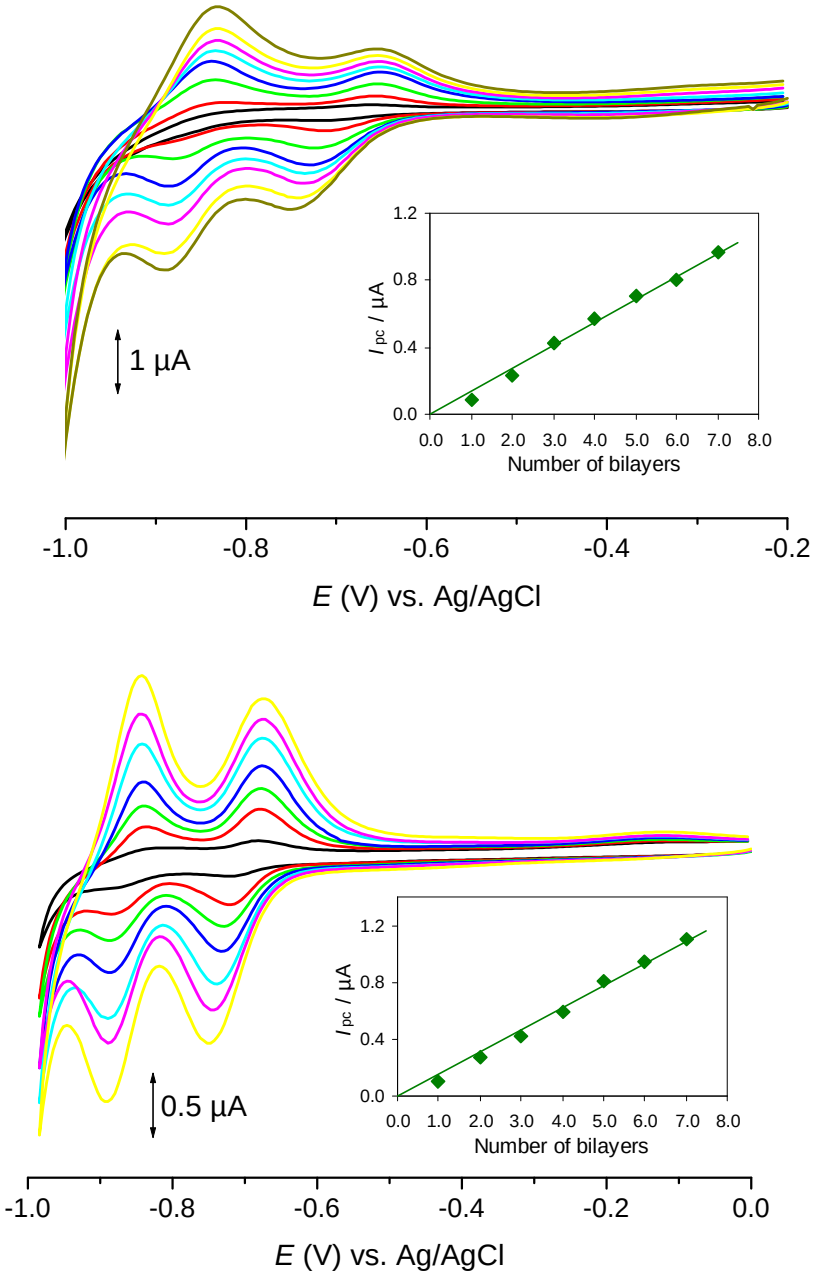

Figure 5.8. Cyclic voltammograms for (a) $(PEI/SiW_{11})_n$ and (b) $(PEI/SiW_{11}Co)_n$ multilayer films in $CH_3COOH/NaCH_3COO$ buffer solution (pH 4.0) for n = 1 – 7, ν = 50 mV s^{-1}. The insets show the peak currents vs. the number of multilayers.

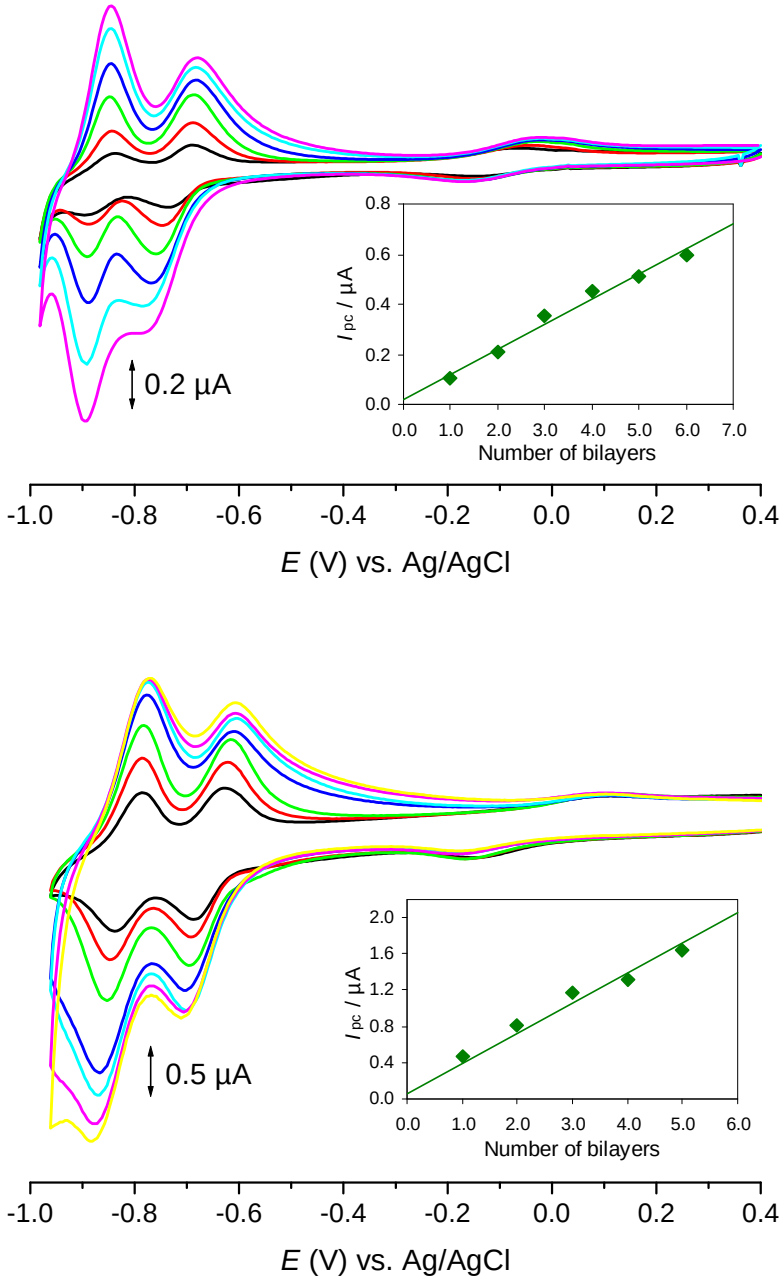

Figure 5.9. Cyclic voltammograms for (a) $(PEI/SiW_{11}Fe)_n$ and (b) $(PEI/PW_{11}Fe)$ multilayer films in $CH_3COOH/NaCH_3COO$ buffer solution (pH 4.0) for n = 6 for $PEI/SiW_{11}Fe$ and 7 for $PEI/PW_{11}Fe$, ν = 10 mV s^{-1}. The insets show the peak currents vs. the number of multilayers.

In order to gain more insight into the requisites for the good deposition of multilayer films, the influence of two polycation solutions with different pH values on the growth characteristics of $PEI/SiW_{11}Fe$ multilayers was studied. Different adsorption times of the polycation PEI and polyanion $SiW_{11}Fe$ were also tested.

The effect of pH on the layer-by-layer self-assembly method is evident, but complex [32]. Apart from any changes in the ionic strength of the buffer solutions used, a change in pH may modify the charge density of polyelectrolytes due to protonation-deprotonation equilibria: an increased charge density of the adsorbing polymer will favour thinner adsorption layers, whereas increasing charge density at the surface will favour thicker adsorbed layers [41]. Therefore, the effect of pH on layer-by-layer film growth is not clear *a priori.* To study the pH effect, two 5mg/mL PEI solutions were used in LbL film preparation of (PEI/$SiW_{11}Fe$), one in a pH 9.0 and the other in a pH 4.0 buffer solution. No differences in the peak potentials were observed and peak currents increased linearly with the number of layers in both cases. However, the peak currents were lower when using the modified electrodes prepared with the PEI solution at pH 4.0 than at pH 9.0, although the peaks obtained were better resolved.

The influence of deposition time on the growth of multilayer films on the glassy carbon electrodes was tested for (PEI/$SiW_{11}Fe$) using different immersion times per anionic or polycationic layer (60, 30, 20, 15 and 10 min). Since saturation was achieved using 20 min deposition times only 20, 15 and 10 min will be discussed here. For these three adsorption times, there was no difference in the peak currents up to the $(PEI/SiW_{11}Fe)_4$ multilayer but differences became apparent for $(PEI/SiW_{11}Fe)_5$ and subsequent multilayers. An adsorption time of 20 min results in the largest amount of adsorbed material (higher peak currents). For 10 and 15 min adsorption times, after the $(PEI/SiW_{11}Fe)_6$ multilayer, peak current saturation is obtained. Several studies indicate that polyelectrolyte adsorption is a two-step process where most polymer chains are anchored during a fast initial step and then the growth of the film slows down until the surface charge becomes completely inverted [28-30,42]. This second step may take much longer. Taking this into account, it is probable that the 10 and 15 min immersion times are not sufficient to achieve total charge reversal with respect to the previous layer, thus leading a smaller adsorption of the next layer and consequent lower peak currents.

Surface coverage can be calculated from cyclic voltammetry according to the equation:

$$\Gamma = (4I_{pa}RT) / (n^2F^2vA) \qquad (5.2)$$

where I_{pa} is the anodic peak current (amperes), n is the number of electrons transferred (2 in this case), ν is the scan rate (V s^{-1}), A is the geometric area of the electrode (0.0725 cm^2), R is the gas constant (8.314 J K^{-1} mol^{-1}), T is the temperature (298K) and F is

Faraday's constant (96485 C mol^{-1}) [40]. In order to obtain the surface coverage, peak currents were plotted against scan rate (10 to 100 mV s^{-1} for $SiW_{11}Fe$ and $PW_{11}Fe$ and 10 to 300 mV s^{-1} for SiW_{11} and $SiW_{11}Co$) and the value of I_{pa}/ν obtained was used to calculate surface coverage using equation (5.2). This led to a surface coverage of 1.29 x 10^{-10} mol cm^{-2} for $PW_{11}Fe$, 1.09 x 10^{-10} mol cm^{-2} for $SiW_{11}Fe$, 1.50 x 10^{-11} mol cm^{-2} for SiW_{11} and 1.82 x 10^{-11} mol cm^{-2} for $SiW_{11}Co$.

Assuming a close geometric packing of POM clusters and the data from scanning tunnelling microscopy observation of Keggin clusters deposited on a gold surface [43] to estimate monolayer coverage, Wang *et al* [33] calculated a value of 1.25x10^{-10} mol cm^{-2}. Comparing this with our values of surface coverage obtained by cyclic voltammetry for $SiW_{11}Fe$ and $PW_{11}Fe$, ours corresponds to monolayer coverage. The values of surface coverage obtained using, in the electrode preparation, a solution of PEI with pH = 4.0 indicate that in those cases (SiW_{11} and $SiW_{11}Co$) a sub-monolayer coverage is achieved. Nevertheless, the surface coverages estimated by UV-visible spectroscopy are somewhat higher (2.72x10^{-10} mol cm^{-2} for $PW_{11}Fe$, 3.04x10^{-10} mol cm^{-2} for $SiW_{11}Fe$, 2.88x10^{-10} mol cm^{-2} for SiW_{11} and 2.63x10^{-10} mol cm^{-2} for $SiW_{11}Co$), but are calculated assuming that the molar absorption coefficients of the polyoxometalates are the same in solution and in the films, which is not certain. The surface coverages reported in the literature calculated by cyclic voltammetry are usually lower than those obtained from UV-visible spectroscopy [2,32].

5.7. Permeability of multilayer films

Electrochemistry can be employed to assess film permeability and as a sensitive probe of structural changes in the $(PEI/POM)_n$ films. In particular, the passivating abilities of different films can be compared using cyclic voltammetry via peak currents and voltammogram shapes. Many groups have used the $[Fe(CN)_6]^{3-/4-}$ redox couple to study the permeability of multilayer films [2,16,44-46]; however, studies of electron transfer at films containing polyoxometalates are few. Liu *et al.* showed that the permeability towards these species can be tailored through the multilayer construction and deposition conditions [2]. Also, Gao *et al.* investigated how the number of multilayer films influences the shape of the cyclic voltammograms [16].

Cyclic voltammetry was also used to study the properties of the multilayer films towards the negatively charged $[Fe(CN)_6]^{3-/4-}$ and the positively charged $[Ru(NH_3)_6]^{3+/2+}$

redox probes. Electrostatic attraction between the multilayer surface and the redox probe when they have opposite charges should facilitate the interfacial electron transfer process, whereas repulsion when they have the same charge would make the electron transfer reaction more difficult. A more reversible voltammogram indicates better access to the electrode substrate, which should result in higher peak currents.

Figure 5.10 shows, as example, cyclic voltammograms of $[Fe(CN)_6]^{3-/4-}$ at the electrode modified with $(PEI/SiW_{11}Co)_n$ for n = 1, 2, 4 and 6. These results show that for an electrode coated with a single $(PEI/SiW_{11}Co)$ bilayer the cyclic voltammogram exhibits quasi-reversible properties, indicating that the probe diffuses freely through the layer and undergoes electron transfer at the electrode surface. Increasing the number of multilayers from one to four leads to a decrease in peak currents and peak broadening and ultimately to an electrode with plateau-shaped current characteristics (Fig. 5.10a). These observations show that an increased number of multilayers leads to a decrease in the number of hexacyanoferrate ions which reach the electrode substrate whenever the terminal layer consists of negatively charged $SiW_{11}Co$ anion. This is attributable to electrostatic repulsion of $[Fe(CN)_6]^{3-/4-}$ by the external negatively charged $SiW_{11}Co$ anion. When the outermost layer is the positively charged PEI the quasi-reversible properties in the cyclic voltammogram of $[Fe(CN)_6]^{3-/4-}$ are restored (Fig. 5.10b), due to the electrostatic attraction of $[Fe(CN)_6]^{3-/4-}$ from the terminal positively-charged PEI layer. The voltammogram is similar to that of a bare glassy carbon electrode, and is independent of film thickness (number of bilayers).

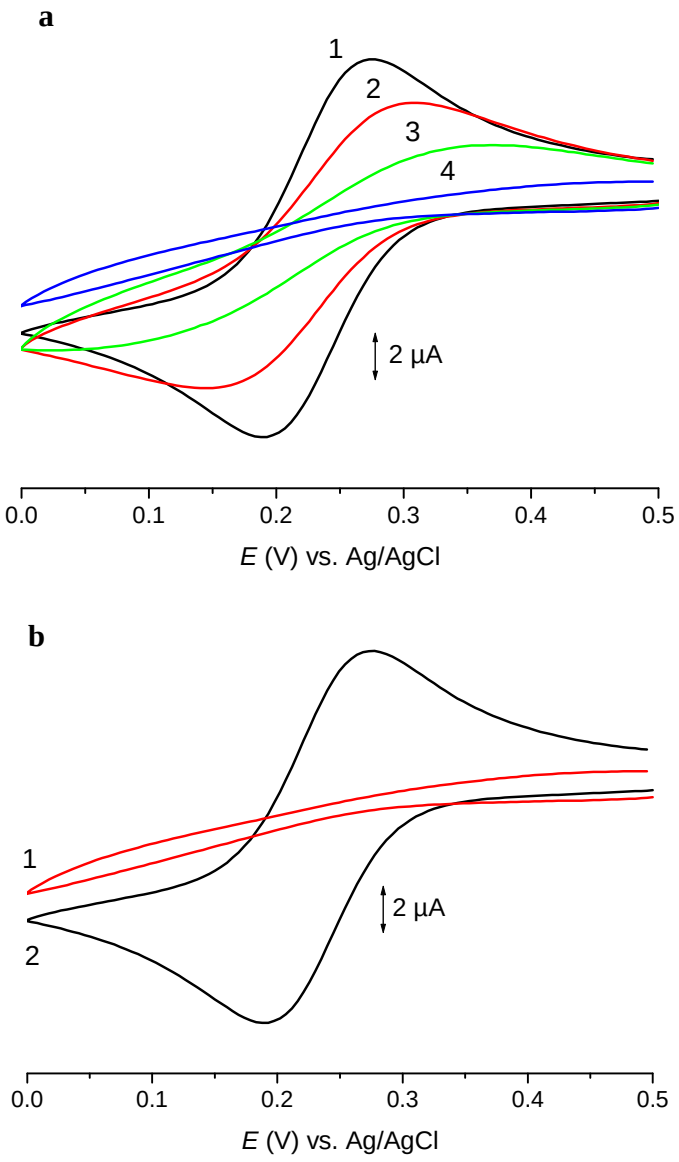

Figure 5.10. Cyclic voltammograms of $[Fe(CN)_6]^{3-/4-}$ (1 mM, 1 M KCl) ν = 100 mV s^{-1}, at modified electrodes with (a) $(PEI/SiW_{11}Co)_n$ for (1) n = 1; (2) 2; (3) 4 and (4) 6; (b) 1 - $(PEI/SiW_{11}Co)_6$ and 2 - $(PEI/SiW_{11}Co)_6$/PEI.

When the positively charged $[Ru(NH_3)_6]^{3+/2+}$ redox probe is used at the $(PEI/SiW_{11}Co)_n$ (with n = 1, 2 and 4) modified electrode, the changes observed are not so significant (Fig. 5.11a). The cyclic voltammograms for n = 1 and 2 are almost identical and there is a slight decrease in the peak currents and an increase in the peak-to-peak separation on increasing the number of bilayers to four. However, after the addition of a layer of PEI on the $(PEI/SiW_{11}Co)_1$ modified electrode (Fig. 5.11b), the peak current of $[Ru(NH_3)_6]^{3+/2+}$ decreases significantly and the peak-to-peak separation increases. This is

attributable to electrostatic repulsion of $[Ru(NH_3)_6]^{3+/2+}$ by the positively charged PEI. The same tests were performed for (PEI/$PW_{11}Fe$) and (PEI/$SiW_{11}Fe$) and the results were identical.

The electrostatic attractions or repulsions have significant effects on the kinetics of the redox reactions. With an increasing number of (PEI/POM) bilayers the peak current of both redox probes decrease gradually, and the peak-to-peak separation increase, owing to kinetic and/or thermodynamic constraints associated with increase film thickness.

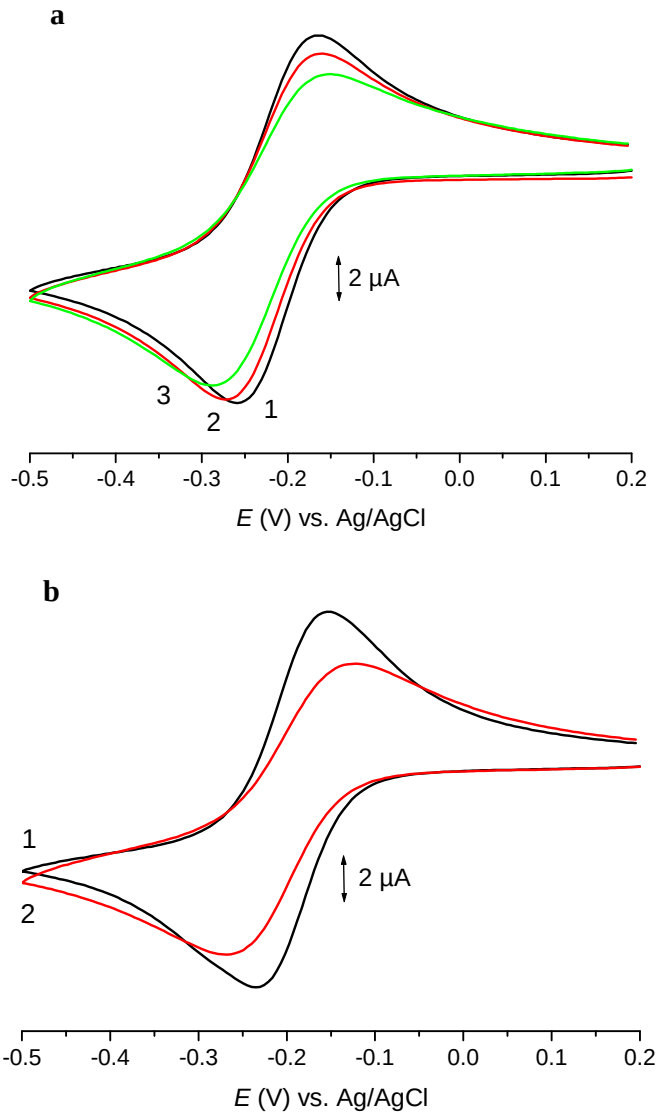

Figure 5.11. Cyclic voltammograms of $[Ru(NH_3)_6]^{3+/2+}$ (1 mM, 1 M KCl) ν = 100 mV s^{-1}, at modified electrodes with (a) $(PEI/SiW_{11}Co)_n$ for (1) n = 1; (2) 2 and (3) 4; (b) 1 - $(PEI/SiW_{11}Co)_1$ and 2 - $(PEI/SiW_{11}Co)_1$/PEI.

To test the reproducibility of these LbL modified electrodes five electrode assemblies were prepared under identical conditions and the cyclic voltammograms recorded in $CH_3COOH/NaCH_3COO$ buffer solution (pH 4.0). The relative standard deviation of the peak current for the first tungsten reduction wave was 14.9% for $(PEI/PW_{11}Fe)_n$, 4.3% for $(PEI/SiW_{11}Fe)_n$, 3.8% for $(PEI/SiW_{11}Co)_n$ and 4.6% for $(PEI/SiW_{11})_n$. Peak potentials did not change significantly. To test stability, modified electrodes were used all day long and kept overnight in their protecting case for 1, 3 or 8 days. No change in the shape and height of the redox waves was observed. Fig. 5.12 shows, as an example, the cyclic voltammograms for the $(PEI/SiW_{11}Co)_7$ electrode.

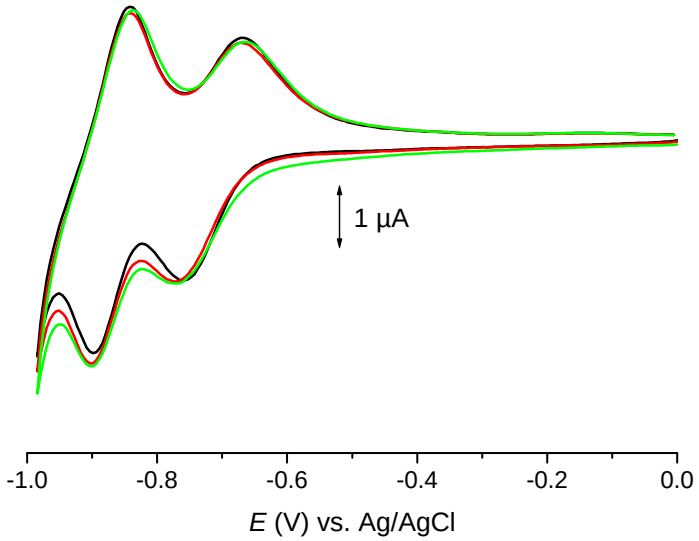

Figure 5.12. Cyclic voltammograms for $(PEI/SiW_{11}Co)_7$ multilayer films in $CH_3COOH/NaCH_3COO$ buffer solution (pH 4.0), $\nu = 25$ mV s^{-1} at first (black), second (red) and eighth working day (green).

5.8. Electrochemical impedance characterisation

Electrochemical impedance spectroscopy can be used to examine the electrical properties of the multilayer assembly which should change as it is built up and provide information which is complementary to that of cyclic voltammetry during the step deposition of the charged PEI and POM layers. Impedance spectra were recorded after the deposition of each layer of PEI and POM in order to investigate the effect of the structure and thickness of the multilayer on the overall interfacial properties in 3 mM

$K_3[Fe(CN)_6]$/0.1 M KCl and in $[Ru(NH_3)_6]Cl_3$/0.1M KCl at 250 mV and -200 mV vs. Ag/AgCl, respectively.

Figures 5.13 and 5.14 show impedance spectra at glassy carbon electrodes with different numbers of PEI/POM bilayers using $[Fe(CN)_6]^{3-/4-}$ and $[Ru(NH_3)_6]^{3+/2+}$ redox probes, respectively. Changes can be clearly seen in the spectra during the stepwise formation of the multilayer assemblies. The impedance spectra comprise a semicircle in the high frequency range that corresponds to the kinetic control of the charge-transfer process and a linear part at lower frequencies, attributable to diffusion control. The diameter of the semicircle increases with an increasing number of PEI/POM bilayers, which can be ascribed to the increase in film thickness and change in the apparent charge transfer resistance.

For the glassy carbon electrode (GCE) covered with only one layer of the positively-charged PEI, tested in the $K_3Fe(CN)_6$ solution, no semicircle was observed. A similar behavior was found for GCE and GCE/$(PEI/POM)_1$ in the solution containing $[Ru(NH_3)_6]^{3+/2+}$. This suggests that the semicircle region is very small and the spectrum is dominated by the Warburg impedance, and thence diffusion control, over nearly the whole range of frequencies examined.

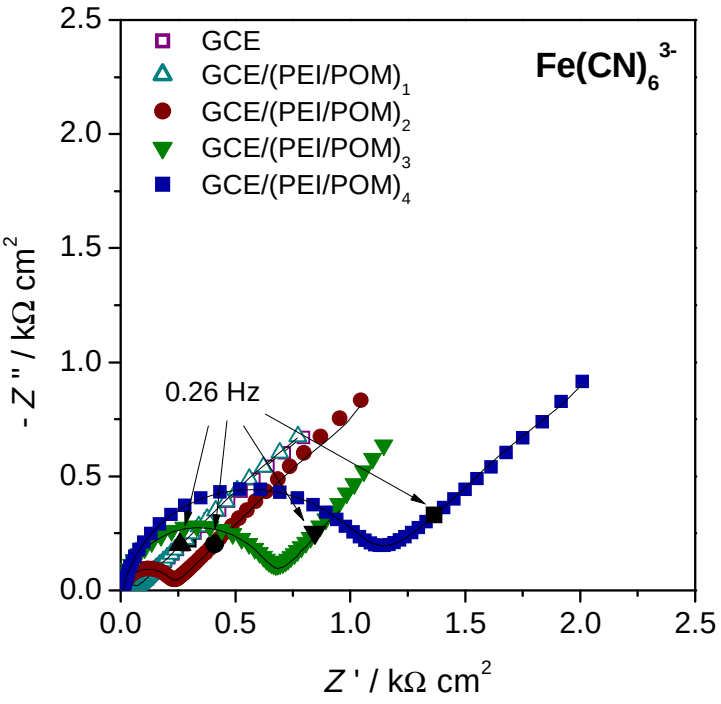

Figure 5.13. Complex plane impedance spectra of different modified electrodes in the presence of 3 mM $K_3Fe(CN)_6$ at +250 mV. Lines indicate equivalent circuit fitting.

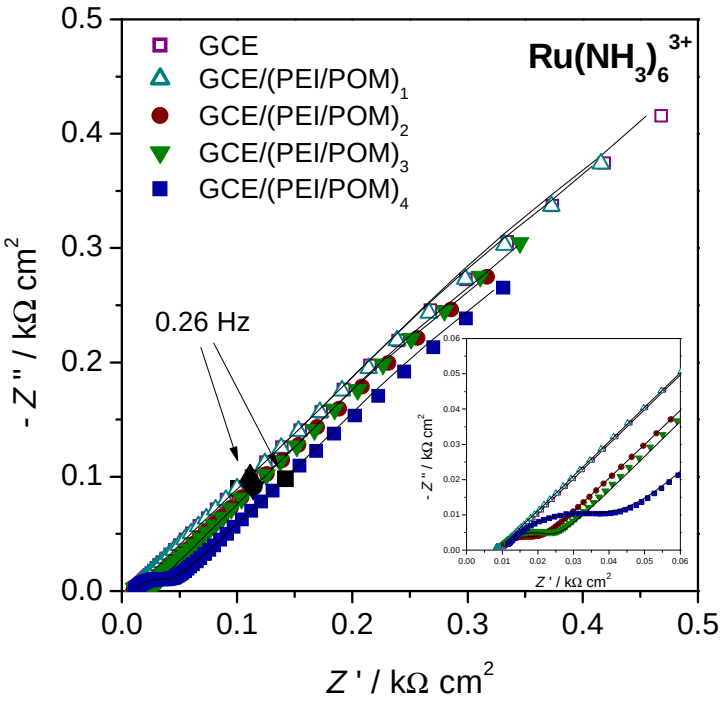

Figure 5.14. Complex plane impedance spectra of different modified electrodes in the presence of 3 mM $Ru(NH_3)_6Cl_3$ at - 200 mV, with amplitude of 10 mV in the frequency range from 65 kHz to 0.01 Hz. In the inset a magnification of the spectra is presented. Lines indicates equivalent circuit fitting.

Quantitative information can be obtained by analysis using appropriate electrical equivalent circuits, Fig. 5.15, and extraction of the electrical parameters. The fitting circuit in Fig.5.15a is a typical Randles circuit that has been used to fit some other similar LbL-assembled structures containing POMs [47-49]. The circuit comprises a cell resistance, R_Ω, in series with a parallel combination of a constant phase element, CPE and a charge transfer resistance, R_{ct}, together with a Warburg impedance, Z_W. The CPE was modeled as a non-ideal capacitor, given by $CPE = -1/(Ci\omega)^n$, where C is the capacitance, which describes the charge separation at the double layer interface, ω is the frequency in rad s^{-1} and the n exponent is due to the heterogeneity of the surface. The Warburg impedance was modeled as an open circuit infinite Warburg element which includes a diffusion resistance, R_{dif}. The circuit in Fig. 5.15b is a simplified version of that in Fig. 5.15a, comprising the cell resistance and the Warburg element, used where no semicircle appeared. The cell resistance, $R_{\Omega,}$ is 9.7 ± 0.5 Ω cm^2 in all cases at the GCE and the Warburg element exponent was always close to 0.50.

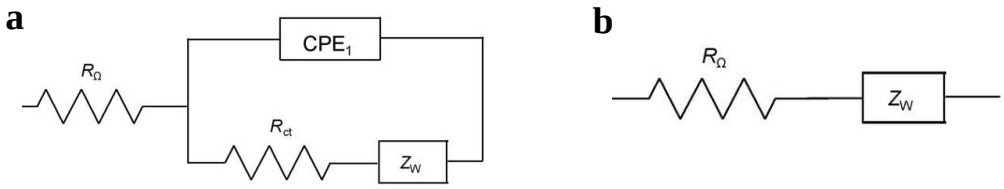

Figure 5.15. Equivalent electrical circuits used to fit the impedance spectra.

Table 5.1 shows values of charge transfer resistance for both redox probes at the bare electrode and for $(PEI/SiW_{11}Fe)_n$ multilayers (n = 1 to 4). The circuit element of most interest is R_{ct} because it can be related directly to the access to the substrate in the modified GCE electrode, where electron transfer of the electroactive species in solution occurs.

Table 5.1. Parameters obtained from impedance spectra of the $(PEI/POM)_n$ multilayer assemblies at GCE in the presence of 3 mM $[Fe(CN)_6]^{4-/3-}$ and 3 mM $[Ru(NH_3)_6]^{2+/3+}$ redox probes by fitting to equivalent circuits in Fig. 5.15.

Redox probe	Number of bilayers	R_{ct} / Ω cm^2	C / μF cm^{-2} s^{n-1}	n	R_{dif} / kΩ cm^2 (W_0)
$[Fe(CN)_6]^{4-/3-}$	0	56	6.0	0.82	3.0
	1	55	11.9	0.86	2.9
	2	210	6.8	0.80	2.9
	3	643	7.2	0.83	1.6
	4	1056	9.5	0.81	3.5
$[Ru(NH_3)_6]^{2+/3+}$	0	---	---	---	1.7
	1	---	---	---	1.6
	2	11.0	106	0.67	1.2
	3	14.9	69	0.69	1.3
	4	32.1	140	0.65	1.2

Considering hexacyanoferrate (III) anion, with just one (PEI/$SiW_{11}Fe$) bilayer assembled on the electrode, R_{ct} is almost the same as at the bare electrode, which indicates that the probe is able to diffuse easily through the bilayers, despite the probe and outer layer having the same charge, and undergo electron transfer at the electrode surface. This is in agreement with cyclic voltammetry that showed a quasi-reversible cyclic voltammogram for $(PEI/SiW_{11}Fe)_1$. As the number of layers increases, as well as the thickness of the multilayer structure, the difficulty of reaching the electrode substrate becomes more pronounced indicating a multilayer with less pores that traverse the film. Assuming that this model is correct, comparing with the bare electrode/one-bilayer system the increase in apparent charge transfer resistance implies a reduction in accessible substrate surface area down to 27 % (2 bilayers) 9 % (3 bilayers) and 5 % (4 bilayers). This is in agreement with other results in the literature, e.g. [50], which suggest that the coverage of the surface by self-assembly is not usually perfect and such defects are progressively removed as the number of bilayers is increased. Interestingly, the values of capacitance are relatively small and change little as do the values of the CPE exponent at around 0.8.

For the ruthenium (III) electroactive species, for zero or one bilayers there is no measurable apparent charge transfer resistance, the process being entirely controlled by diffusion. Resistance to charge transfer only becomes evident for 2 and more bilayers, supporting this explanation. When access does become physically limited, for 2 or more bilayers, it is still much easier than with hexacyanoferrate (III), as would be expected, and charge separation is much greater, with capacitance values an order of magnitude higher. The diffusion resistance values are correspondingly lower. Nevertheless, the CPE exponent is lower suggesting that non-uniformities in the surface play a much larger role when the sign of the charges of the electroactive species and the outermost layer are opposite.

Analysis of the spectra for these two redox species clearly demonstrates that the electrostatic attraction or repulsion between the redox probe and the surface of the multilayer assemblies plays a significant role in the charge transfer process, repulsion for $[Fe(CN)_6]^{3-/4-}$ and attraction for $[Ru(NH_3)_6]^{3+/2+}$, with the negatively-charged layer of POM. On the other hand, adsorption of the next layer, positively charged PEI, reverses the surface charge and the electrostatic interaction creates attraction of the negatively charged $[Fe(CN)_6]^{3-/4-}$ and repulsion of the positively charged $[Ru(NH_3)_6]^{3+/2+}$, leading to higher charge transfer resistances for the $[Ru(NH_3)_6]^{3+/2+}$ redox probe.

The impedance spectra for electrodes terminated with a PEI layer, tested with both redox probes, were also recorded and presented the same general features as those terminated with a POM layer, and the conclusions are the same, so are not further discussed.

Comparative experiments using $[Fe(CN)_6]^{3-/4-}$ were carried out on indium tin oxide electrode substrates in order to assess the influence of the electrode substrate on which the multilayer films are formed (Fig. 5.16).

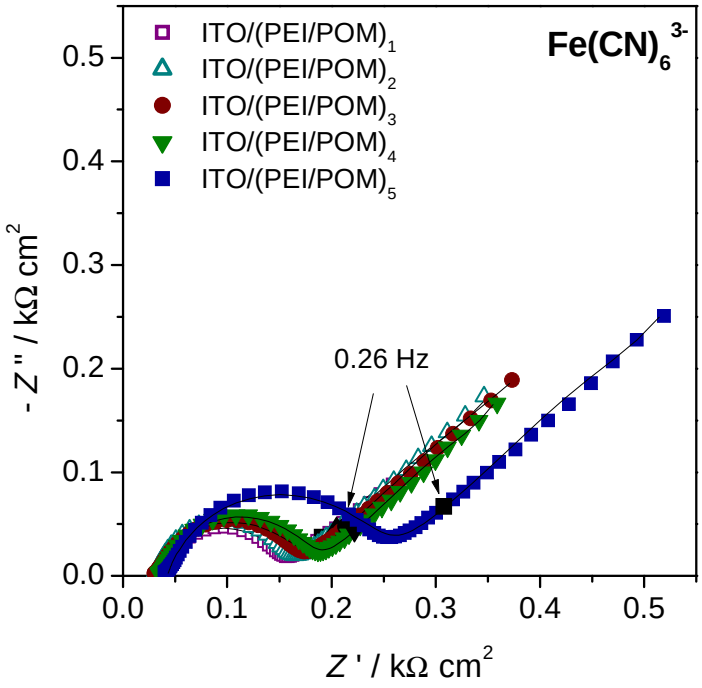

Figure 5.16. Complex plane impedance spectra of different ITO modified electrodes in the presence of 3 mM $K_3Fe(CN)_6$ at 250 mV, with amplitude of 10 mV in the frequency range from 65 kHz to 0.01 Hz. Lines indicate equivalent circuit fitting.

The same trends were observed with respect to different numbers of bilayers as at glassy carbon, see Table 5.2. However, although an increased number of bilayers leads to higher values of the apparent charge transfer resistance, the values, which are initially larger than at glassy carbon electrodes by a factor of two, increase less, less than doubling after 5 bilayers. This suggests that the deposition by layer-by-layer self-assembly is occurring in a different way and the identity of the substrate is important. In particular, there is evidence that imperfections due to incomplete coverage on parts of the substrate surface which are not covered by the first bilayers continue. Additionally, the values of the

capacitance are much higher in this case than at glassy carbon electrodes and the diffusion resistance is lower giving indications that the multilayer also has a different internal structure.

Table 5.2. Parameters obtained from impedance spectra of the $(PEI/POM)_n$ multilayer assemblies at ITO electrodes in the presence of 3 mM $[Fe(CN)_6]^{4-/3-}$ redox probe by fitting to the equivalent circuit in Fig. 5.15a.

Number of bilayers	R_{ct} / Ω cm^2	C / µF cm^{-2} s^{n-1}	n	R_{dif} / kΩ cm^2 (W_0)
1	117	65	0.82	0.47
2	126	29	0.86	0.66
3	138	60	0.80	0.79
4	146	57	0.83	0.61
5	206	50	0.81	0.97

5.9. Electrocatalytic properties of (PEI/POM) multilayer films

The applicability of POM species as a reduction electrocatalyst, is based on the fact that the reduced form, which is the catalytic mediator, can provide a large number of electrons at a suitable, not too negative, potential. Heteropolyanions, in general, have been proved to be excellent catalysts for the electroreduction of various species [51-53] and have been extensively exploited. For example, in Chapter 3 it was observed that TBA-$SiW_{11}Fe$ modified electrodes can reduce nitrite: Dong et al observed that the parent $[SiW_{12}O_{40}]^{4-}$ could be used as electrocatalyst for the reduction of nitrite [54] and Toth and Anson applied the iron-substituted Keggin-type POMs, $[XW_{11}Fe^{(III)}(H_2O)O_{39}]^{n-}$, where X = P, As, Si, Ge as catalysts for the reduction of hydrogen peroxide and nitrite [37,51]. Nitrite was one of the analysts chosen to test the electrocatalytic properties of $(PEI/SiW_{11}Fe)_n$ and $(PEI/SiW_{11}Co)_n$ multilayer films. Under the present experimental conditions, multilayer films of $(PEI/SiW_{11})_n$ did not show electrocatalytic effects towards these compounds, as observed previously [35,51].

In acidic solutions, nitrite is protonated to HNO_2 which can disproportionate (see equations 3.1 and 3.2), although the rate of this process is known to be low. It is normally

assumed that nitrous acid is the reactive form of nitrite between pH 2 and 8 in the case of the electrocatalysis with iron-substituted polyoxotungstates [51].

Figure 5.17a presents cyclic voltammograms for the $(PEI/SiW_{11}Fe)_7$ multilayer film modified electrode in the absence and in the presence of increasing concentrations of nitrite in the interval from 0 to 0.7 mM, at scan rate 10 mV s^{-1}. The inset of Fig. 5.17 (a) shows the catalytic peak current at -0.77 V vs. the concentration of nitrite up to 0.7 mM with a detection limit of $6.8x10^{-5}$ M.

As is known, the electroreduction of nitrite requires a large overpotential, and no response is observed in the range of potentials used at the glassy carbon electrode in a solution containing NO_2^-. At pH 4.0, the reduction wave associated with the $Fe^{III/II}$ couple is almost unaffected by the addition of NO_2^-, but the two-electron reduction waves of the $SiW_{11}Fe$ anion that appear at more negative potentials are significantly enhanced by the addition of nitrite. Similar behaviour was observed by Toth and Anson [51] when performing studies at pH 5.0. A linear range for the catalytic current can be defined for a nitrite concentration up to 0.7 mM, as shown in the inset.

Although the $Fe^{III/II}$ couple is almost unaffected by the addition of nitrite, the presence of the iron centre is essential for catalysis because nitrite has no effect on the cyclic voltammograms of the lacunary derivative $KSiW_{11}$, despite the fact that this anion exhibits a voltammetric response at potentials similar to those of $KSiW_{11}Fe$ anions. Also for the $SiW_{11}Co$, the presence of the metal seems determinant since this compound also presented electrocatalytic properties although the cobalt peak is not seen in the working potential window.

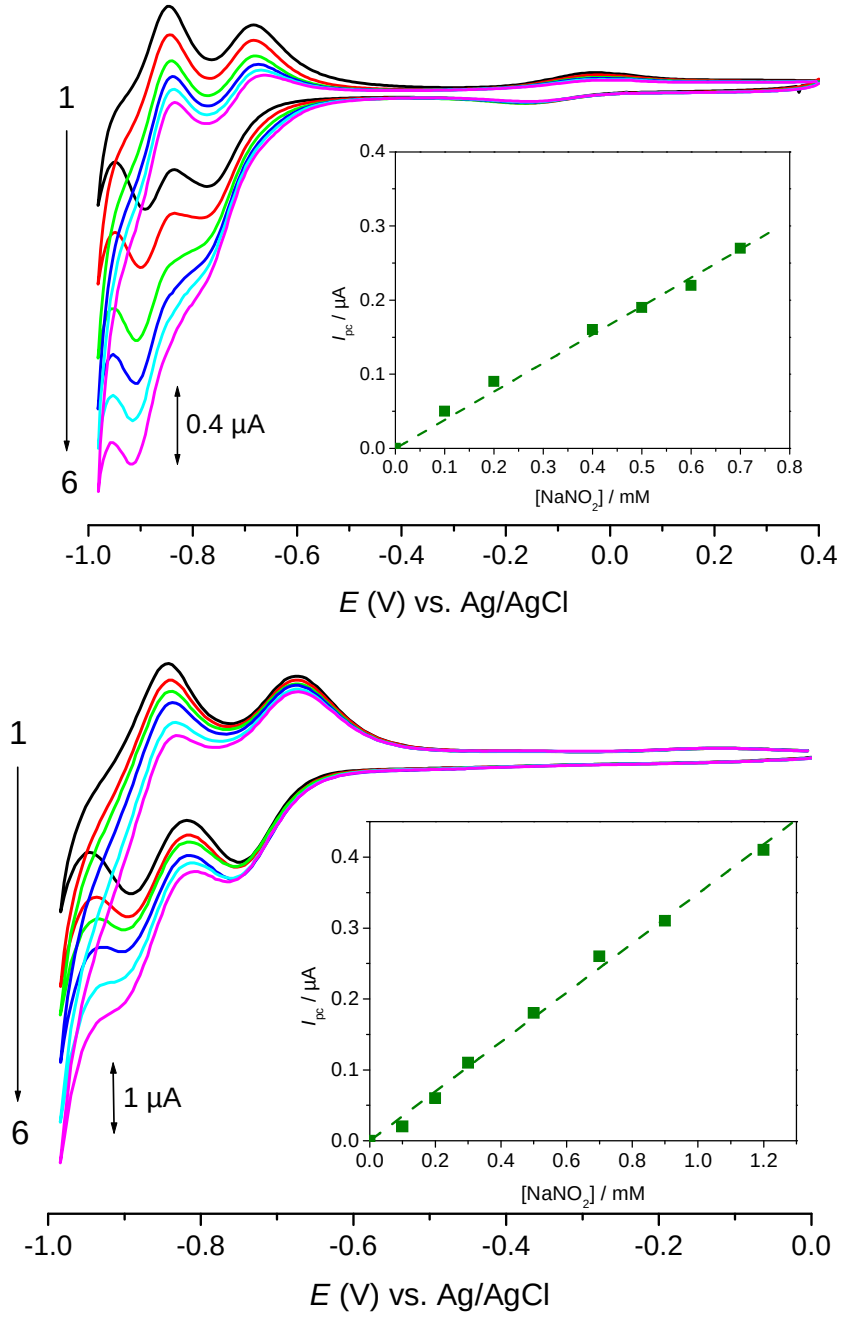

Figure 5.17. Cyclic voltammograms of GCE/(PEI/POM)$_7$ in pH 4.0 buffer solution obtained in the absence and in the presence of added concentrations of nitrite: (a) $SiW_{11}Fe$, 1) 0; 2) 0.2; 3) 0.4; 4) 0.5; 5) 0.6 and 6) 0.7 mM, scan rate 10 mV s^{-1}, (b) $SiW_{11}Co$ 1) 0; 2) 0.2; 3) 0.3; 4) 0.5; 5) 0.9 and 6) 1.2 mM, scan rate 25 mV s^{-1}. The inset shows the catalytic peak current at -0.77 V for $SiW_{11}Fe$ and at -0.90 V vs. the concentration of nitrite for $SiW_{11}Co$.

Figure 5.17b presents cyclic voltammograms for the (PEI/$SiW_{11}Co$)$_7$ multilayer film modified electrode in the absence and in the presence of increasing concentrations of

nitrite in the interval from 0 to 1.2 mM, at scan rate 25 mV s^{-1}. At pH 4.0, the second reduction wave of the $SiW_{11}Co$ anion that appears at more negative potential is significantly enhanced by the addition of nitrite, whereas the first one is less affected. The increase of the peak current at -0.9V indicates that nitrite is being catalytically reduced at the modified electrode. The processes may be described by equations 5.3 to 5.5 [55]. The first two equations correspond to electrochemical reactions taking place at the electrode. It is known that at the pH used, HNO_2, as the reactive form of nitrite, takes part in reaction corresponding to eq. 5.5 [51]:

$$SiW_{11}{}^{VI}Co(H_2O)O_{39}{}^{6-} + 2e^- + 2H^+ \rightarrow H_2SiW_2{}^{V}W_9{}^{VI}Co(H_2O)O_{39}{}^{6-} \quad (5.3)$$

$$H_2SiW_2{}^{V}W_9{}^{VI}Co(H_2O)O_{39}{}^{6-} + 2e^- + 2H^+ \rightarrow H_4SiW_4{}^{V}W_7{}^{VI}Co(H_2O)O_{39}{}^{6-} \quad (5.4)$$

$$H_4SiW_4{}^{V}W_7{}^{VI}Co(H_2O)O_{39}{}^{6-} + nHNO_2 \rightarrow H_2SiW_2{}^{V}W_9{}^{VI}Co(H_2O)O_{39}{}^{6-} + nN \text{ products} \quad (5.5)$$

The linear range for the catalytic current is up to a nitrite concentration of 1.2 mM, as shown in the inset, with a detection limit of 7.2 x 10^{-5} M. This value is very similar to the one obtained for $(PEI/SiW_{11}Fe)_7$. Although in the literature references to the catalytic reduction of nitrite by Keggin type polyoxometalates can be found, the authors usually do not give the values of detection limits. However, some examples can be found, such as the one obtained with a PMo_{12} modified electrode (1 x 10^{-4}) [56]. Compared with these values the ones obtained for $SiW_{11}Fe$ and $SiW_{11}Co$ are better. Additionally, these modified electrodes allow us to reach higher concentration of nitrite than with electrodes modified by other methodologies such as for example the droplet evaporation methodology.

Bromate and iodate were also chosen as analytical systems to test the electrocatalytic properties of $(PEI/SiW_{11}Co)_n$ multilayer films since this anion is not usually used for electrocatalytic studies, unlike the $SiW_{11}Fe$ anion.

Figure 5.18 shows cyclic voltammograms for the $(PEI/SiW_{11}Co)_7$ multilayer film modified electrode in the absence and in the presence of increasing concentrations of bromate (a) and iodate (b) in the interval from 0 to 1.0 mM for bromate and to 0.5 mM for iodate, at scan rate 50 mV s^{-1}. The inset of Fig. 5.18a and 5.18 b shows the catalytic peak current at -0.9 V vs. the concentration of bromate up to 0.6 mM and of iodate up to 0.5 mM.

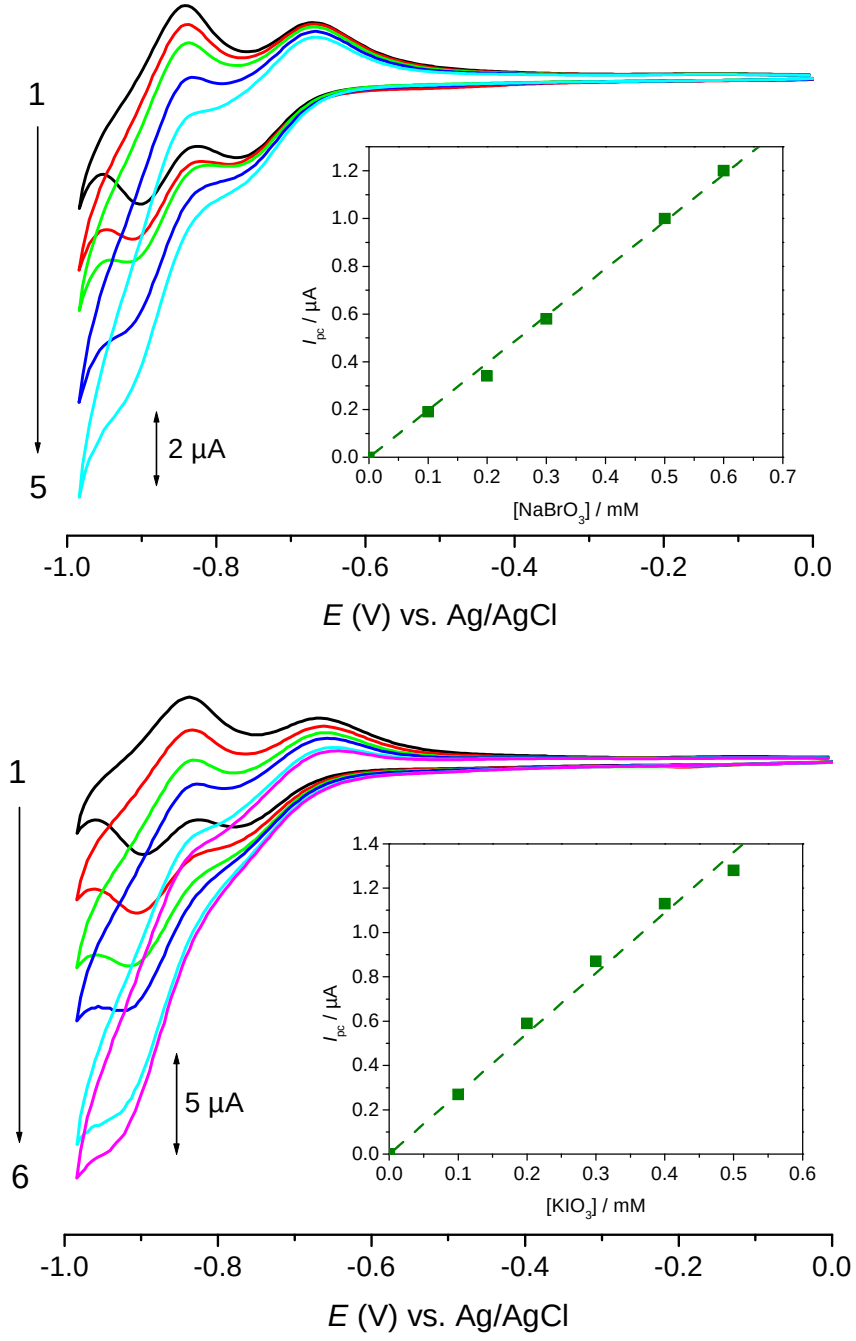

Figure 5.18. Cyclic voltammograms of GCE/(PEI/$SiW_{11}Co)_7$ in pH 4.0 buffer solution obtained in the absence and in the presence of added concentrations of (a) bromate: 1) 0; 2) 0.1; 3) 0.3; 4) 0.6 and 5) 1.0 mM, scan rate 50 mV s^{-1} and (b) iodate: 1) 0; 2) 0.1; 3) 0.2; 4) 0.3; 5) 0.4 and 6) 0.5 mM, scan rate 50 mV s^{-1}. The insets show the catalytic peak current at -0.90 V vs. analyte concentration.

The results obtained for the reduction of bromate and iodate have similar characteristics. As occurred for nitrite, the wave associated with the first tungsten reduction is little affected by the addition of bromate or iodate, but the peak current of the second tungsten reduction wave is greatly enhanced (Fig. 5.18a and 5.18b). The linear range for the catalytic current is up to 0.6 mM for bromate and for iodate is up to 0.5 mM, as shown in the insets. The detection limits were 3.7 x 10^{-5} and 5.8 x 10^{-5} M for bromate and iodate, respectively. These results indicate that the second cathodic wave has catalytic activity towards BrO_3^- and IO_3^-. The electrochemical processes involved are the same as in equations 5.3 and 5.4 and the catalytic chemical steps are:

$$3H_4SiW_4^{V}W_7^{VI}Co(H_2O)O_{39}^{6-} + BrO_3^- \rightarrow 3H_2SiW_2^{V}W_9^{VI}Co(H_2O)O_{39}^{6-} + Br^- + 3H_2O \quad (5.6)$$

$$3H_4SiW_4^{V}W_7^{VI}Co(H_2O)O_{39}^{6-} + IO_3^- \rightarrow 3H_2SiW_2^{V}W_9^{VI}Co(H_2O)O_{39}^{6-} + I^- + 3H_2O \quad (5.7)$$

Although the linear range of concentrations is not very high, the values of detection limit are good. Compared with, for example, the value obtained for the detection of bromate with a $[SiW_{11}Ni(H_2O)O_{39}]^{6-}$ modified electrode, ours is similar [39]. The main importance of this $SiW_{11}Co$ modified electrode is that, even if this compound was already used in other types of modified electrode, this is the first time it showed catalytic activity. Previous work with $SiW_{11}Co$ electrodes prepared by the droplet evaporation methodology showed no catalytic activity towards nitrite (see Chapter 3).

An additional important point is that after use in these electrocatalytic reactions, the electrodes could be totally recovered, i. e. the original voltammograms could be restored.

5.10. Conclusions

It has been demonstrated that $(PEI/PW_{11}Fe)_n$, $(PEI/SiW_{11}Fe)_n$, $(PEI/SiW_{11})_n$ and $(PEI/SiW_{11}Co)_n$ multilayer films can be successfully prepared on glassy carbon electrodes using layer-by-layer self–assembly and that the electrochemical properties of the POMs are maintained. The effect of scan rate in cyclic voltammetry leads to the conclusion that the tungsten reduction process is a surface-confined process. UV–VIS spectroscopy

demonstrated that the amount of POM adsorbed per deposition step is almost constant, up to a certain limit.

Use of $[Fe(CN)_6]^{3-/4-}$ and $[Ru(NH_3)_6]^{3+/2+}$ electrochemical probes in cyclic voltammetry showed that attractions or repulsions at the electrode surface have significant effects on the kinetics of the redox reactions, either accelerating or decelerating the processes. It was also found that with an increasing number of PEI/POM bilayers the peak current of both redox probes gradually decreased, and the peak-to-peak separation increased, indicating that, in general, the kinetics of the redox reactions become slower.

The behaviour of self-assembled multilayer films in the presence of redox probes can also be successfully investigated using electrochemical impedance spectroscopy. In particular, the charge transfer reactions at the surface of a $(PEI/POM)_n$ modified electrode can be affected by the thickness of the multilayer assembly and by the electrostatic attraction and repulsion between the surface of the assembly and the electroactive species in solution. With the negatively charged hexacyanoferrate (III) the outermost negatively charged POM leads to electrostatic repulsion as well as less penetration through to the electrode surface, which causes the apparently higher charge transfer resistance observed. If another layer is deposited so that the outermost layer is positively charged, this resistance becomes lower again. The opposite is true with the positively charged hexaammineruthenium(III) species. Impedance data are able to show differences between such assemblies more clearly than the information obtained from cyclic voltammetry. Additionally, impedance spectra are sensitive to and can distinguish multilayer construction on different substrates, as seen with glassy carbon and indium tin oxide.

The $(PEI/SiW_{11}Fe)_n$ multilayer films also exhibited electrocatalytic activity towards the reduction of nitrite and $(PEI/SiW_{11}Co)_n$ multilayer films towards the reduction of nitrite, bromate and iodate.

5.11. References

[1] G. Decher, *Science* 277 (1997) 1232.

[2] S. Liu, D.G. Kurth, B. Bredenkotter, D. Volkmer, *J. Am. Chem. Soc.* 124 (2002) 12279.

[3] M. Skunik, B. Baranowska, D. Fattakhova, K. Miecznikowski, M. Chojak, A. Kuhn, P. J. Kulesza, *J. Solid State Electrochem.* 10 (2006) 168.

[4] P. J. Kulesza, M. Skunik, B. Baranowskaa, K. Miecznikowski, M. Chojak, K. Karnicka, E. Frackowiak, F. Béguin, A. Kuhn, M. Delville, B. Starobrzynska, A. Ernst, *Electrochim. Acta* 51 (2006) 2373.

[5] D. Fan, J. Hao, *J. Phys. Chem. B* 113 (2009) 7513.

[6] B. Xu, L. Xu, G. Gao, W. Guo, S. Liu, *J. Colloid Interface Sci.* 330 (2009) 408.

[7] S. Gao, R. Cao, C. Yang, *J. Colloid Interface Sci.* 324 (2008) 156.

[8] M. Sadakane, M.E. Steckhan, *Chem. Rev.* 98 (1998) 219.

[9] Y. Wang, C. Guo, Y. Chen, C. Hu, W. Yu, *J. Colloid Interface Sci.* 264 (2003) 176.

[10] Y. Feng, Z. Han, J. Peng, J. Lu, B. Xue, L. Li, H. Ma, E. Wang, *Mater. Lett.* 60 (2006) 1588.

[11] S. Li, E. Wang, C. Tian, B. Mao, Y. Song, C. Wang, L. Xu, *Mater. Res. Bull.* 43 (2008) 2880.

[12] L. Cheng, J. Liu, S. Dong, *Anal. Chim. Acta* 417 (2000) 133.

[13] S. Zhai, Y. Chen, S. Wang, J. Jiang, *Talanta* 63 (2004) 927.

[14] L. Cheng, S. Dong, *J. Electroanal. Chem.* 481 (2000) 168.

[15] J. Liu, L. Cheng, S. Dong, *Electroanalysis* 14 (2002) 569.

[16] S. Gao, T. Li, X. Li, R. Cao, *Mater. Lett.* 60 (2006) 3622.

[17] C. Li, X. Wang, H. Ma, F. Wang, Y. Gu, *Electroanalysis* 20 (2008) 1110.

[18] F. Caruso, D.G. Kurth, D. Volkmer, M.J. Koop, A. Müller, *Langmuir* 14 (1998) 3462.

[19] D.G. Kurth, D. Volkmer, M. Ruttorf, B. Richter, A. Müller, *Chem. Mater.* 12 (2000) 2829.

[20] C.M.A. Brett, A.M. Oliveira Brett, Electrochemistry, Principles, Methods and Applications, Oxford University Press, Oxford, 1993, ch 11

[21] H.O. Finklea, D.A. Snider, J. Fedyk, E. Sabatani, Y. Gafni, I. Rubinstein, *Langmuir* 9 (1993) 3660.

[22] H. Taira, K. Nakano, M. Maeda, M. Takagi, *Anal. Sci.* 9 (1993) 199.

[23] A. Bardea, F. Patolsky, A. Dagan, I. Willner, *Chem. Commun.* (1999) 21.

[24] A. J. Bard, L. R. Faulkner, Electrochemical Methods: Fundamentals and Applications, Wiley, New York, 2001.

[25] K. Nomiya, Y. Sugie, K. Amimoto, M. Miwa, *Polyhedron* 6 (1987) 519.

[26] M. Fournier, R. Massart, *C. R. Acad. Sc. Paris, Série C* 276 (1973) 1517.

[27] T. J. R. Weakley, S. A. Malik, *J. Inorg. Nucl. Chem.* 29 (1967) 2935.

[28] S.T. Dubas, J.B. Schlenoff, *Macromolecules* 32 (1999) 8153.

[29] P. Bertrand, A. Jonas, A. Laschewsky, R. Legras, *Macromol. Rapid Commun.* 21 (2000) 319.

[30] D.G. Kurth, R. Osterhout, *Langmuir* 15 (1999) 4842.

[31] Y. Lvov, K. Ariga, M. Onda, I. Ichinose, T. Kunitake, *Colloid Surf. A - Physicochem. Eng. Asp.* 146 (1999) 337.
[32] G. Decher, J.B. Schlenoff, Multilayer Thin Films, Wiley – VCH, 2003.
[33] B. Wang, R.N. Vyas, S. Shaik, *Langmuir* 23 (2007) 11120.
[34] M.T. Pope, Heteropoly and Isopoly Oxometalates, Springer Verlag, Berlin, 1983.
[35] D.M. Fernandes, S.M.N. Simões, H.M. Carapuça, A.M.V. Cavaleiro, *Electrochim. Acta* 53 (2008) 6580.
[36] F.A.R.S. Couto, A.M.V. Cavaleiro, J.D. Pedrosa de Jesus, J.E.J. Simão, *Inorg. Chim. Acta* 281 (1998) 225.
[37] J. E. Toth, F. C. Anson, *J. Electroanal. Chem.* 256 (1988) 361.
[38] A. Kuhn, F.C. Anson, *Langmuir* 12 (1996) 5481.
[39] C. Chen, Y. Song, L. Wang, *Electrochim. Acta* 54 (2009) 1607.
[40] L. Cheng, J.A. Cox, *Electrochem. Commun.* 3 (2001) 285.
[41] D. Yoo, S. Shiratori, M. Rubner, *Macromolecules* 31 (1998) 4309.
[42] F. Hua, Y.M. Lvov in: V. Erokhin, M. Ram, Z. Yavuz (Eds), The New Frontiers of Organic and Composite Nanotechnology, Elsevier Science, 2007.
[43] W.G. Klemperer, C.G. Wall, *Chem. Rev.* 98 (1998) 297.
[44] J.J. Harris, M.L. Bruening, *Langmuir* 16 (2000) 2006.
[45] V. Pardo-Yissar, E. Katz, O. Lioubashevski, I. Willner, *Langmuir* 17 (2001) 1110.
[46] J. Dai, A.W. Jensen, D.K. Mohanty, J. Erndt, M.L. Bruening, *Langmuir* 17 (2001) 931.
[47] S. Zhai, S. Gong, J, Jiang, S. Dong, J. Li, *Anal. Chim. Acta* 486 (2003) 85.
[48] Z. Cheng, L. Cheng, Q. Gao, S. Dong, X. Yang, *J. Mater. Chem.* 12 (2002) 1724.
[49] G. Yang, H. Guo, M. Wang, M. Huang, H. Chen, B. Liu, S. Dong, *J. Electroanal. Chem*. 600 (2007) 318.
[50] C. Picart, Ph. Lavalle, P. Hubert, F.J.G. Cuisinier, G. Decher, P. Schaaf, J.C. Voegel, *Langmuir* 17 (2001) 7414.
[51] J. E. Toth, F. C. Anson, *J. Am. Chem. Soc.* 111 (1989) 2444.
[52] T. McCormac, B. Fabre, G. Bidan, *J. Electroanal. Chem*. 427 (1997) 155.
[53] L. Wang, D. Xiao, E. Wang, L. Xu, *J. Colloid Interface Sci*. 285 (2005) 435.
[54] S. Dong, X. Xi, M. Tian, *J. Electroanal. Chem*. 385 (1995) 227.
[55] Y. Li, W. Bu, L. Wu, C. Sun, *Sensors Actuator B* 107 (2005) 921.
[56] Y. Liang, P. He, Y. Ma, Y. Zhou, C. Pei, X. Li, *Electrochem. Commun*. 11 (2009) 1018.

CHAPTER 6

MODIFIED ELECTRODES WITH SILICOTUNGSTATES AND PEDOT

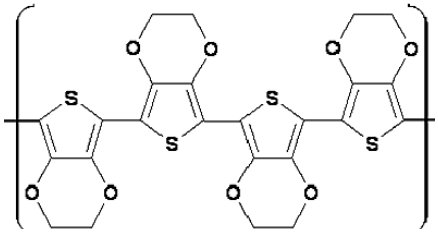

6.1. Introduction

Over the past several years there has been growing interest in conducting and redox polymer films due to the prospect of their application in different fields such as sensors, molecular electronics, corrosion protection, displays and light emitting diodes [1-3]. The most commonly studied conducting polymers used in electrode modification are of the polyaniline or polypyrrole types, which can be doped with anionic species such as redox-active Keggin-type polyoxometalates [4-13]. It has been established that incorporation of polyoxometalates in such conducting polymers produces composite (hybrid) materials in which the polymeric structure is retained, whereas the inorganic clusters are largely responsible for the system integrity and overall electroactivity. Polythiophene and poly(3-methylthiophene) have also been studied as hosts for heteropolyanions, incorporating phosphometalates and silicometalates [14-16].

Poly(3,4-ethylenedioxythiophene) (PEDOT), a derivative of polythiophene with dioxyethylene [17], is an alternative organic polymer and has the advantage of being one of the most stable commercially available conducting polymers (arising from dioxy-ring electron donation and a favourable geometry) [18-20]. In addition, it participates to a small extent in side reactions with oxygen and hydrogen ions, which can be beneficial from the point of view of interference elimination [21]. PEDOT has excellent electrical conductivity and optoelectronic properties [19,22-24], useful for different applications. For example, PEDOT has been used as an antistatic coating [25], a conductive electrode in light emitting diodes and as a material for electrochromic devices [26].

PEDOT is frequently prepared by electropolymerization of 3,4-ethylenedioxythiophene (EDOT) by potential cycling in aqueous or nonaqueous solvents, as described in Chapter 1. It is commonly accepted that PEDOT is very stable in its doped oxidized state [27]. The exact nature of electrochemical processes occurring in PEDOT films is fairly complex [28]. The system is believed to undergo several overlapping fast redox transitions characterized by high diffusion coefficients for charge propagation [29]. The above properties make PEDOT attractive as a potential material for fabrication of composite matrices. Some work has already been done using PEDOT and Keggin anions. Kulesza *et al.* prepared electrodes containing $[PMo_{12}O_{40}]^{3-}$ and carbon nanoparticles [30], platinum nanoparticles [31] or nanotubes [32,33] dispersed in PEDOT films. They also produced hybrid films of PEDOT and $[PMo_{12}O_{40}]^{3-}$ or $[PW_{12}O_{40}]^{3-}$ by electrodeposition [34]. White *et al.* have used PEDOT and polyoxometalates to prepare electrodes using the vapour transport method [35].

The present work concerns the preparation and electrochemical characterization of PEDOT-modified electrodes doped with $[SiW_{11}Fe^{III}(H_2O)O_{39}]^{5-}$ ($SiW_{11}Fe$), $[SiW_{11}Co^{II}(H_2O)O_{39}]^{6-}$ ($SiW_{11}Co$), $[SiW_{11}O_{39}]^{8-}$ (SiW_{11}), and, for comparison, $[SiW_{12}O_{40}]^{4-}$ (SiW_{12}). These modified electrodes are prepared by controlled electrodeposition of composite (hybrid) films of PEDOT with the Keggin type silicotungstates. The electrochemical behaviour of the immobilized POMs was examined by cyclic voltammetry and the effect of solution pH and scan rate on the voltammetric behaviour of the modified electrodes was evaluated. Furthermore, the electrodes modified with $SiW_{11}Fe$ were studied by electrochemical impedance spectroscopy.

6.2. Experimental

6.2.1. Reagents and solutions

Sulphuric acid (Fluka), sodium sulphate (Sigma-Aldrich) and 3,4-ethylenedioxythiophene (Aldrich) were used as received. The potassium salts of the α-Keggin silicotungstates $K_8[SiW_{11}O_{39}]\cdot 13H_2O$, $K_5[SiW_{11}Fe^{III}(H_2O)O_{39}]\cdot 13H_2O$ and $K_6[SiW_{11}Co^{II}(H_2O)O_{39}]$ were prepared as described in Chapter 2. Silicotungstic acid, $H_4[SiW_{12}O_{40}]\cdot xH_2O$ (Merck), was used as received.

Electrolyte buffer solutions within the pH range 1.5-3.5, used for voltammetry, were prepared by mixing appropriate amounts of a 0.2 M H_2SO_4 solution with a 0.5 M Na_2SO_4 solution.

The solutions used for the film preparation were used immediately after their preparation and degassed with pure nitrogen for at least 10 min.

6.2.2. Instrumentation and methods

Cyclic voltammetry experiments were carried out as referred previously in Chapter 3. The working electrode was used bare or surface-modified with the POM salts.

Electrochemical impedance measurements were carried out as referred to in Chapter 5.

6.2.3. Preparation of POM doped PEDOT films

Prior to coating, the GCE (3 mm diameter, BAS, MF-2012) was conditioned by the procedure described in 5.2.3. Electrochemical pre-treatment of the electrode was performed by applying 20 consecutive potential scans, between -0.8 V and 0.8 V, at a scan rate of 0.1 V s^{-1} in NH_4Ac/HCl (pH 3.4; 1.0 M NH_4Ac / 0.5 M HCl) buffer solution.

Unless otherwise stated, the POM-doped PEDOT films were prepared by potential cycling (5 cycles) at 100 mV s^{-1} from -0.75 to 1.1 V vs. Ag/AgCl in a solution containing SiW_{12}, SiW_{11}, $SiW_{11}Fe$ or $SiW_{11}Co$ (0.25 mM) and PEDOT (5 mM) in 0.2 M H_2SO_4. All measurements were made at room temperature (~25º C).

6.3. Cyclic voltammetry of the POM doped PEDOT films

6.3.1. Film formation and stability

The electrodeposition of PEDOT films doped with Keggin-type polyoxotungstates on glassy carbon electrodes, was carried out by potential cycling in solutions containing the chosen POM ($SiW_{11}Fe$, $SiW_{11}Co$, SiW_{12} or SiW_{11}) and EDOT in 0.2 M H_2SO_4. PEDOT's

electronic structure (Fig. 6.1) is controlled by the applied potential, switching between the conductive (oxidized) and the insulating (reduced) states. Oxidized PEDOT has a transparent sky blue color that turns dark purple upon reduction [36]. The polymer and POM are expected to interact electrostatically with each other during the deposition process, because oxidized PEDOT is positively charged and the polyoxometalate is anionic.

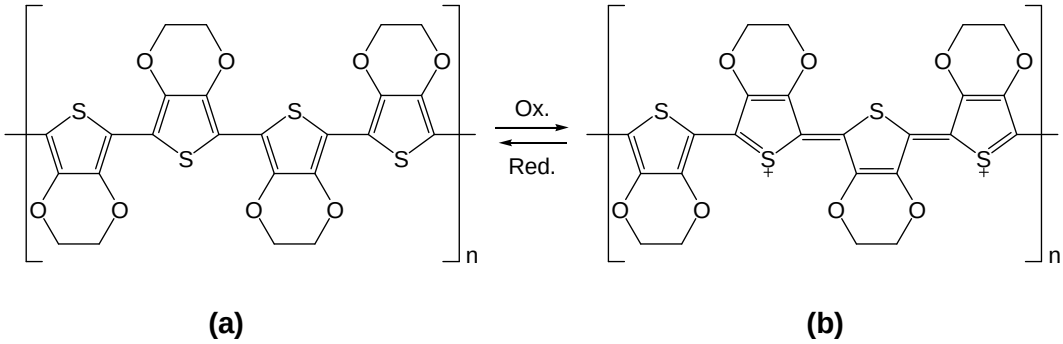

(a) **(b)**

Figure 6.1. Neutral PEDOT (a) is oxidized to form a conducting polycation (b) in the presence of charge-balancing anions. Oxidized PEDOT has a transparent sky blue color that turns dark purple upon reduction.

Figure 6.2 shows cyclic voltammograms that demonstrate the growth of $SiW_{11}Fe$-doped PEDOT films. PEDOT is generated on the electrode surface during positive scans [2,34], with simultaneous attraction of compensating anions during the potential cycling and growth of the film, which leads to increased stability of the composite film. The fact that all voltammetric peak currents increase almost linearly with each cycle in Fig. 6.2 implies a linear growth of the film. The cyclic voltammograms for the other three silicotungstates were similar.

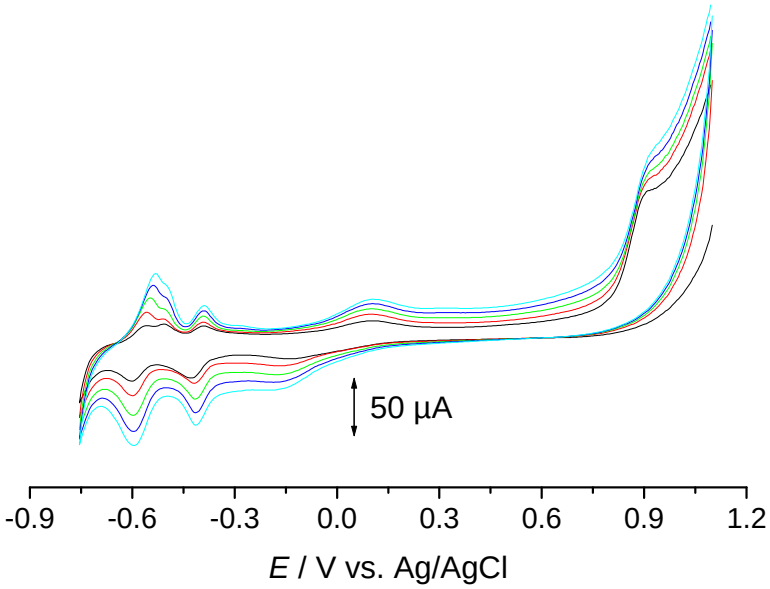

Figure 6.2. Electropolymerization and formation of hybrid films by potential cycling in 5 mM EDOT / 0.25 mM $SiW_{11}Fe$ / 0.2 M H_2SO_4 solution. Potential range -0.75 to 1.1 V; scan rate: 100 mV s^{-1}.

Figure 6.3 shows cyclic voltammograms in the potential range from -0.75 to 0.0 V vs. Ag/AgCl for $SiW_{11}Fe$ doped PEDOT films at three different times after film preparation. Shortly after the films were prepared, the voltammetric response was characterized by three pairs of peaks. Scans were recorded every day during six days at the beginning and at the end of the day; at the end of each day, the electrode was left to rest in its protecting case. It can be observed that the pair of peaks at less negative potential, corresponding to the $Fe^{III/II}$ process did not change, but there were significant changes in the cyclic voltammograms, corresponding to the tungsten (VI) reduction peaks. At the end of the first day (~6–8 h after electrode preparation), the observed change in the peak positions and heights corresponding to tungsten reduction suggests some reorganization of the structure. It seems that these peaks were altered from two reduction processes of one and three electrons to the typical two reductions of two-electrons, inferred from the changes in the peak heights. After six days this behaviour was maintained and after longer time periods no further significant changes were observed in the cyclic voltammograms. According to these results, it appears that the prepared modified electrodes should be left to rest for at least one day in order to attain reproducible cyclic voltammograms. For the other POM-doped PEDOT films a similar electrochemical behaviour, with alteration during the first 24 h after preparation, was observed.

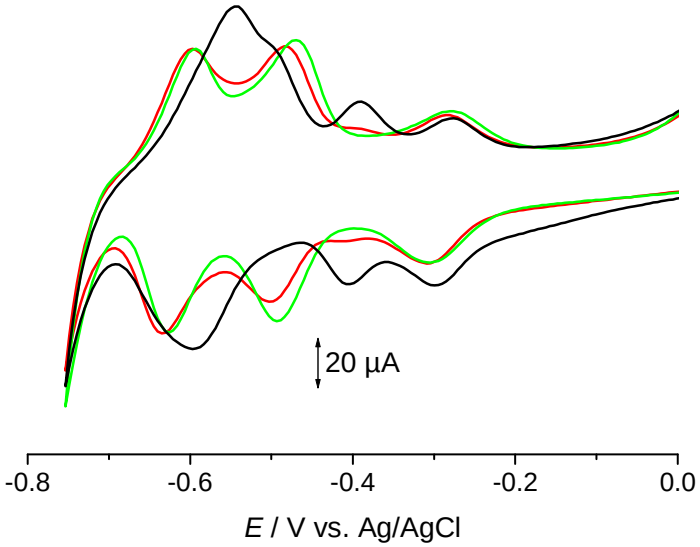

Figure 6.3. Cyclic voltammograms for $SiW_{11}Fe$ doped PEDOT obtained in 0.2 M H_2SO_4 solution, ν = 100 mV s^{-1}: (black) after deposition; (red) end of the first day; (green) six days later.

Figure 6.4 shows cyclic voltammograms, in the same potential range, of a $SiW_{11}Fe$-doped PEDOT modified electrode (6 days after preparation) and, for comparison, the cyclic voltammogram of a PEDOT film prepared by the same procedure as the previous one but without POM. The results demonstrate that the contribution of PEDOT to the overall electrochemical response of the POM-doped films is relatively low, the voltammetric behaviour of the produced films being dominated by the redox characteristics of the polyoxometalates. In the cyclic voltammogram of $SiW_{11}Fe$ in Fig. 6.4, two reduction waves can be observed, at -496 and -628 mV, corresponding to the reduction of tungsten atoms. Another reduction peak is observed at -305 mV which corresponds to the reduction of Fe^{III}.

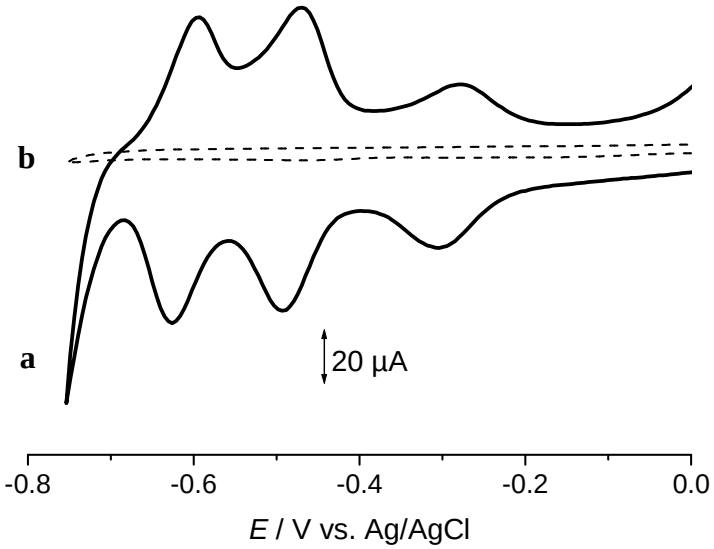

Figure 6.4. Cyclic voltammograms for: (a) $SiW_{11}Fe$-doped PEDOT and (b) PEDOT film. Electrolyte: 0.2 M H_2SO_4 solution, ν = 100 mV s^{-1}.

6.3.2. Film characterisation

All the electrochemical characterisation experiments were carried out in acidic aqueous solutions, as it is known that the silicotungstates used in this work may undergo a series of hydrolytic processes as the pH increases. Cyclic voltammograms of the SiW_{12} and SiW_{11} doped films reveal two clearly resolved 2-e^- reduction waves, as can be seen for the SiW_{12} anion in Fig. 6.5a. The peak potentials do not differ much from each other (Table 6.1), but the voltammograms are better defined for the parent anion. Cyclic voltammograms of SiW_{12} in H_2SO_4 aqueous solution usually show three redox couples corresponding to two one-electron waves followed by one two-electron wave [37]. However, Keita and Nadjo reported that in strong acid aqueous solutions ($HClO_4$ and HCl) and in DMF, with stepwise addition of perchloric acid [38], significant changes of the waves are observed; in particular, the first voltammetric wave changes from a one-electron, diffusion-controlled process to an overall, apparently direct, two-electron transfer. So it is possible that the PEDOT environment where the SiW_{12} is immobilized may favour similar changes in the number of reduction waves.

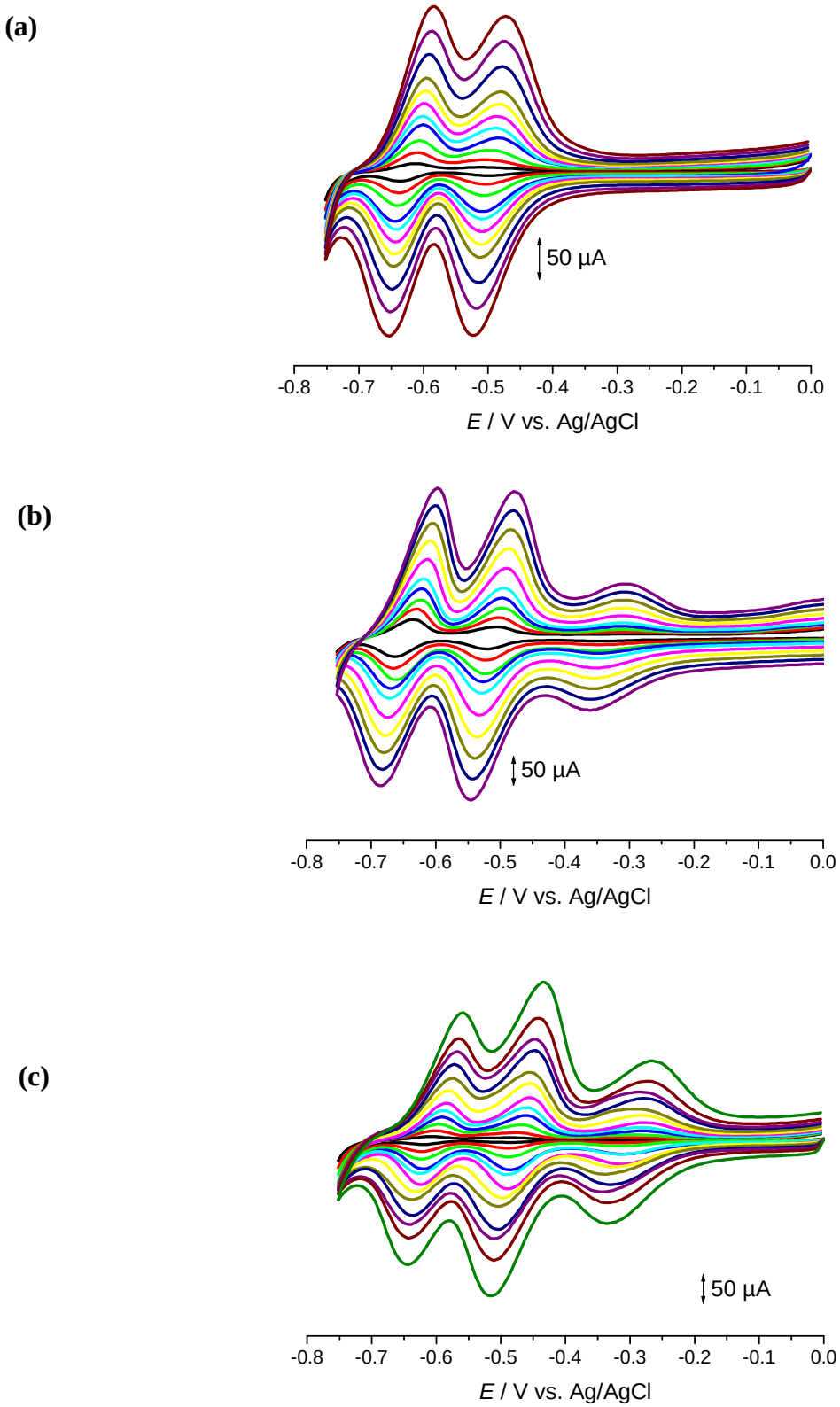

Figure 6.5. Cyclic voltammograms of (a) $SiW_{12,}$ (b) $SiW_{11}Co$ and (c) $SiW_{11}Fe$ doped PEDOT modified electrodes 0.2 M H_2SO_4 solution at scan rates of 25, 50, 75, 100, 125, 150, 175, 200,250, 300, 350 and 400 mV s^{-1}.

For the $SiW_{11}Co$ anion in aqueous solution [39] or immobilized on electrodes (see chapter 3), the cyclic voltammograms usually have two 2-electron reduction peaks, due to the reduction of tungsten atoms, and no peaks corresponding to cobalt redox processes, within the potential window used. However, the cyclic voltammograms of $SiW_{11}Co$-doped PEDOT on the modified electrode revealed a third reduction peak at approximately -350 mV vs Ag/AgCl, in addition to those corresponding to the reduction of tungsten atoms (Fig. 6.5b). Because the cyclic voltammograms of SiW_{12} and SiW_{11} have only two reduction waves of almost equal height (Fig 6.5a), the possibility of formation of such species in these conditions was ruled out. Also, the fact that a third peak is not observed in the cyclic voltammograms of SiW_{12} or SiW_{11} shows that this peak cannot be attributed to the polymer. Thus, this third reduction peak is possibly due to a process occurring at the substituting metal. A much higher redox potential was determined for the $SiW_{11}Co^{III/II}$ couple (+1.10 V vs NHE) [40] and no reasonable explanation could be found for its change. We consider much more probable that the observed peak, with $E_{1/2}$ near -340mV, corresponds to the $Co^{II/I}$ redox couple. For cobalt, oxidation states lower than +2 usually need the stabilizing effects of π-acceptor ligands. Some type of interaction may be established between cobalt and the thiophene rings, that may stabilise Co(I). Many examples may be found of electrochemical studies involving $Co^{II/I}$ redox couples, namely cobalt complexes with bipyridine [41,42], porphyrins [42,43], phthalocyanines [44,45] and Schiff bases [46]. The observed redox potentials vary over a large range, depending on the ligands.

The effect of scan rate was investigated for SiW_{12}, $SiW_{11}Fe$ and $SiW_{11}Co$ in 0.2 M H_2SO_4 solution (Fig. 6.5). The cathodic and anodic peak currents are directly proportional to scan rate, which indicates a surface-confined process, and the ratio of oxidation to reduction peak currents is close to 1. The anodic/cathodic peak-to-peak separation (ΔE_p) was ca. 5 – 50 mV instead of zero, which would be expected for a reversible surface process.

Table 6.1 presents the voltammetric data of the first tungsten reduction peak and of the metal for the four silicotungstates studied and, for comparison, the values in aqueous solution. The values of $|E_p-E_{p/2}|$ close to 30 mV indicate a 2-electron reduction process as referred previously. Also, as a consequence of immobilization, there were no significant differences between the potential of the first tungsten reduction process upon metal substitution, in contrast to aqueous solutions. A similar behaviour was observed for these POMs immobilized on modified electrodes by the droplet evaporation method (Chapter 3) or by the layer-by-layer method (Chapter 5).

Table 6.1. Cyclic voltammetric data of the first W reduction process for silicotungstate doped PEDOT modified electrodes at 100 mV s^{-1} in 0.2 M H_2SO_4.

POM	E_{pc} *	$\lvert \Delta E_p \rvert$ *	$\lvert E_{pc} - E_{p/2} \rvert$ *	E_{pc} (M´) *	$E_{pc\ (aq)}$ #
SiW_{12}	-509	15	35	-	-
SiW_{11}	-521	29	33	-	-501
$SiW_{11}Fe$	-495	28	34	-305	-563
$SiW_{11}Co$	-522	26	32	-350	-566

* mV vs. Ag/AgCl; # E_{pc} values for the polyoxoanions in aqueous solution (mV vs. Ag/AgCl) at pH 2.0, v = 50 mV s^{-1}.

The pH of the electrolyte solution has a marked effect on the voltammetric behaviour of POM-doped PEDOT modified electrodes. With increasing pH, the peak potentials shift to more negative potentials. Additionally the peak currents gradually decrease. With the raise of pH there occurs an increase in the concentration of Na^+ in the buffer (with replacement of H^+ by the bulky cations), and, thus, slower penetration (charge propagation) of bulkier cations to the active centres which may explain the decrease of current.

Plots of peak potential versus pH in the range from 1.5 to 3.5 gave a slope of -70 mV/pH unit for SiW_{12}, -89 mV/pH unit for $SiW_{11}Fe$ and -86 mV/pH unit for $SiW_{11}Co$. The effect of pH at SiW_{11}-doped PEDOT modified electrodes were not determined because the reduction waves of this anion tend to overlap with increasing pH, and the potentials of the individual peaks were difficult to determine accurately. The slopes show that the redox mechanism at the tungsten atoms immobilized on the PEDOT film requires the involvement of protons. So, in the present experimental conditions, assuming a Nernstian behaviour, the first W reduction in SiW_{12} is a two-electron/two-proton global process. For the metal-substituted anions the slopes are slightly higher, indicating that the two-electron reduction is probably accompanied by addition of two to three protons as already observed in chapter 3 for the TBA-silicotungstates immobilized by the droplet evaporation methodology.

The stability of POM-doped PEDOT modified electrodes was studied, by cycling 100 times in 0.2 M H_2SO_4 solution between -0.75 and 0.0 V at 100 mV s^{-1}. The peak currents decreased less than 5%. After this, the electrodes were left immersed in this solution for one month: there was no decrease in peak current but the peak potentials shifted to

slightly more positive potentials. The reason for this high stability may be the strong electrostatic interaction between the polyoxometalate and the conductive PEDOT polymer.

6.4. Electrochemical impedance spectroscopy of the POM doped PEDOT films

Electrochemical impedance spectroscopy (EIS) was used to examine the interfacial properties of the PEDOT/$SiW_{11}Fe$ modified electrode.

Two series of experiments were performed. First, measurements were carried out in pH 2.0 H_2SO_4/Na_2SO_4 buffer solution at three different potentials (-329, -512 and -648 mV vs. Ag/AgCl) chosen to encompass the redox reactions of silicotungstate. Secondly, measurements were carried out at four different pH values at -512 mV vs. Ag/AgCl.

Complex plane impedance spectra in pH 2.0 H_2SO_4/Na_2SO_4 buffer solution are illustrated in Fig. 6.6a. There are clear differences between the spectra obtained at the three potentials. The spectrum recorded at -329 mV was a straight line and for the other two potentials, the spectra included a semicircle in the high frequency range that corresponds to kinetic control of the charge-transfer process and a linear part characteristic of the lower frequency attributed to a diffusion process. The diameter of the semicircle is greater for spectra recorded at -648 mV. This increase in the diameter can be due to the interfacial charge transfer process becoming slower with increasing negative potentials.

Spectra obtained at -512 mV in H_2SO_4/Na_2SO_4 buffer solutions of different pH values also presented the same profile, Fig. 6.6b. The diameter of the semicircle increases with increase of pH, due to electron transfer becoming more difficult because of the consumption of protons, as already seen by cyclic voltammetry.

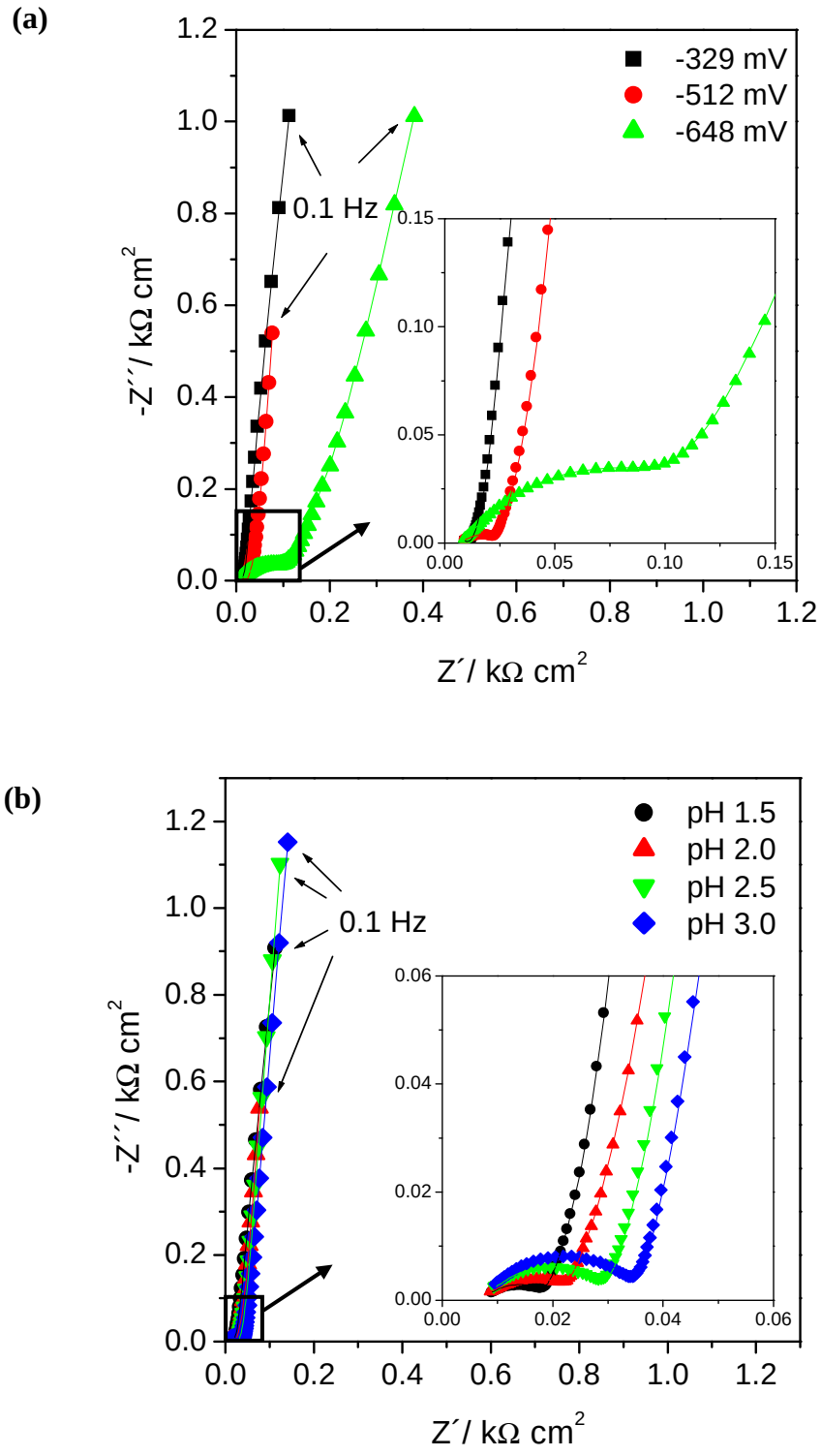

Figure 6.6. Complex plane impedance spectra of PEDOT/$SiW_{11}Fe$ modified electrode in H_2SO_4/Na_2SO_4 buffer solution (a) pH 2.0, at different applied potentials (b) at -512 mV vs. Ag/AgCl at different values of pH.

The spectra were fitted to the equivalent circuit shown in Fig. 6.7. The fitting circuit comprises a cell resistance, R_Ω, in series with a parallel combination of, a constant phase element, CPE, and a charge transfer resistance, R_{ct}, with a Warburg element, Z_W. The CPE was modeled as a non-ideal capacitor, given by CPE= $-1/(C\mathrm{i}\omega)^n$, where C is the capacitance, which describes the charge separation at the double layer interface, ω is the frequency in rad s^{-1} and the n exponent is due to the heterogeneity of the surface. The Warburg element was modeled as an open circuit finite Warburg element, W_0 where Z_W (W_o) = R_{dif} ctnh ($[\mathrm{i}\tau\omega]^\alpha$) / $(\mathrm{i}\tau\omega)^\alpha$, R_{dif} being a diffusion resistance.

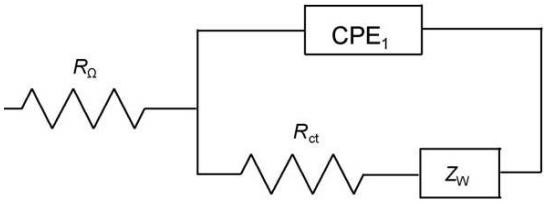

Figure 6.7. Equivalent circuit used to fit the spectra.

Tables 6.2 and 6.3 show the values of the parameters obtained. The circuit elements R_{ct} and R_{dif} relate directly to the accessibility of the electrode substrate and the flow of species at the electrode substrate and though the film, respectively. Both of these depend on the applied potential and on the pH of electrolyte used. In all cases α(W_o) is 0.46 or 0.47 which close to the value of 0.50 for a perfectly uniform surface although the CPE exponent is lower, suggesting a greater non-uniformity at the multilayer/electrode interface. Values of capacitance become a little lower as the pH is increased.

Table 6.2. Parameters obtained from impedance spectra of the $SiW_{11}Fe$ doped PEDOT modified electrode in pH 2.0 H_2SO_4/Na_2SO_4 buffer solution by fitting to the equivalent circuit in Fig. 6.7.

Potential (mV)	R_{ct} / Ω cm^2	C / μF cm^{-2} s^{n-1}	n	R_{dif} / Ω cm^2	α (W_o)
-329	- *	- *	- *	11.8	0.46
-512	12.2	56.5	0.71	16.2	0.46
-648	87.5	107.1	0.72	81.5	0.46

* Element not included

Table 6.3. Parameters obtained from impedance spectra of the $SiW_{11}Fe$ doped PEDOT modified electrode at -512 mV in H_2SO_4/Na_2SO_4 buffer solutions with different pH values by fitting to the equivalent circuit in Fig. 6.7.

pH	R_{ct} / Ω cm^2	C / μF cm^{-2} s^{n-1}	n	R_{dif} / Ω cm^2	α (W_o)
1.5	8.1	60.7	0.73	14.2	0.46
2.0	12.2	56.5	0.71	16.2	0.46
2.5	19.5	50.0	0.72	18.4	0.47
3.0	25.5	34.7	0.71	20.4	0.47

The impedance results are in agreement with those from cyclic voltammetry. In particular, the shift of peak potentials in cyclic voltammetry to more negative values together with a decrease in current as the pH of the electrolyte solution increases is in agreement with the increase of the charge transfer resistance in the impedance spectra.

6.5. Conclusions

The feasibility of preparation of hybrid films of $[SiW_{12}O_{40}]^{4-}$, $[SiW_{11}O_{39}]^{8-}$, $[SiW_{11}Fe^{III}(H_2O)O_{39}]^{5-}$ or $[SiW_{11}Co^{II}(H_2O)O_{39}]^{6-}$ and PEDOT, under aqueous conditions, on the surface of glassy carbon electrodes has been demonstrated. The electrochemical behaviour of these modified electrodes was studied by cyclic voltammetry and electrochemical impedance spectroscopy. Cyclic voltammograms of the prepared films showed, in all cases, two well resolved 2-electron waves attributable to tungsten redox processes and one 1-electron wave attributable to the substituting metal, when present. The effect of scan rate in cyclic voltammetry leads to the conclusion that the first tungsten reduction process is surface-confined and the study at different pH indicates that the reductions are proton dependent. The electrodes have high stability, which can be attributed to strong electrostatic interaction between the polyoxometalate and the conducting PEDOT polymer. The impedance results showed that the charge transfer resistance increased with increasing pH and for higher values of potentials used.

6.6. References

[1] C. Barbero, M. C. Miras, B. Schnyder, O. Haas, R. Kotz, *J. Mater. Chem.* 4 (1994) 1775.

[2] G. Inzelt, M. Pineri, J. W. Schultze, M. A. Vorotyntsev, *Electrochim. Acta* 45 (2000) 2403.

[3] J. F. Rubinson, H. B. Mark Jr., Interfacial Electrochemistry, Conducting Polymer Films as Electrodes, New York (1999) p.689.

[4] A.M. White, R.C.T. Slade, *Electrochim. Acta* 48 (2003) 2583.

[5] A.M. White, R.C.T. Slade, *Synth. Met.* 139 (2003) 123.

[6] A. Balamurugan, S. M. Chen, *J. Solid State Electrochem.* 11 (2007) 1679.

[7] P. C. Lekha, S. Subramanian, D. P. Padiyan, *J. Mater. Sci.* 44 (2009) 6040.

[8] P. Gomez-Romero, M. Chojak, K. Cuentas-Gallegos, J. A. Arsensio, P. J. Kulesza, N. Casan-Pastor, M. Lira-Cantu, *Electrochem. Commun.* 5 (2003) 149.

[9] P. Gomez-Romero, M. Lira-Cantu, *Adv. Mater.* 9 (1997) 144.

[10] E. F. C. Chimamkpam, F. Hussain, A. Engel, A. Schilling, G. R. Patzke, *Z. Anorg. Allg. Chem.* 635 (2009) 624.

[11] T. F. Otero, S. A. Cheng, F. Huerta, *J. Phys. Chem. B* 104 (2000) 10522.

[12] T. F. Otero, S. A. Cheng, D. Alonso, F. Huerta, *J. Phys. Chem. B* 104 (2000) 10528.

[13] S. Cheng, T. F. Otero, E. Coronado, C. J. G. García, E. M. Ferrero, C. G. Saiz, *J. Phys. Chem. B* 106 (2002) 7585.

[14] B. Fabre, G. Bidan, D. Fichou, *J. Chim. Phys. Phys.-Chim. Biol.* 89 (1992) 1053.

[15] M. Lapkowski, G. Bidan, M. Fournier, *Synth. Met.* 41 (1991) 407.

[16] J.L. Sauvajol, J.P. Lereporte, C. Chorro, G. Poussigue, *J. Phys.-Conders. Matter* 4 (1992) 3179.

[17] F. Petraki, S. Kennou, S. Nespurek, *J. Appl. Phys.* 103 (2008) 033710.

[18] G. Heywang, F. Jonas, *Adv. Mater.* 4 (1992) 116.

[19] M. Dietrich, J. Heinze, G. Heywang, F. Jonas, *J. Electroanal. Chem.* 369 (1994) 87.

[20] H. Yamoto, O. Ohwa, W. Wernet, *J. Electroanal. Chem.* 397 (1995)163.

[21] Y. Yang, Y. Jiang, J. Xu, J. Yu, *Thin Solid Films* 516 (2008) 1191.

[22] M. Granstrom, M. Berggren, O. Inganas, *Science* 267 (1995) 1479.

[23] M. Mastragostino, C. Arbizzani, A. Bongini, G. Barbarella, M. Zambianchi, *Electrochim. Acta* 38 (1992) 135.

[24] C. Kvarnstrom, H. Neugebauer, S. Blomquist, H. J. Ahonen, J. Kankare, A. Ivaska, *Electrochim. Acta* 44 (1999) 2739.

[25] F. Jonas, G. Heywang, *Electrochim. Acta* 39 (1994) 1345.

[26] P. M. Beaujuge, J. R. Reynolds, *Chem. Rev.* 110 (2010) 268.

[27] J. C. Lacroix, K. K. Kanazawa, A. D. Diaz, J. *Electrochem. Soc.* 136 (1989) 1308.

[28] X. Chen, O. Inganas, *J. Phys. Chem.* 100 (1996) 15202.

[29] J. Bobacka, A. Lewenstam, A. Ivaska, *J. Electroanal. Chem.* 89 (2004) 17.

[30] M. Skunik, B. Baranowska, D. Fattakhova, K. Miecznikowski, M. Chojak, A. Kuhn, P. J. Kulesza, *J. Solid State Electrochem.* 10 (2006) 168.

[31] K. Karnicka, M. Chojak, K. Miecznikowska, M. Skunik, B. Baranowska, A. Kolary, A. Piranska, B. Palys, L. Adamczyk, P. J. Kulesza, *Bioelectrochemistry* 66 (2005) 79.

[32] M. Skunik, P. J. Kulesza, *Anal. Chim. Acta* 631 (2009) 153.

[33] P. J. Kulesza, M. Skunik, B. Baranowska, K. Miecznikowski, M. Chojak, K. Karnicka, E. Frackowiak, F. Béguin, A. Kuhn, M. H. Delville, B. Starobrzynska, A. Ernst, *Electrochim. Acta* 51 (2006) 2373.

[34] L. Adamczyk, P. J. Kulesza, K. Miecznikowski, B. Palys, M. Chojak, D. Krawczyk, J. *Electrochem. Soc.* 152 (2005) E98.

[35] M. White, R. C.T. Slade, *Electrochim. Acta* 49 (2004) 861.

[36] J. P. Lock, J. L. Lutkenhaus, N. S. Zacharia, S. G. Im, P. T. Hammond, K. K. Gleason, *Synth. Met.* 157 (2007) 894.

[37] M. T. Pope, Heteropoly and Isopoly Oxometalates, Spring Verlag, 1983.

[38] B. Keita, L. Nadjo, *J. Electroanal. Chem.* 227 (1987) 77.

[39] F.A.R.S. Couto, A.M.V. Cavaleiro, J.D. Pedrosa de Jesus, J.E.J. Simão, *Inorg. Chim. Acta* 281 (1998) 225.

[40] S.A. Malik, T.J.R. Weakley, *J. Chem. Soc. (A)* (1968) 2647.

[41] S. A. Richert, P. K. S. Tsang, D. T. Sawyer, *Inorg. Chem.* 28 (1989) 2471.

[42] W. Zhu, M. Sintic, Z. Ou, P. J. Sintic, J. A. McDonald, P. R. Brotherhood, M. J. Crossley, K. M. Kadish, *Inorg. Chem.* 49 (2010) 1027.

[43] J. A. Claussen, G. Ochoa, M. Páez, J. Costamagna, M. Gulppi, T. Nyokong, F. Bedioui, J. H. Zagal, *J. Solid State Electrochem.* 12 (2008) 473.

[44] M. N. Yarasir, M. Kandaz, B. F. Senkal, A. Koca, B. Salih, *Dyes and Pigments* 77 (2008) 7.

[45] P. C. Gach , J. A. Karty, D. G. Peters, *J. Electroanal. Chem.* 612 (2008) 22.

[46] J. D. L. Holloway, W. L. Bowden, W. E. Geiger, Jr., *J. Am. Chem. Soc.* 99 (1977) 7089.

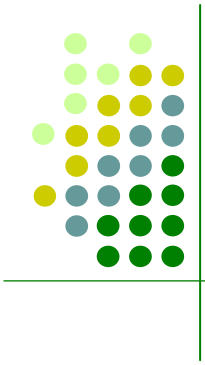

CHAPTER 7

CONCLUSIONS

Polyoxometalates represent an important subject of current research due to the discovery of several types of application of these compounds over recent decades. Since the use of polyoxometalates in the field of modified electrodes is one of their important applications, this thesis was focused on the study of different possible approaches to modify electrodes with these anions and on their characterization and potential applications in electrocatalysis. These studies were restricted to Keggin-type polyoxotungstates, with particular emphasis on Fe- and Co-substituted polyoxotungstates. The electrodes were designed for the purpose of being used in aqueous solutions. The production of new devices involving POMs is becoming even more common and several papers devoted to the parent Keggin polyoxometalates can be found in the literature. Much less studies are available concerning the lacunary and the mono-substituted anions.

Several compounds were used in this work in the preparation of modified electrodes, namely the tetra-butylammonium (TBA) and potassium (K) salts of lacunary, $TBA_xH_y[XW_{11}O_{39}]$ and $K_x[XW_{11}O_{39}]$, and mono-substituted anions, $TBA_xH_y[XW_{11}M(H_2O)O_{39}]\cdot nH_2O$ and $K_x[XW_{11}M(H_2O)O_{39}]\cdot nH_2O$, with X = P and Si and M = Fe^{III} and Co^{II}. All compounds were prepared and characterized. The TBA salts, being insoluble in water, are convenient in preparative methods involving the direct deposition or incorporation of a polyoxotungstate salt in the electrode. The potassium salts were used whenever the anions were incorporated in the electrode in association with cationic polymeric counter-ions.

The electrochemical study of the lacunary and mono-substituted silicotungstates was performed by cyclic voltammetry in aqueous H_2SO_4/HAc/NaAc buffer solutions. These anions presented reversible or quasi-reversible redox processes associated with

the reduction of tungsten atoms ($W^{VI} \rightarrow W^{V}$) and in the case of iron-substituted silicotungstate the redox process of iron ($Fe^{III} \rightarrow Fe^{II}$). In the case of the metal-substituted anions, the first electron to enter the structure is received by the transition metal, the remaining electrons being accepted by the tungsten atoms. For the lacunary anion the first tungsten reduction appears at a less negative potential than for the metal substituted. A study of the scan rate effect showed that the peak currents were diffusion controlled and altering the pH revealed that the first and second tungsten reductions of the lacunary anion are two two-electron/two-proton processes and for the metal substituted anions are two-electron/two or three-proton processes. A knowledge of these redox properties is important for the studies of the immobilized polyoxotungstates.

The preparation of modified electrodes with TBA-silicotungstates (TBA-SiW_{11}, TBA-$SiW_{11}Fe$ and TBA-$SiW_{11}Co$) by solvent evaporation methodology from acetonitrile solutions seems to be the simpler and most straightforward process used. This method was used only once before in our laboratory and, to our knowledge, this is the only report in the literature. These electrodes proved to be fairly reproducible and stable. Optical and scanning electron microscopy examination revealed non-uniform electrode surfaces with areas indicating a fast growth of crystals. The morphology of the TBA-POM deposits was similar to the powder compounds. Cyclic voltammetry showed that for all the immobilized POMs, the tungsten reduction processes were diffusion controlled with the uptake of protons from solution. The TBA-$SiW_{11}Fe$ modified electrodes showed electrocatalytic properties towards nitrite. However, the total recovery of the initial electrode surface was not possible.

The second approach chosen for the immobilization of POMs was the use of carbon paste electrodes due to their known advantages. The POMs used were TBA-PW_{11} and TBA-$PW_{11}Co$. A traditional CPE preparative method was used as well as a new method for chemical modification. In this, a drop of a mixture of graphite, poly(hexylmethacrylate) and POM was deposited on the surface of a CPE. Cyclic voltammetry showed that the first tungsten redox processes were also controlled by diffusion and accompanied by the uptake of protons. Modification using poly(hexylmethacrylate) slightly improves the electrode sensitivity for the same amount of POMs. These electrodes were more stable than the ones prepared by solvent evaporation methodology.

In order to overcome some of the problems in these two approaches another immobilization method was tested, the layer-by-layer method, using potassium salts of polyoxotungstates (K-SiW_{11}, K-$SiW_{11}Fe$, K-$SiW_{11}Co$ and K-$PW_{11}Fe$) and poly(ethylenimine) as the polycation. UV-vis spectroscopy was used after the deposition

of each bilayer to monitor film growth and revealed that the amount of POM adsorbed per deposition step was almost constant. Scanning electron microscopy was also used for evaluation of surface morphology. Images showed that for all the polyoxotungstates used a completely-covered surface was achieved but these presented a considerable number of cracks which underneath revealed a high density of irregular shaped domains of small micrometric dimensions. Voltammetric studies showed that the electrochemical properties of the four POMs studied are maintained in the multilayer films. Unlike the other two methodologies, here it was found that the cathodic and anodic peak currents of the first tungsten wave were directly proportional to scan rate, indicating a surface confined process. Use of $[Fe(CN)_6]^{3-/4-}$ and $[Ru(NH_3)_6]^{3+/2+}$ electrochemical probes in cyclic voltammetry showed that attractions or repulsions at the electrode surface have significant effects on the kinetics of the redox reactions. It was also found that with an increasing number of PEI/POM bilayers the peak current of both redox probes gradually decreased, and the peak-to-peak separation increased, indicating that, in general, the kinetics of the redox reactions become slower. The behaviour of multilayer films was also investigated using electrochemical impedance spectroscopy. With the negatively charged hexacyanoferrate (III) the outermost negatively charged POM led to electrostatic repulsion as well as less penetration through to the electrode surface, which causes the apparently higher charge transfer resistance observed. If another layer is deposited so that the outermost layer is positively charged, this resistance becomes lower again. The opposite is true with the positively charged hexammineruthenium(III) species. Additionally, impedance spectra are sensitive to and can distinguish multilayer construction on different substrates, as seen with glassy carbon and indium tin oxide. The $(PEI/SiW_{11}Fe)_n$ multilayer films exhibited electrocatalytic activity towards the reduction of nitrite and $(PEI/SiW_{11}Co)_n$ multilayer films towards the reduction of nitrite, bromate and iodate. This methodology gave better results compared with the droplet evaporation because a total recovery of the electrodes was possible after catalysis and here the $SiW_{11}Co$ showed electrocatalytic activity. These electrodes also presented good stability.

Entrapment of POMs in polymer matrices can also be achieved by electrodeposition with conducting polymers. In addition to their conductivity, conducting polymers often feature reversible redox chemistry and ionic transport and can provide an ideal network where polyoxoanions can be integrated. The preparation of modified electrodes with poly(3,4-ethylenedioxythiophene) and silicotungstates ($K\text{-}SiW_{12}$, $K\text{-}SiW_{11}$, $K\text{-}SiW_{11}Fe$ and $K\text{-}SiW_{11}Co$) showed that the main POM features are also maintained by this methodology and that the first tungsten reduction process is surface confined. The electrodes revealed

high stability, which can be attributed to strong electrostatic interaction between the polyoxotungstates and the conducting polymer. The behaviour of the film was also investigated using electrochemical impedance spectroscopy and the results demonstrated that the charge transfer resistance increased with increasing pH and at higher potentials.

The studies presented in this thesis have the aim of contributing to the knowledge of new modified electrodes with polyoxotungstates. The electrochemical properties of polyoxotungstates when immobilized were studied and the different types of electrodes characterized by a number of techniques. Even though the electrochemical features of POMs were similar in terms of number of redox waves and of the pH effect on these waves, the influence of scan rate brought out differences. The layer-by-layer and electrodeposition methods showed a surface confined behaviour expected for electrodes with immobilized species. Some electrodes were more stable than others the ones prepared by the droplet evaporation method being the less and the electrodes prepared by electrodeposition the more stable. The same anion also presented distinct electrocatalytic activity depending on the method used for its immobilization. The more obvious result was the non-activity of $SiW_{11}Co$ when immobilized by droplet evaporation and its good activity of the same anion when the layer-by-layer assembly was employed.

In summary, the knowledge acquired through these studies will aid in the development of POM-based modified electrodes and it is clear that there are several factors that can affect the performance of these modified electrodes. However, it is important to continue with the study of new ways to improve the already existing methodologies as well as the use of new ones because POMs offer a large range of practical applications. For example, from the materials science point of view, one of the most important POMs functionalities is its photo- and electrochromic properties. The fabrication of film by electropolymerization involving other conducting polymers and different types of POMs from those used here can be a promising subject of study. Polyoxomolybdates can be employed instead of polyoxotungstates, because their less negative reduction potentials is a key factor in the design of photo- and electrochromic systems. Besides GCE electrodes other electrode materials (transparent Pt, ITO glass/PET etc.) can be used in order to study the influence of the substrate. Also, other transition-metals, such as Mn, Ni and Cu, may be introduced into mono-substituted anions, providing additional redox behaviour which can be helpful when employing the modified electrodes in electrocatalysis.